ALBUMIN IN ARTIFICIAL LIVER SUPPORT SYSTEMS

by

Richard Hollis Miller

B. S. in Chemical Engineering, University of Pittsburgh, 2002

Submitted to the Graduate Faculty of

the Swanson School of Engineering in partial fulfillment

of the requirements for the degree of

Doctor of Philosophy

University of Pittsburgh

2012

UNIVERSITY OF PITTSBURGH

SWANSON SCHOOL OF ENGINEERING

This dissertation was presented

by

Richard Hollis Miller

It was defended on

July 3, 2012

and approved by

Mohammad Ataai, PhD, Professor, Department of Chemical and Petroleum Engineering

Robert M. Enick, PhD, Professor, Department of Chemical and Petroleum Engineering

Carl F. Lagenaur, Associate Professor, PhD, Department of Neurobiology

George V. Mazariegos, Professor, MD, Department of Surgery

Dissertation Director: John F. Patzer II, Associate Professor, PhD, Department of Bioengineering

ALBUMIN IN ARTIFICIAL LIVER SUPPORT SYSTEMS

Richard Hollis Miller, PhD

University of Pittsburgh, 2012

While liver transplantation is the only accepted therapy for liver failure, bound solute dialysis (BSD) may provide an alternative. Current BSD methods, MARS and SPAD, are unfortunately poorly characterized. The studies presented here address basic questions involved in making BSD effective. First, Biacore surface plasmon resonance (SPR) was used to measure binding and reaction rate constants of albumin-solute pairs relevant to designing and testing BSD systems. Much is known about albumin equilibrium binding properties, but little is known regarding albumin-solute binding kinetics. Additionally, testing and clinical application of BSD systems are often done at different temperatures (i.e. room temperature (22°C) and body temperature (37°C)), and changes in reaction rates and binding constants with temperature need to be considered. Human and bovine serum albumin were immobilized on Biacore sensor chip surfaces, and reacting solutes (bilirubin, FK506, cyclosporine A, cholate, deoxycholate, and glycocholate) flowed across the surfaces. The SPR response was tracked during the association and dissociation of the albumin-solute complex. Reactions were performed at 22°C and 37°C. Equilibrium constants consistent with previously reported values and reaction rates were determined for all reactions tested except cyclosporine A. Second, I developed a mathematical model describing the removal of albumin bound solutes using BSD that incorporates albumin-solute reaction kinetics. Previous BSD models focused on the amount of binder in the dialysate, ultrafiltration, and the use of solid adsorbents. The new model relaxes the assumption of reaction equilibrium built into previous BSD models. For a given equilibrium binding constant

and set of mass transport parameters, the model was solved for several reaction rates. In all cases tested, the equilibrium BSD model overestimated removal compared to the kinetic model, but the kinetic model displayed greater numerical instability. A third project explored methods to direct visualize protein deposition in and on commercial dialysis membranes during use. A novel slide dialyzer design incorporating commercial renal dialyzer membranes was developed and tested.

TABLE OF CONTENTS

LIST OF TABLES

LIST OF FIGURES

PREFACE

I would like to thank my wife, Charlotte, and my children, Vincent and Camille, for their love and patience. Thank you Mom and Dad. I love you both dearly, and I would have never been able to make it this far without your help. The help of our dear friend, nonna Christine, has been invaluable during my academic pursuits.

I would like to thank my advisor, Dr. John Patzer. You were one of my first professors my freshman year as an undergraduate, and your advice and knowledge has provided me with direction and focus. I would be remiss in not mentioning my mentor and good friend Dr. Carl Lagenaur. Your help and advice has made my work possible.

ACRONYMS AND ABREVIATIONS

ACLF	Acute on chronic liver failure
ALF	Acute liver failure
ALSS	Artificial liver support system
BAL	Bioartificial liver
BLSS	Bioartificial liver support system
BSD	Bound solute dialysis
CVVHD	Continuous veno-venous hemodialysis
CVVHDF	Continuous veno-venous hemodiafiltration
DMSO	Dimethyl sulfoxide
EDC	1-Ethyl-3-(3-dimethylaminopropyl) carbodiimide hydrochloride
EQ	Equilibrium
FDA	Food and Drug Administration
FPSA	Fractionated plasma separation and adsorption
HE	Hepatic encephalopathy
HepC	Hepatitis C virus
HRS	Hepatorenal syndrome
HSA	Human serum albumin
ICU	Intensive care unit

ID	Inner diameter
LDLT	Living donor liver transplantation
MAP	Mean arterial pressure
MARS	Molecular Adsorbent Recirculating System
MELD	Model for End-Stage Liver Disease
n/a	Not available
NAPQI	N-acetyl-p-benzoquinone imine
NHS	N-Hydroxysuccinimide
OD	Outer diameter
ODE	Ordinary differential equation
OLTx	Orthotopic liver transplantation
OPTN	Organ Procurement and Transplantation Network
PBS	Phosphate buffered saline
PELD	Pediatric End-Stage Liver Disease Model
PES	Polyethersulfone
RTV	Room temperature vulcanization
RU	Response units
SMT	Standard medical therapy
SPAD	Single pass albumin dialysis
SPR	Surface plasmon resonance
UNOS	United Network for Organ Sharing
UPMC	University of Pittsburgh Medical Center

1.0 INTRODUCTION

Liver disease and liver failure remain medically intransigent in the United States and abroad and are responsible for many deaths each year. Whether acute fulminant liver failure or acute decompensation of function on chronic liver disease, orthotopic liver transplantation (OLTx) is the only treatment that has been proven effective for acute liver failure.[1-3] Despite the success of liver transplantation surgery, many patients die while waiting for a liver to become available. At any given time approximately 16,000 people are on the waiting list for a liver, but only 6319, 6320, and 6291 transplants were performed in 2008, 2009, and 2010 respectively. During the years 2000 – 2010 between 1500 and 2000 people per year have died while waiting for liver transplantation.[4] The lack of treatment alternatives and the number of deaths attributed to liver failure argue for a need for new treatment methods to bridge patients to transplant or recovery.

Several artificial and bioartificial (BAL) liver support systems have undergone preclinical and clinical evaluation with varying levels of success. BAL detoxification systems use liver cells cultured in a bioreactor to treat the patient's blood in an extracorporeal circuit. Cell-based therapy is perceived to have the ability to replace part of the metabolic and synthetic function normally seen in the liver, but several hurdles have prevented cell-based therapy from gaining widespread acceptance (including cell source, seeding or encapsulation matrix, and oxygenation method). [3, 5-9]

Non-biological artificial liver support systems (ALSS) have the potential to provide a new standard in the treatment of liver failure. ALSS treats a patient's blood in an extracorporeal circuit using dialysis, solid state adsorbents, or both. ALSS utilizing solid state adsorbents, such as HemoCleanse–DT (also referred to as Biologic-DT, Liver Dialysis Unit or the Unit) (HemoCleanse, Lafayette, Indiana, USA) and the Prometheus system (Fresenius Medical Care, Bad Homburg, Germany) use activated carbon, neutral polymer adsorbents, charged exchange resins, or combinations of adsorbents as a sink for the removal of molecules typically cleared by the liver.[10-13] Solid state adsorbent systems have been clinically shown to improve patient blood chemistries, but have not been proven to improve patient survival in randomized prospective trials.[3, 6, 7, 14, 15]

Albumin dialysis, or more generally bound solute dialysis (BSD), as practiced by the Molecular Adsorbent Recycling System (MARS) (Gambro AB, Stockholm, Sweden) and single pass albumin dialysis (SPAD), has shown proof of principal in the clinical setting. *In vitro* and clinical tests have shown both MARS and SPAD capable of increasing the rate of removal of solutes refractory to aqueous dialysis by four-fold or more over conventional intensive care unit (ICU) dialysis methods.[3, 7, 16-23]

BSD systems are targeted toward the removal of solutes that are bound to proteins or other carriers in the blood, primarily albumin, that are normally metabolized and removed by the liver and that cannot be removed by conventional aqueous dialysis and other ICU methods.[6, 24] The removal of such bound solutes has the potential to reduce further liver and kidney damage due to the persistence of higher than normal concentrations of protein bound solutes. Unfortunately, the current BSD methods, MARS and SPAD, were heuristically designed and are poorly characterized. Application of engineering principles to characterize the thermodynamics,

kinetics, and transport phenomena involved in BSD can be used to answer many of the basic questions involved in making BSD an effective treatment approach.

1.1 THE HUMAN LIVER

The liver is the largest human internal organ. The liver accounts for approximately 3.8% of a newborn's body mass and approximately 2% of the body mass of a typical adult.[25] The liver is located toward the right side of the body just under the diaphragm, and is roughly divided into four lobes. The classical description of the division of the lobes, based on the topography of the liver, has been replaced by divisions based on the blood flow through the liver and the ability to surgically resect parts of the liver. The blood flow to the liver is fed by two vessels, the portal vein and the hepatic artery. The portal vein accounts for approximately two thirds of the flow into the liver. The portal vein is fed by the absorptive surfaces of the digestive tract. All ingested and absorbed drugs, nutrients, and toxins therefore pass through the liver before entering the systemic circulation. The hepatic artery accounts for the remaining third of the blood supply to the liver, and provides oxygenated blood the liver. Blood on its way to the systemic circulation leaves the liver via the hepatic vein which joins the inferior vena cava on its way to the heart.[26, 27]

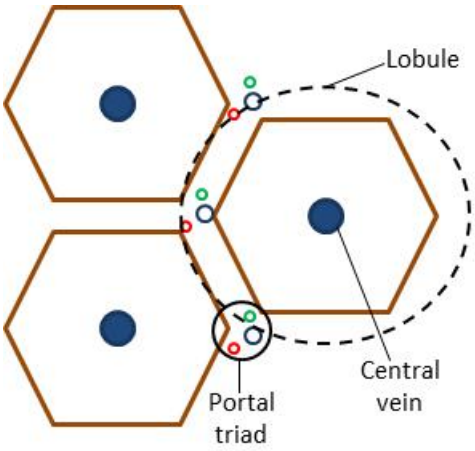

Figure 1.1. Schematic representation of the lobule concept of the histological arrangement of the liver. The lobule concept of the histological arrangement of the liver consists of hexagonal plates of hepatocytes with a central vein at the center of the lobule. Three to six portal triads feed into each lobule.[6, 26-28]

The cellular anatomy (histological organization) of the liver is arranged into regular functional subunits. The architecture of the liver's subunits are described as either lobules or acini. A lobule is a hexagonal construct with a portal triad (a bile duct, a branch of the hepatic artery, and a branch of the portal vein) at three to six of its corners and a central vein at its center (Figure 1.1). The central vein is a branch of one of the hepatic veins. Blood vessels running through the portal tract connect the portal triads at either end of the portal tract to each other, and the blood vessels in the portal tract branch into sinusoids lined with hepatocytes as the blood flows to the central vein. About 70% of a hepatocyte's surface faces the sinusoids and about 15% face bile canaliculi (branches of the bile duct). While this description based on the lobule structure has the central vein at the center of each subunit, the acinus view has the portal triad at the center of a roughly circular complex acinus with three central veins around its edges (Figure 1.2).[6, 26-28]

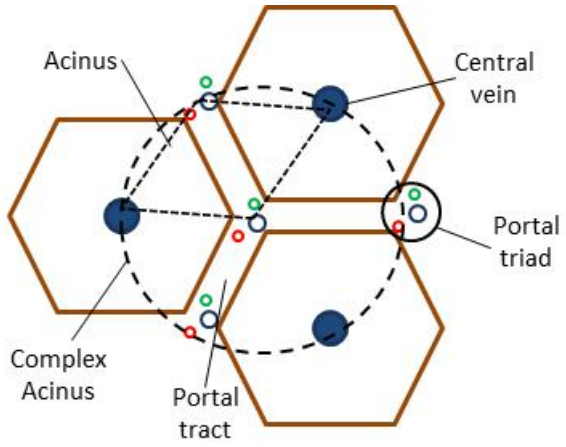

Figure 1.2. Schematic representation of the acinus concept of the histological arrangement of the liver. The acinus concept of the histological arrangement of the liver consists of two portal triads and the portal tract that runs between them at the center and a central vein at the ends (dotted rhombus). Blood vessels run between the portal triads, and blood flows through the hepatocytes as the blood flows between the portal tract on the way to the central vein. A complex acinus consists of three adjacent acini (dotted circle).[6, 26-28]

The liver is connected to the digestive tract by the bile canaliculi and bile ducts. Bile is a solution of metabolic wastes and cholesterol derived salts called bile acids (or bile salts). Bile produced by the hepatocytes flows into the bile canaliculi, into the bile ducts, and is either fed into the intestinal lumen or stored in the gallbladder. The main function of bile (other than as metabolic waste) is to buffer the mixture of partially digested food and digestive fluids (chyme) as it leaves the stomach and to facilitate the action of digestive enzymes.[26-28]

The metabolic and synthetic functions of the liver are numerous. The liver performs first pass (and subsequent) metabolism on all drugs and nutrients from the portal drainage of the digestive tract before they become accessible to the rest of the body. Many endogenous metabolites and waste products as well as exogenous compounds are modified and removed by the liver, particularly compounds that are poorly soluble and not removed by the kidneys. The metabolism and removal of compounds by the liver frequently involves the action of low

specificity enzymes to chemically modify the compounds to make them more polar through the addition of charged groups. Making a molecule more polar has the effect of making it more soluble in water and also makes it more difficult for the molecule to cross the hydrophobic membranes of cells. Although the chemical modification of compound by the liver is meant to detoxify and make compounds more easily removable from the circulation, it also has the potential to produce toxic metabolites. Acetaminophen (also called N-acetyl-para-aminophenol (APAP), Tylenol®, or paracetamol) is a common analgesic that is sold in the United States as a pain killer and is also found in many drug formulations including over the counter cold remedies and the prescription narcotics Percocet® and Vicodin®. Most of the acetaminophen that is ingested by an individual will be metabolized by the glucuronidation pathway producing glucuronic acid. Small amounts of acetaminophen are metabolized by cytochrome P-450s to produce N-acetyl-p-benzoquinone imine (NAPQI). Most of the NAPQI that is produced is then conjugated with glutathione, but once glutathione is depleted the remainder reacts with proteins and nucleic acids causing liver cell death. In cases of extreme overdoses, if the person taking the drug has a glutathione deficiency, such as happens with alcoholics, or if the drug is taken concurrently with alcohol, NAPQI will be produced in larger amounts and cannot be removed. NAPQI persisting in high concentrations causes a large amount of liver cell death, and the high degree of liver cell death can lead ultimately to acute liver failure. Acetaminophen overdosing is the leading cause of acute liver failure in the US accounting for nearly 50% of all ALF cases.[29, 30]

The liver has many functions in addition to the metabolism of endogenous and exogenous compounds. The conversion of glucose to glycogen and back again is performed by the liver. The production of a number of serum proteins is performed by the liver, including clotting

factors and serum albumin. Although this is hardly an all-inclusive list, it highlights the varied functions of the liver.[6, 26-28]

1.2 LIVER FAILURE

Liver failure is characterized by the inability of the liver to perform normal metabolic and synthetic functions at a level that is necessary to sustain life. Liver failure can be the result of either an acute insult such as poisoning or drug overdose (termed fulminant or acute liver failure (ALF), and defined as sudden onset of liver failure of less than eight weeks post insult with no prior history of liver disease) or the end result of an underlying disease state such as hepatitis C (HepC) or alcoholism (acute-on-chronic liver failure (ACLF), long term history of liver disease). Liver failure is often broken down to further define the etiology (fatty liver disease, viral hepatitis, alcoholic or nonalcoholic cirrhosis, and acute drug intoxication, for example). Despite the range of causal factors associated with liver failure, the presentation of liver failure follows a fairly well defined progression (including elevated blood bilirubin and bile acid concentrations, renal dysfunction, and hepatic encephalopathy).[6, 26-28, 31-33]

1.3 LIVER TRANSPLANTATION

Better critical care management methods for ALF and ACLF patients have improved patient survival rates without transplantation (100% mortality 50 years ago compared to 40-60% mortality now depending on etiology). In many cases standard medical therapy is not sufficient

for patients to recover, and the patients require liver transplantation.[34-37] The first human liver transplantations were performed in 1963 and early 1964 on seven critically ill patients (five by Starzl at the University of Colorado, one in Boston, and one in Paris). None of the seven lived more than three months. The transplantation by Starzl in July 1967 was the first one year survival of a liver graft recipient. Liver transplantation was considered experimental until the introduction of the immunosuppressant drug cyclosporine A (FDA approved in 1983), leading to a 5 year survival exceeding 50%. The approval of the immunosuppressant drug tacrolimus (also known as FK506) (Astellas Pharma, Inc., Tokyo, Japan) in 1994 along with improved organ preservation techniques has led to a current one-year survival rate for liver transplantation of 85-90% (depending on the underlying etiology).[33, 34, 38]

Regardless of the improvements that have been achieved in recipient survival, many patients still die waiting for liver transplantation. Many patients in need of transplantation never receive a liver owing to the lack of livers available for transplantation. Of those patients that do receive a liver, about 8% require re-transplantation.[33] Most transplantation is done using whole or partial (referred to as split liver transplantation) deceased donor (cadaveric) livers. The allocation of cadaveric livers that are obtained for transplantation is performed by the United Network for Organ Sharing (UNOS).[33] Patients that are most in need of liver transplantation surgery are prioritized using the Model for End-Stage Liver Disease (MELD). The MELD is a prognostic scoring method that has been shown to predict the survival of patients in liver failure. The prognostic scoring method prioritizes the allocation of livers to patients that are most likely to die without transplantation, rather than the patients that have been on the waiting list for liver transplantation the longest. UNOS uses MELD scoring to prioritize liver transplantation for

patients older than 12 years of age and the Pediatric End-Stage Liver Disease (PELD) scoring for patients 11 and younger.

Living donor liver transplantation (LDLT) is when part of a living donor's liver is given to the recipient. Given the liver's ability to regenerate, a significant portion of the donor's liver can be removed without permanent detriment to the donor. LDLT is an especially important option for small pediatric patients and patients that have been ruled out as candidates for liver transplantation for one reason or another based on the current deceased donor liver allocation system. Although patient survival is better with LDLT than with cadaveric liver transplantation, the LDLT procedure creates risk to both donor and recipient, and both require support post-transplant.[34, 39]

1.4 ARTIFICIAL LIVER SUPPORT

The lack of an alternative to liver transplantation and supportive care for the treatment of liver failure has argued for the development of new therapies to bridge liver failure patients to either recovery or transplantation and to support patients post transplantation. Extracorporeal liver support systems have been introduced as alternatives to standard medical therapy. Several bio- and mechanical artificial liver support systems have undergone preclinical and clinical evaluation with varying levels of success. Extracorporeal liver support systems can be lumped into two categories: those that contain cells (bioartificial liver support system, BLSS) and those that do not (artificial liver support system, ALSS).

1.4.1 Bioartificial Liver Support Systems

Bioartificial liver support systems (BLSSs) have the potential to provide metabolic and synthetic support that standard medical therapy alone cannot provide. In a BLSS, liver cells are cultured in a bioreactor, called a bioartificial liver (BAL). As the patient's blood or plasma flows through the BAL in an extracorporeal circuit, the cells contained in the bioreactor perform some portion of their normal (or possibly altered and abnormal) metabolic and synthetic processes on the patient's blood. Several BLSS configurations have undergone some degree of preclinical and clinical evaluation, but a number of hurdles have prevented cell-based therapy from gaining widespread acceptance (including cell source, seeding or encapsulation matrix and method, and oxygenation method). Although proof of principal has been shown by these trials, no BLSS device has been approved for use by the FDA.[3, 5-9, 14, 15, 40]

1.4.2 Non-biological Artificial Liver Support System

Non-biological artificial liver support systems (ALSS) have the potential to provide non-metabolic, non-synthetic, support to the patient at a substantially lower risk and cost than current BLSS.[7, 14, 15, 20] Systems have been developed that use solid state binders such as activated carbon or exchange resins (ionic, neutral, or both), but most research to date has focused on albumin dialysis systems. Both albumin dialysis and solid state sorption can be termed bound solute dialysis (BSD). BSD is the use of a high affinity binder on the sweep fluid side of a dialysis system to increase the rate of removal of albumin bound solutes from the patient's blood. The basic medical hypothesis underlying the use of BSD systems is that the removal of albumin bound solutes that are normally metabolized and removed by the liver will mitigate further liver

and other organ damage from toxins and metabolites persisting in higher than safe concentrations.[6, 24]

1.4.3 Bound solute dialysis systems using solid state adsorbents

BSD systems utilizing solid state adsorbents have been developed using activated carbon, synthetic and natural resins, combinations of carbon and resin adsorbents, combinations of soluble adsorbents (albumin dialysis) and solid state adsorbents (e.g. MARS), and combinations of bioreactors and solid state adsorbents.

Ash *et al* have developed systems based on sorption suspension dialysis. The HemoCleanse – DT (also referred to as Biologic-DT, Liver Dialysis Unit or the Unit, HemoCleanse, Lafayette, Indiana, USA) and the HemoCleanse – DTPF use finely divided activated carbon as the binding agent. The patient's blood passes on one side of a semipermeable dialysis membrane while dialysate containing finely divided activated carbon flows through the other side of the dialysis membrane (Figure 1.3). Conflicting reports exist as to whether the carbon containing dialysate stream is recirculated or is single pass through the dialyzer.[3, 6, 10, 11, 14]

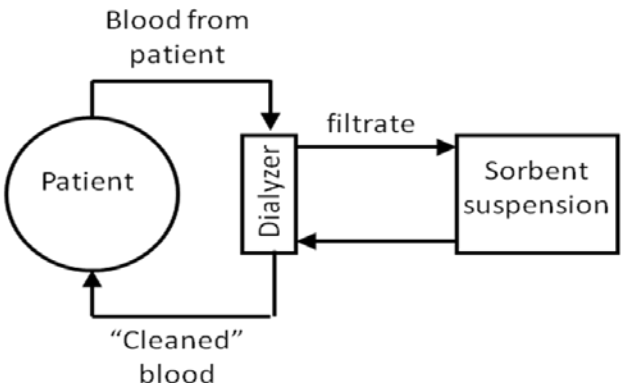

Figure 1.3. Schematic of the HemoCleanse-DT (also called The Unit for liver detoxification or Biologic DT). The patient's blood flows across one side of a flat plate dialyzer and a suspension of finely divided charcoal adsorbent is circulated on the other side of the dialyzer.[10, 11]

The Prometheus system (Fresenius Medical Care, Bad Homburg, Germany) passes the patient's blood through a plasma filter, and the plasma stream is run over two adsorbent columns (containing neutral resin and an anion exchanger) (Figure 1.4). After passing through the two adsorption columns, the plasma is recombined with the patient's blood in the extracorporeal circuit, and the patient's blood is sent through a conventional aqueous dialyzer. The Prometheus system has not been well evaluated in clinical trials.[12, 13, 41, 42]

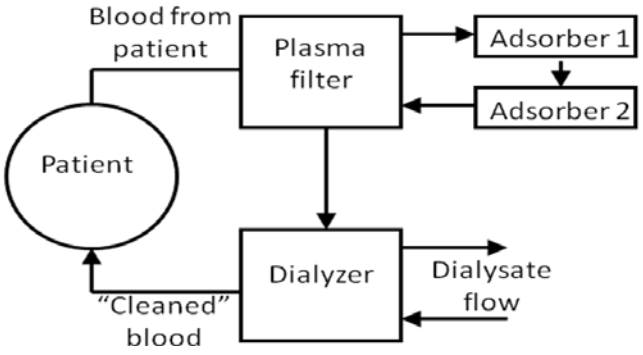

Figure 1.4. Schematic of the Prometheus system. The original design (fractionated plasma separation and adsorption (FPSA)) had the dialyzer in the secondary loop after the two adsorption columns.[41]

2.0 ALBUMIN DIALYSIS

Albumin dialysis uses an albumin solution on the sweep fluid side of a dialysis system as a sink for toxins and metabolites that will bind to albumin and that are refractory to removal by conventional dialysis. The basic medical hypothesis underlying the use of albumin dialysis systems (and all BSD systems) is that the removal of protein bound solutes normally metabolized and removed by the liver and that cannot be removed by conventional detoxification methods has the potential to reduce further liver and kidney damage from protein bound solutes persisting at higher than normal concentrations. Current approaches to albumin dialysis (the molecular adsorbent re-circulating system (MARS) and single pass albumin dialysis (SPAD)) have not been well characterized. Application of engineering principles to characterize the thermodynamics, kinetics, and transport phenomena involved in albumin dialysis can be used to answer many of the basic questions involved in making albumin dialysis an effective treatment option.

2.1 THERMODYNAMICS OF BOUND SOLUTE DIALYSIS

Solute molecules, *S*, complex with a site on the binder (albumin), *A*, to form a binder-solute complex according to the reaction

$$S + A \underset{k_d}{\overset{k_a}{\rightleftharpoons}} S \bullet A \qquad \textbf{Equation 2.1}$$

k_a (L mol^{-1} s^{-1}) and k_d (s^{-1}) are the rate constants for solute-binder complex formation and for the dissociation of the complex, respectively. The equilibrium affinity binding constant is given by

$$K_B = \frac{k_a}{k_d} = \frac{C_{S \bullet A,eq}}{C_{S,eq} C_{A,eq}} \qquad \textbf{Equation 2.2}$$

K_B (L mol^{-1}) is the equilibrium binding constant, and $C_{i,eq}$ (mol L^{-1}) is the concentration of species *i* when the system is at equilibrium. Although the reactions are presented here as 1:1 binding, that is not necessarily the case. Albumin has more than one binding site (of varying affinity) for many molecules. Albumin can also bind several different molecules at various sites at the same time.[43] Many chemical species that are typically removed or metabolized by the liver have an extremely high affinity binding constant with albumin, making them refractory to removal by conventional dialysis. The albumin affinity binding constants for several compounds that are of interest in the modeling or treatment of liver failure or in the *in vitro* testing of artificial liver support systems are presented in Table 2.1. Compounds with affinity binding

constants greater than K_B = 10^3 L mol^{-1} are considered refractory to conventional aqueous dialysis.[18, 19, 44]

Table 2.1. Human albumin-solute affinity binding constants.[43, 45]

	Binding constant, K_B (L mol^{-1})	
Solute	Primary Site	Secondary Site
Bilirubin	1.5 - 9.5 x 10^7	0.3 - 1.01 x 10^7
Bile Acids		
Lithocholate	20.0 x 10^4	
Chenodeoxycholate	5.5 x 10^4	
Deoxycholate	4 x 10^4	
Copper (II)	1.5 x 10^{16}	
Long-chain fatty acids	~1-70 x 10^7	
Exogenous Compounds and Drugs		
Salicylate	1.9 x 10^5	
Warfarin	3.3 x 10^5	
Digitoxin	0.4 x 10^5	
Phenol Red	2.8 x 10^4	
Ibuprofen	2.7 x 10^6	

A dialysis cartridge consists of a bundle of semipermeable fibers encased in a hollow tube (shell) (Figure 2.1). The fibers are potted into place at either end with impermeable glue. A distribution cap at the blood inlet divides the blood flow between the fibers, and a cap at the outlet collects the blood flow from the fiber bundle. The blood flow is then returned to the patient. In conventional aqueous dialysis, blood flows on one side of a semipermeable membrane while dialysate solution (a buffered crystalloid solution that contains concentrations of salts and glucose similar to the plasma of a healthy patient) flows on the other side of the membrane countercurrent to the blood. Solutes that are at a higher concentration on one side of the membrane than the other, and that are smaller than the molecular weight cutoff of the dialysis

membrane, will diffuse down their concentration gradient into the other solution. The concentrations in the dialysate solution are typically set to retain physiological levels of salt, and remove excess salts, urea, and creatinine (compounds normally removed by the kidneys). In some cases a transmembrane pressure gradient is maintained to remove water by ultrafiltration. The albumin molecule and albumin-solute complexes in a patient's blood are too large to pass through a typical dialysis membrane regardless of whether transport occurs by convection or diffusion.

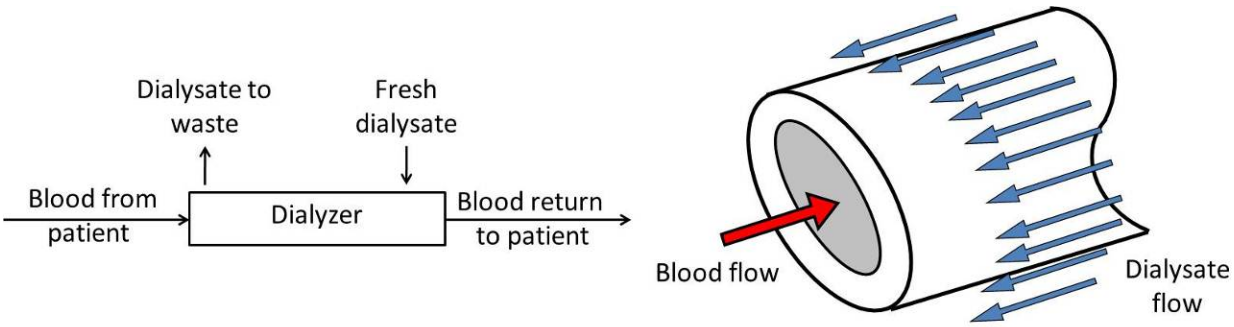

Figure 2.1. Schematic of a hollow fiber renal dialysis cartridge. Blood enters a manifold that divides the flow into the inner lumen of the many hollow fibers encased in the dialyzer. Fresh dialysate enters the shell space of the dialyzer and flows around the outside of the fibers countercurrent to the blood flow. Molecules that are smaller than the pore size of the fibers will diffuse down their concentration gradients from one stream to the other. Bulk fluid transport (ultrafiltration) can occur by maintaining a pressure gradient across the fiber wall.

Unbound solutes that are smaller than the molecular weight cutoff of the dialysis membrane can be removed by aqueous dialysis. The difference in free solute concentration across the dialysis membrane provides the driving force for diffusion, but the free concentration of tightly bound solutes is so small that the removal rate is too slow to be effective for the

removal of solutes of concern in the treatment of liver failure.[18, 19, 44] Additionally, the driving force (the free solute concentration difference) is further reduced once a small amount of the solute has passed across the membrane. The equilibrium free concentration of a solute can be calculated from the total concentrations of the solute and the binder and the binding constant for the binder solute complex. The total concentration of the solute and binder are related to the free concentration of binder and solute and the concentration of the complex by mass balance.

$$C_{S,total} = C_S + C_{S\bullet A} \qquad \textbf{Equation 2.3}$$

$$C_{A,total} = C_A + C_{S\bullet A} \qquad \textbf{Equation 2.4}$$

The concentrations of unbound solute can be calculated by combining Equation 2.2, Equation2.3, and Equation 2.4.

$$K_B C_S^2 + (1 + K_B C_{A,total} - K_B C_{S,total}) C_S - C_{S,total} = 0 \qquad \textbf{Equation 2.5}$$

Since only one solution for this quadratic equation makes physical sense Equation 2.5 can be solved analytically for the free solute concentration, C_S.

$$C_S = \frac{1}{2K_B}\left[K_B(C_{S,total} - C_{A,total}) - 1 + \sqrt{\left[1 + K_B(C_{A,total} - C_{S,total})\right]^2 + 4K_B C_{S,total}} \right] \qquad \textbf{Equation 2.6}$$

At concentrations of albumin and bilirubin typical for liver failure, $C_{A,total}$=0.6x10^{-3} mol L^{-1} and $C_{S,total}$=0.3x10^{-3} mol L^{-1}, respectively, the free concentration of bilirubin (K_B ~10^7 L mol^{-1}) is

C_S=0.2x10^{-6} mol L^{-1} (three orders of magnitude lower than the total concentration).[44] Minimizing the free solute concentration on the dialysate side of the membrane maximizes the concentration gradient, thereby maximizing the rate of solute removal from the patient. Reducing the dialysate side free solute concentration can be accomplished by either increasing the flow rate of the dialysate stream, or by introducing a binder such as albumin to the dialysate side of the membrane. With a molecule that is as tightly albumin bound as bilirubin, little additional benefit to the rate of solute flux is achieved once a blood to dialysate albumin concentration ratio of as little as $(C_{A,total})_D/(C_{A,total})_B$ = 0.04 ($(C_{A,total})_D$ and $(C_{A,total})_B$ are the patient's blood and the dialysate albumin concentrations respectively). Significantly higher albumin concentrations are required to reach the theoretical maximum removal rate for less tightly bound molecules. The increase in removal rate (the impact of adding albumin to the dialysate) is greater for more tightly albumin bound molecules than for less tightly albumin bound molecules.[18, 19, 44]

2.2 THE MOLECULAR ADSORBENT RECIRCULATING SYSTEM (MARS)

The Molecular Adsorbent Recirculating System (MARS) (Figure 2.2) is the ALSS that has received the most attention from researchers and clinicians, including many publications on clinical trials and case studies, in vitro tests, review articles, and theoretical analyses. MARS is a closed loop hybrid albumin dialysis/solid state adsorbent system. The patient's blood is perfused through a proprietary dialyzer countercurrent to a recirculating stream of albumin containing dialysate solution. The MARS dialyzer has a polysulfone membrane with a sieving coefficient of <1% for albumin.[46] The dialysis cartridge is pre-primed with 10% (1% is equivalent to 1 g

dL^{-1} or 10 g L^{-1}) human albumin for 1 hour prior to use. A passivation step with albumin to reduce thrombosis is not unusual with extracorporeal circuits, but in the case of MARS the pretreatment is meant to impregnate the dialysis membrane with albumin, not to passivate the surfaces in the circuit. Solutes that are smaller than the molecular weight cutoff of the membrane transit out of the patient's blood, through the dialyzer membrane, and enter the recirculating albumin containing dialysate stream. The albumin concentration in the recirculating dialysate stream varies in the literature from 5% to 20%. The dialysate stream then passes through an aqueous dialyzer and two adsorption columns that are meant to "regenerate" the albumin stream by removing solutes that were stripped from the blood.

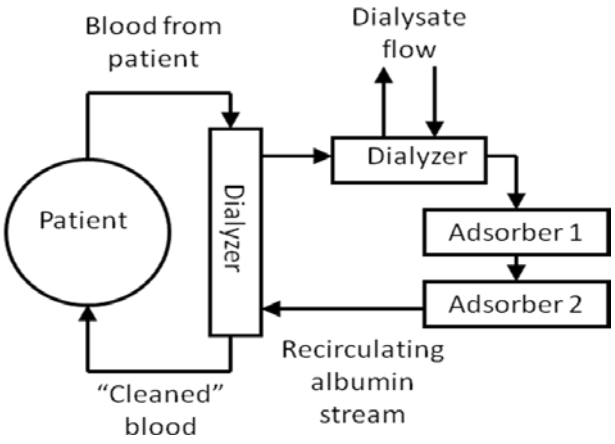

Figure 2.2. Schematic of the Molecular Adsorbent Recirculating System (MARS). The patient's blood passes on one side of a proprietary dialyzer that is impermeable to albumin, and the "cleaned" blood is then returned to the patient. Solutes (both albumin bound and water soluble) transit the dialyzer membrane to a recirculating albumin enriched dialysate stream. The albumin solution then passes through an aqueous dialyzer and two adsorption columns to remove the solutes that were picked up from the patient's blood.[41]

Many case studies, small randomized clinical trials, numerous review articles, and several *in vitro* experiments with the MARS system have been published. Some of the trials and case

studies using MARS reported reductions of biochemical markers such as blood concentrations of bilirubin and creatinine and improvement in hepatic encephalopathy.

One of the earliest studies with MARS randomly assigned 13 patients with hepatorenal syndrome (HRS) to receive either MARS (n=8) or standard medical therapy (SMT) (n=5). A significant improvement in survival was observed (37.5% vs. 0% after 7 days of treatment for MARS and SMT respectively). MARS therapy also resulted in reductions to biochemical markers (including improvements in serum bilirubin and creatinine levels for MARS but not SMT), and increases in mean arterial pressure (MAP) where the control group had a further decrease in MAP over the study period.[47] A later larger randomized study comparing MARS (n=9) versus SMT (n=9) showed no difference in 7 day survival (45% in both groups) or MAP, but significant improvements in encephalopathy grade were seen with MARS but not SMT.

Recent comparisons between patients treated with only standard ICU methods and patients treated with the MARS system as well as conventional care showed a significant improvement in the quality of life adjusted cost effectiveness (a measure of the expense required to improve the quality of life of a patient) of the ICU care of liver failure patients when MARS therapy was used.[48] Despite these seemingly positive results, MARS has not been shown to improve patient survival, and has not been shown to be any more effective than SPAD.

2.3 SINGLE PASS ALBUMIN DIALYSIS (SPAD)

Single pass albumin dialysis (SPAD) uses conventional hemodialysis or hemodiafiltration equipment with albumin added to the dialysate solution. With the exception of the albumin

added to the dialysate stream, SPAD does not require any special equipment or disposables over what is required for conventional renal replacement therapy.

The patient's blood passes countercurrent to an albumin containing dialysate in a conventional hemodialysis filter. With SPAD, the albumin containing dialysate is discarded after it passes through the dialyzer. Continuously supplying fresh dialysate solution maintains maximum diffusion gradients in the dialyzer.

To date little clinical data on SPAD exists, and no randomized controlled prospective studies have been performed using SPAD. A patient with multi-organ failure secondary to acute liver failure and Wilson's disease was successfully bridged to transplant for 59 days using SPAD.[17] During the treatments significant amounts of serum copper and bilirubin were removed (both are tightly albumin bound and not removed well using conventional dialysis methods), an improvement in hepatic encephalopathy (HE) was noted, and kidney function normalized after several days of treatment. Another study looked at using SPAD on three patients with chronic liver failure (one patient with hepatitis B and D, one patient with hepatitis C, and one patient with alcohol induced cirrhosis).[21] All three patients showed improvements in HE and bilirubin levels. Two of the patients were successfully bridged to liver transplantation, and the third patient died from sepsis after 148 days of intermittent SPAD. A third case study describes the use of albumin dialysis to treat a patient with renal insufficiency and intrahepatic cholestasis that developed intractable pruritus.[16] Two sessions of albumin dialysis were run, one using 1.85% HSA in the dialysate and one with 5.0% HSA in the dialysate. The rates of removal of the tightly bound solute bilirubin were comparable for both albumin concentrations. The SPAD treatments were ended after the second treatment since the patient's pruritus showed no improvement.

More recently, a retrospective analysis was performed looking at the efficacy of SPAD compared to MARS.[49] Records of patients treated with SPAD or MARS from July of 2004 to August of 2008 at the university hospital of Friedrich-Schiller University Jena (Jena, Germany) were analyzed to compare the efficacy of the two albumin dialysis methods. MARS was considered by the physicians as their first choice for albumin dialysis therapy. The hospital only had one MARS system, and SPAD was performed if a second patient was to be treated while the MARS device was in use or if the albumin dialysis therapy needed to be started outside of the hospitals regular day shift. In all 57 liver failure patients were treated over the four year span. MARS therapy was performed 126 times and SPAD 37 times. No significant difference in the efficacy or safety between the two devices was noted, but MARS was significantly more expensive. The disposables cost of a single SPAD treatment was approximately €505, and the disposables for a MARS treatment was approximately €2270. In addition to the four fold greater disposables cost, the MARS treatment requires additional equipment and labor costs.

Several *in vitro* tests of SPAD and comparisons of SPAD with MARS have been performed. Awad *et al.* dialyzed recirculating bovine blood spiked with bilirubin against dialysate containing 0, 2%, or 10% albumin with a 0.3 m^2 polysulfone dialyzer.[50] The 2% albumin experiments had a 3.1 fold improvement in the removal rate of bilirubin over no albumin, and 10% albumin in the dialysate resulted in a 4.5 fold improvement in the removal rate of bilirubin over no albumin in the dialysate. The creators of the MARS system performed *in vitro* testing of SPAD and MARS.[51] Their testing showed SPAD to be more effective than MARS for the removal of bilirubin ($K_B = 10^8$ L mol^{-1}) and sulfobromophthalein ($K_B = 10^7$ L mol^{-1}), but MARS more effective at removing the less tightly bound glycocholic acid ($K_B = 10^3$ L mol^{-1}).[43] Sauer *et al.* compared SPAD, MARS, and CVVHDF. SPAD and MARS were both

found superior to CVVHDF at removing several albumin bound compounds, and SPAD was equally effective or superior to the removal capability of MARS.

Patzer *et al.* have published the only mathematical model describing the removal of tightly albumin bound compounds using SPAD.[18, 19, 44] Although albumin was the binder used in the experimental validation of the model, the model is equally applicable to other binders, and was termed more generally as bound solute dialysis (BSD). The model and experimental validation both indicated that dialysate albumin concentrations in excess of 1 g L^{-1} will have a negligible additional impact on the removal rate of tightly albumin bound compounds like bilirubin. This is in contrast to 100-200 g L^{-1} of albumin used in MARS therapy.

3.0 MOTIVATION AND SPECIFIC AIMS OF THIS STUDY

The basic medical hypothesis underlying the use of BSD systems is that removal of solutes that are bound to proteins or other carriers in the blood, primarily albumin, that are normally metabolized and removed by the liver and that cannot be removed by conventional aqueous dialysis and other intensive care unit (ICU) methods will allow the albumin present in blood to perform its normal function (as a carrier of various molecules in the blood). Preventing the buildup of albumin bound substances has the potential to mitigate further liver and kidney damage from albumin bound solutes persisting at higher than normal concentrations. Unfortunately the current BSD methods, MARS and SPAD, were heuristically designed and are poorly characterized. Application of engineering principles to characterize the thermodynamics, kinetics, and transport phenomena involved in BSD can be used to answer many of the basic questions involved in making BSD an effective treatment approach.

Further work is needed to expand on the basic studies of BSD to identify what is necessary to make BSD effective and readily available for any hospital or clinic. The research presented is based on the hypothesis that the nature of the kinetics of binding and unbinding of albumin-solute systems and the interaction of albumin with the dialysis membrane can be harnessed to impact the removal of solutes refractory to aqueous dialysis (including the removal of specific albumin bound solutes and the unwanted stripping of therapeutic drugs). The

research presented is focused on improving the understanding of the use of albumin in ALSS by the following specific aims:

Specific Aim 1 – Analyze the kinetics of association and dissociation of albumin-solute binding pairs of interest in liver failure using Biacore SPR technology. While a significant amount of information in known about the equilibrium binding properties of many albumin-solute pairs, little is known about the reaction kinetics. Biacore SPR can measure the kinetics of association and dissociation of albumin with metabolites that build up in a patient's blood as a result of liver failure (e.g. bile acids) and drugs commonly used after liver transplantation (i.e. the immune suppressants cyclosporine A (CyA) and tacrolimus (FK506)).

Specific Aim 2 – Develop a mathematical description of albumin dialysis taking into account the kinetics of the solute-binder interaction. The equilibrium model developed by Patzer does a good job describing the removal of the tightly albumin bound solute bilirubin from a reservoir, but several phenomena cannot be captured with the simplified reaction scheme used. Most notably, a model that makes use of a more complete description of the binding reactions has the potential to describe what happens when the rates of reaction are on the same time scale as the rate of transport across the dialysis membrane and what happens when there are multiple solutes competing for the same binder. Such questions speak directly to whether the dialysis membranes and binders are appropriate for the removal of specific toxins or drugs, and what might be required to design membranes and binders to target specific solutes.

Specific Aim 3 – Investigate the penetration of albumin into the wall of commercial dialysis fibers by developing small scale slide dialyzers to allow for the direct visualization of the penetration of albumin into the dialysis membrane during use. While a cover slip window could be fit to a conventional dialyzer, it would not be practical to visualize the cartridge under

conditions that would be typical to transplant ICU procedures. The required pumps and fluid reservoirs would be prohibitive in the microscopy facility. Fibers from commercial dialyzers potted into small scale dialyzers designed for use on microscopes reduce space and reagent requirements, while still allowing for realistic flow velocities. The ability of albumin to enter and deposit in the wall of some dialysis membranes during use could for better or worse impact the removal capability of an ALSS. Many blood contacting devices (including MARS) have an albumin priming step prior to use. The formation of a protein layer often reduces the rate of transport, whether by convection or diffusion, of solutes across a dialysis membrane, and albumin penetration and deposition could contribute transport mechanisms in addition to diffusion. Diffusion is typically considered to be the main method of removal in dialysis and albumin dialysis procedures.

Basic studies and mathematical modeling of the properties of albumin dialysis can be used to develop BSD and albumin dialysis into a cost effective treatment for patients in liver failure that provides sufficient support to bridge patients to OLTx or, even better, to recovery of liver function.

4.0 SPECIFIC AIM 1: SURFACE PLASMON RESONANCE MEASUREMENT OF THE BINDING KINETICS OF ALBUMIN WITH BILE ACIDS, BILIRUBIN, AND FK506

Mathematical modeling of albumin dialysis ALSSs indicates that the strength of the interaction between the binder (often albumin in both the patient's blood and in the dialysate) and the solute that is being removed from a patient's blood is a determining factor in the rate of removal of a given solute and the increase in the removal rate over conventional hemodialysis.[44] However, a paucity of information exists on the strength of the interaction between albumin and solutes of interest in the treatment of liver failure (pre or post liver transplantation, e.g. tacrolimus (FK506), bilirubin, N-acetyl-p-benzoquinone imine (NAPQI), bile acids, etc.). Surface plasmon resonance (SPR) biosensor devices (i.e. Biacore AB, Uppsala, Sweden/GE Healthcare Life Sciences Piscataway, NJ) have the potential to provide high throughput analysis of both the kinetics and equilibrium binding constants of solute-albumin interactions.[52] Biacore SPR tracks the association and dissociation of unlabeled reactants in real time, which allows for the determination of reaction rates of association and dissociation and the equilibrium binding constant. Knowledge of the albumin-solute binding reaction rates and the equilibrium binding constant may provide an *a priori* method for determining whether albumin dialysis is likely to increase the observable rate of removal of a given solute over conventional dialysis.

4.1 THEORY

Binder-solute interaction: The reaction of the binder (albumin), *A*, with a given solute, *S*, is typically considered a 1:1 reaction (Equation 2.1). Although a single albumin molecule may bind several different molecules or several of the same molecule at the same time, most albumin-solute interactions at concentrations typically seen physiologically can be considered to follow the simple 1:1 reaction scheme.[52] The equilibrium binding (association) constant for the reaction in Equation 2.1 is

$$K_B = \frac{1}{K_D} = \frac{C_{S\bullet A,eq}}{C_{S,eq}C_{A,eq}} \qquad \textbf{Equation 4.1}$$

K_B (L mol^{-1}) and K_D (mol L^{-1}) are the association and dissociation, respectively, equilibrium constants for the complex, C_i (mol L^{-1}) is the concentration of species *i*, and the subscript *eq* denotes a concentration at equilibrium. The equilibrium constant can be expressed in terms of the association and dissociation reaction rate constants as

$$K_B = \frac{k_a}{k_d} \qquad \textbf{Equation 4.2}$$

Effect of temperature variation on binding properties: The *in vitro* testing of medical devices and the analysis of albumin binding properties is frequently done at temperatures other than physiological (37°C).[19, 52] The difference in temperatures can have a dramatic effect on the strength of binding and kinetics of albumin-solute binding reaction rates.

Albumin-solute binding can be either endothermic (negative heat of reaction) or exothermic (positive heat of reaction). Measurement of the equilibrium binding constant at multiple temperatures is needed to determine trends for a given binding pair. Changes in the equilibrium binding constant as temperature changes typically follow the von't Hoff equation

$$\ln\frac{K_2}{K_1} = \frac{-\Delta H_{rxn}}{R}\left(\frac{1}{T_2} - \frac{1}{T_1}\right) \qquad \textbf{Equation 4.3}$$

K_1 and K_2 (L mol^{-1}) are the equilibrium association binding constants at absolute temperatures T_1 and T_2 (in Kelvin, K), respectively, R (J mol^{-1} K^{-1}) is the ideal gas constant, and ΔH_{rxn} (J mol^{-1}) is the heat of reaction (binding).[53] Changes in the binding reaction rate constants with temperature can typically be found using the Arrhenius equation

$$\ln\frac{k_1}{k_2} = \frac{E_a}{R}\left(\frac{1}{T_2} - \frac{1}{T_1}\right) \qquad \textbf{Equation 4.4}$$

where k_1 and k_2 are the reaction rate constants (either association or dissociation) at temperatures T_1 and T_2, respectively and E_a (J mol^{-1}) is the activation energy.[53-55]

Biacore surface plasmon resonance (SPR): Biacore SPR devices track the interaction of two reactants in real time. Tracking the reaction in real time provides sufficient information to determine both the equilibrium constant and kinetic rate constants. Neither of the reactants needs to be labeled. A Biacore CM5 sensor chip like the one used in these experiments consists of a glass support layer with a 50 nm thick gold layer (Figure 4.1). An approximately 100 nm thick layer of carboxymethyl dextran is covalently attached to the gold surface. One of the

reactants of interest is attached either covalently (as is the case with the measurements presented here) or by another capture method to the dextran surface. The binding partner and buffer flow past the surface of the chip. As the immobilized reactant on the surface and the binding partner flowing past the surface react, there is an increase in the local density at the sensor chip surface. The change in density at the chip surface inside of the flow chamber causes the angle of totally reflected light incident on the back of the chip to change. The change in the angle of totally reflected light, measured in dimensionless relative response units (RU), is tracked as the SPR response.

In the case of our experiments, albumin is immobilized on the sensor chip surface and the reacting partner (solute) flows across the chip's surface. The formation of the albumin-solute complex at the chip's surface results in an increase in the local density and causes a change in the refractive index. The increase of density at the chip surface is tracked as an increase in the SPR response.

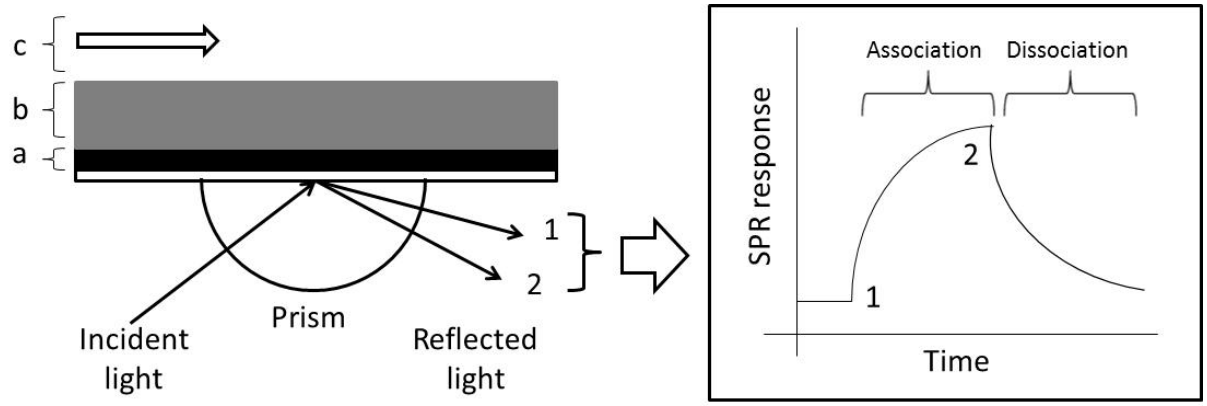

Figure 4.1. A Biacore sensor chip consists of a glass support layer with a 50 nm thick gold layer (a). An ~100 nm thick layer of carboxymethyl dextran (b) is covalently attached to the gold surface. Reactants and buffer flow past the surface of the chip (c). As reactions occur at the chip surface, the angle of reflected light at the back of the chip changes (1 to 2 in the plot on the right).

The equilibrium binding constants can be determined by fitting the equilibrium portion of the response curves to an independent binding site model

$$R_{eq} = \sum_i \frac{K_{B,i} C_j R_{\max,i}}{1 + K_{B,i} C_j}$$ **Equation 4.5**

R_{eq} (RU) is the equilibrium binding response, C_j (mol L^{-1}) is the injection concentration of the solute sample that is flowing across the surface, and R_{max} (RU) is the maximal response possible for the surface when it is saturated with a given solute. For a 1:1 binding interaction i=1, and for multiple independent binding sites i is the number of binding sites for a given solute.[52]

The kinetic rate constants can be determined by fitting the SPR response vs. time curves to the integrated reaction rate equations. The rate equations that result in Equation 4.5, Equation 4.6, Equation 4.7 and are provided in Appendix B. For the association phase the integrated rate equation is

$$R = \frac{k_a C_j R_{\max}}{k_a C_j + k_d} \left(1 - e^{-(k_a C_j + k_d)t}\right)$$ **Equation 4.6**

where t (s) is time, R (RU) is the transient SPR response, and C_j (mol L^{-1}) is the injection concentration of the solute. The integrated rate equation for the dissociation phase is

$$R = R_0 e^{-k_d (t - t_0)}$$ **Equation 4.7**

where R_0 (RU) and t_0 (s) are the SPR response and time, respectively, at the start of the dissociation phase.[56]

4.2 METHODS

Surface plasmon resonance analysis was performed under contract by the University of Utah's Center for Biomolecular Interaction Analysis (Director Dr. D.G. Myszka) using a Biacore S51 (Biacore AB, Uppsala, Sweden/GE Healthcare Life Sciences Piscataway, NJ). Research grade CM5 sensor chips and amine coupling reagents were obtained from GE Healthcare Life Sciences (Piscataway, NJ). Research grade DMSO, cholic acid, deoxycholic acid, glycocholic acid, bilirubin, FK506, cyclosporine A, and bovine albumin (BSA) were obtained from Sigma-Aldrich (St. Louis, MO). Medical grade 25% human albumin (HSA) solution was from Baxter Healthcare Corporation (Westlake Village, CA).

Biosensor analysis: The Biacore S51 device used has hydrodynamically addressing flow cells that, by changing the relative flow rates of the two inlets, allow two different reaction surfaces and a reference surface to be located in the same flow cell (Figure 4.2).

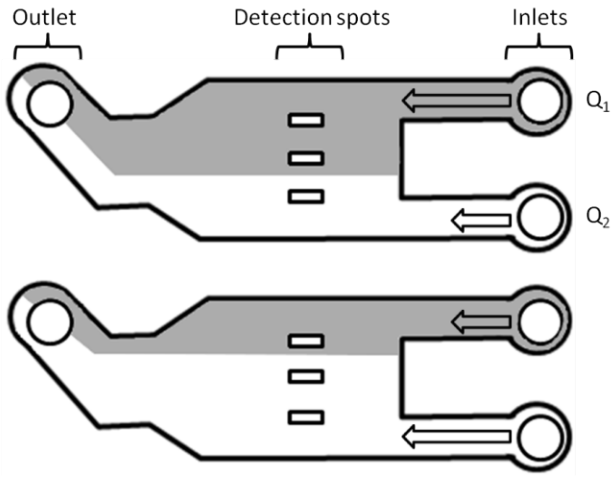

Figure 4.2. The hydrodynamically addressing flow cells in the Biacore S51 device allow separate ligands to be isolated on the two outside detection spots by controlling the flow rates of the two inlets. The center detection spot is left as a reference surface.[57]

Approximately 10,000 relative response units (RU) of BSA and HSA were immobilized on two of the three spots of flow cell one on a CM5 sensor chip using standard amine coupling chemistry, and the third detection spot was left as a reference for nonspecific binding.[58] The dextran surface of the sensor chip was functionalized using a 1:1 mixture of 0.1 mol L^{-1} 1-Ethyl-3-(3-dimethylaminopropyl) carbodiimide hydrochloride (EDC) and 0.1 mol L^{-1} N-Hydroxysuccinimide (NHS). The functionalized surface was then incubated with the albumin being immobilized on the surface at a concentration of 30 μg mL^{-1} in sodium acetate (pH=5.2). Any remaining reactive amine groups on the dextran surface were then blocked with 1 mmol L^{-1} ethanolamine (pH=8.0). All three detection spots used in the experiments were functionalized and blocked, but no protein was isolated on detection spot 3. Detection spot 1 and detection spot 2 had 10,300 RU of BSA and 9,980 RU of HSA, respectively, immobilized on the dextran surface. The third detection spot was used as a reference for nonspecific solute binding. Phosphate buffered saline (PBS, 53 mmol L^{-1} Na_2HPO_4, 12.5 mmol L^{-1} KH_2PO_4, 70 mmol L^{-1}M

NaCl, pH 7.4) was used for preparing solute samples and for performing the binding experiments. PBS used for binding experiments and preparing solute samples was supplemented with 3% DMSO. Binding experiments for glycocholic acid, cholic acid, and deoxycholic acid acids were conducted at 300 μmol L^{-1} and nine 2-fold serial dilutions. Less soluble compounds (CyA, bilirubin and FK506) were studied at 30 μmol L^{-1} and nine 2-fold serial dilutions. All compounds were tested on HSA and BSA surfaces at 22°C and 37°C. Each dilution was run at each temperature one time across each surface. Binding curve data analysis and curve fitting were performed using the SCRUBBER-2 software package developed by the Center for Biomolecular Interaction Analysis. The SCRUBBER-2 software uses a nonlinear least squares fitting method for curve fitting, but the specific numerical methods used for curve fitting and determining error bound for the results are proprietary.

4.3 RESULTS

Response versus time curves were obtained for all compounds except CyA. CyA was insoluble in 3% DMSO solutions, and displayed unusually large responses (>1000 RU) that were indicative of aggregates of CyA binding to the surface. SCRUBBER-2 software algorithms were used to zero, align, subtract the reference flow cell response, and correct the data for changes in the refractive index caused by the density change resulting from dissolving the solutes in DMSO solutions. As the solute flows across the sensor surface an increase in the response signal is seen as solute is bound by the immobilized albumin at the sensor chip surface (Figure 4.3). After the sample injection ends (at 30 seconds in these experiments) buffer (without the solute) flowing

across the sensor chip surface removes solute molecules from the reaction site as the solute-albumin complex dissociates.

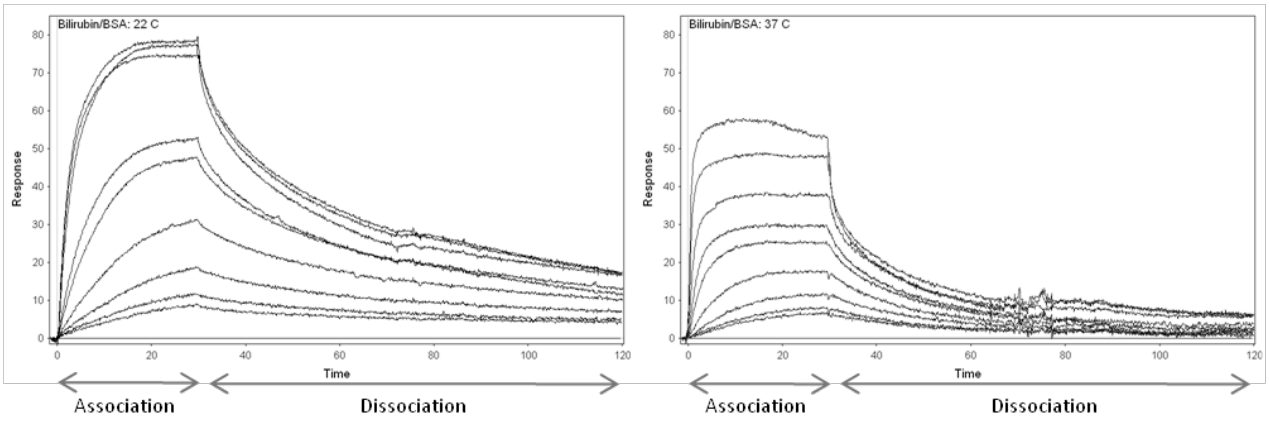

Figure 4.3. As buffer containing the solute (in this case bilirubin) flows across the sensor chip surface, there is an increase in the SPR response as solute molecules are bound by the immobilized albumin at the sensor chip surface (association phase). After the sample injection ends (at 30 seconds in these experiments) the SPR signal decreases as buffer flowing across the sensor chip surface removes solute molecules as the solute-albumin complex dissociates (dissociation phase).

Equilibrium binding constants: The equilibrium portions of the response versus time curves (last 3-5 seconds of the association phase) were plotted as a function of solute injection concentration and fitted using the non-linear least squares fitting routine built into SCRUBBER-2 with either a one (bilirubin and FK506) or two (cholic acid, deoxycholic acid, and glycocholic acid) independent site model (Equation 4.5, Figure 4.4). The calculated equilibrium association binding constants (K_B) for each interaction are reported in Table 4.1 together with previously reported literature values for comparison. With the exception of bilirubin, the reported binding constants are similar to (within an order of magnitude) those found using other more conventional methods. The binding constants for bilirubin varied from reported values by 1 to 2

orders of magnitude. The binding constants decreased with a temperature increase from 22°C to 37°C with the exception of FK506, which showed a greater than ten-fold enhancement of the binding strength with increased temperature.

Table 4.1. Equilibrium binding constants (K_B, L mol^{-1}) for albumin/small molecule binding reactions obtained by fitting the equilibrium portion of SPR response curves for a binding pair at a given temperature to Equation 4.5. K_{B1}, K_{B2}, and the R_{max} values (K_{B1} and K_{B2} have separate R_{max} values associated with them) were the adjustable parameters in the curve fits. Detailed results with standard errors and R_{max} values can be found in Appendix B.[43, 45, 59-61]

		BSA		HSA		Previously reported values			
		K_{B1}	K_{B2}	K_{B1}	K_{B2}	K_{B1}	K_{B2}	Albumin type	Temp.
Bilirubin	22°C	1.03×10^{6}	---	1.15×10^{6}	---	1.5×10^{7}	1.0×10^{6}	Human	---
	37°C	8.40×10^{5}	---	4.81×10^{5}	---	9.5×10^{7}	3×10^{6}	Human	37°C
FK506	22°C	1.04×10^{3}	---	1.37×10^{3}	---	$1.5\text{-}2.5\times10^{3}$	---	Human	22°C
	37°C	1.33×10^{4}	---	6.33×10^{3}	---	---	---	---	---
Colic acid	22°C	8.77×10^{4}	5.95×10^{3}	2.38×10^{4}	3.57×10^{3}	6.8×10^{4}	2.8×10^{2}	Bovine	20°C
	37°C	5.24×10^{4}	2.70×10^{3}	1.56×10^{4}	1.99×10^{3}	3.3×10^{3}	3×10^{2}	Human	37°C
Deoxycholic acid	22°C	1.45×10^{5}	3.03×10^{3}	8.62×10^{4}	1.82×10^{3}	2.0×10^{5}	3×10^{3}	Bovine	20°C
	37°C	1.35×10^{5}	3.13×10^{3}	5.29×10^{4}	1.56×10^{3}	4.0×10^{4}	7×10^{2}	Human	37°C
Glycocholic acid	22°C	2.44×10^{4}	2.86×10^{3}	2.70×10^{6}	2.16×10^{3}	---	---	---	---
	37°C	1.67×10^{4}	1.61×10^{3}	2.00×10^{4}	1.41×10^{3}	2.6×10^{3}	4×10^{2}	Human	37°C

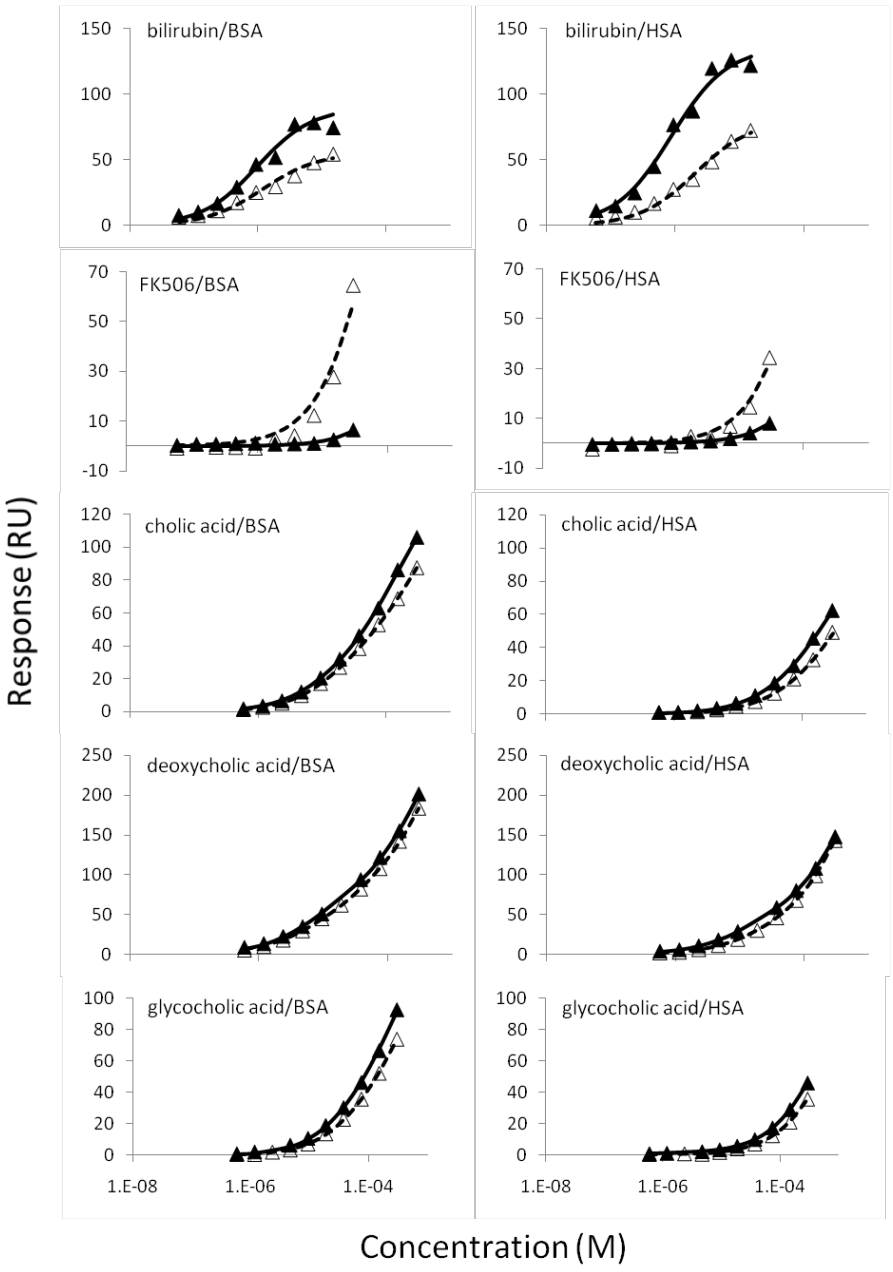

Figure 4.4. The equilibrium binding response (points) is plotted versus concentration and curve fit (lines) with a one (bilirubin and FK506) or two (colic, deoxycholic, and glycocholic acids) independent site model (Equation 4.5). With the exception of FK506, a higher affinity was seen at room temperature (22°C, solid triangles, and solid fit line) than at a more physiological temperature (37°C, open triangles and dashed fit line). FK506 displayed a 10 fold higher affinity at the higher temperature. Note that the y-axis scales are the same for each solute species, but differ from solute to solute.

Binding rate constants: While only the equilibrium portion of the response curves were used to calculate the equilibrium binding constants, the entire data set for each solute/albumin pair at a given temperature was used to calculate the kinetic rate constants. The response versus time curves were globally fit to the rate equations (Equation 4.6 and Equation 4.7) using the nonlinear least squares fitting routine built into SCRUBBER-2 (Figure 4.5).[62] The rate constants (k_a and k_d) and the R_{max} values were the adjustable parameters in the curve fit. The rate constants for binding and unbinding (k_a and k_d respectively) for each interaction are presented in Table 4.2.

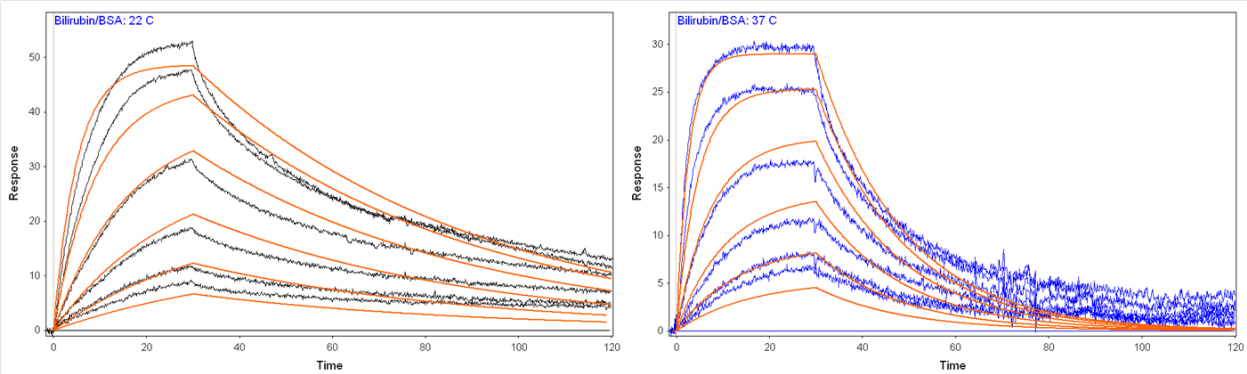

Figure 4.5. The SPR response curves (jagged curves) were fit to the rate equations (smooth lines, Equation 4.6 and Equation 4.7) using the non-linear least squares fitting methods built into SCRUBBER-2. The association (k_a) and dissociation (k_d) rates and maximal response (R_{max}) were the adjustable parameters in the fit. These are the same SPR curves presented in Figure 4.3 with the high concentration curves removed to restrict the binding reaction to the higher affinity binding site.

Table 4.2. Association reaction rate constants, dissociation reaction rate constants, and equilibrium binding constants for albumin/small molecule binding reactions obtained by globally fitting SPR response curves for a binding pair at a given temperature to Equation4.6 and Equation 4.7. R_{max}, k_a, and k_d were the adjustable parameters in the curve fits. The number in parentheses is the error associated with the last significant digit.

		BSA			HSA		
		k_a (L mol^{-1} s^{-1})	k_d (s^{-1})	k_a/k_d (L mol^{-1})	k_a (L mol^{-1} s^{-1})	k_d (s^{-1})	k_a/k_d (L mol^{-1})
Bilirubin	22°C	1.010(6)x10^5	0.0175(2)	5.8x10^5	6.55(5)x10^4	0.0282(3)	2.3x10^6
	37°C	1.70(2)x10^5	0.0535(8)	3.2x10^6	1.60(4)x10^5	0.128(3)	1.3x10^6
FK506	22°C	94.4(6)	0.0100(1)	9.4x10^3	----------	----------	----------
	37°C	9.3(2)x10^3	0.81(1)	1.2x10^5	6.0(5)x10^3	0.60(1)	1.0x10^4
Colic acid	22°C	1.09(3)x10^5	2.33(6)	4.7x10^4	7.2(3)x10^4	4.5(2)	1.6x10^4
	37°C	1.10(4)x10^5	3.2(1)	3.4x10^4	8.7(7)x10^4	6.4(5)	1.4x10^4
Deoxycholic acid	22°C	1.35(1)x10^5	0.845(8)	1.6x10^5	1.62(3)x10^5	2.09(4)	7.8x10^4
	37°C	1.41(1)x10^5	1.35(1)	1.0x10^5	2.13(7)x10^5	6.1(2)	3.5x10^4
Glycocholic acid	22°C	4.4(2)x10^4	1.77(6)	2.5x10^4	6.1(5)x10^4	3.7(3)	1.6x10^4
	37°C	4(2)x10^3	2.4(1)	1.7x10^3	1.1(8)x10^4	13(2)	8.5x10^2

4.4 DISCUSSION

Although considerable work has been done developing albumin dialysis artificial liver support systems of several types, no *a priori* method exists to determine how effectively a specific molecule can be removed by albumin dialysis. Mathematical modeling of albumin dialysis has been shown to be predictive of the removal rate of the tightly albumin bound solute bilirubin, but more detailed modeling methods have been limited by the availability of information on albumin-solute binding properties. Developing a proper understanding of the albumin-solute binding reaction kinetics is a necessary step in understanding the behavior of albumin dialysis

systems and developing albumin dialysis into an effective and cost effective therapy for patients in liver failure.

Fitting the equilibrium SPR response at several concentrations to a one or two independent site model (Equation 4.5) has been shown to provide reasonable and reproducible binding constants for albumin-small molecule binding reactions. Although a large degree of variation in reported albumin-solute binding constants is often seen as a result of the purification methods used in the production of the albumin, the binding constants determined here by SPR have been shown to agree well with other methods used to measure binding constants.[63, 64] Of the reacting pairs tested in these experiments, only bilirubin varied by more than an order of magnitude from previously reported values (Table 4.1). The reason for the large variation in the binding constant for bilirubin in the experiments versus previously reported values is not known, but the very low aqueous solubility of bilirubin and the isomerization of bilirubin to more soluble forms by exposure to light may have both contributed to the difference seen in the SPR measurements presented here and results obtained using other methods.[65]

To obtain kinetic rate constants, the SPR response curves for each binding pair (not just the equilibrium response) were globally fit to the reaction rate equations (Equation 4.6 and Equation 4.7). The ability to measure the binding reaction rate constants is a necessary step toward developing more realistic mathematical models of albumin dialysis. Additionally, the value of the equilibrium binding constant obtained by taking the ratio of the reaction rate constants (Equation 4.2) provides an additional check for the accuracy and validity of values for the equilibrium binding constants obtained using the equilibrium SPR response. Only the values of the binding constants for glycocholic acid determined by the two curve fitting methods varied by more than an order of magnitude. Better estimates of the equilibrium constants are not

necessarily determined by curve fitting the rate equations to the entire data set for a binding pair instead of only the equilibrium response. When only the equilibrium SPR response is used a larger concentration range can be used in the curve fit allowing for the determination of equilibrium constants for secondary binding sites. Higher concentration curves were removed from the curve fitting to determine the reaction rate constants to prevent secondary binding sites from contributing to the SPR response. Global curve fitting to determine the rate constants for the secondary sites may be mathematically possible, but is not possible with the SCRUBBER-2 software package used in the analysis of the data presented here.

Although the two temperatures used in this study do not provide enough information to determine general trends for changes in the reaction rates and binding constants with changes in temperature, it is readily evident that the temperature needs to be considered for the testing and operation of albumin dialysis systems. With the exception of FK506, the tested compounds showed higher affinities at 22°C than at 37°C. FK506, however, had 12.7 and 3.7 (BSA and HSA, respectively) fold increases in the affinity binding constants at the higher temperature.

4.5 CONCLUSION

Surface plasmon resonance (SPR) provides a tool for examining the properties of albumin binding to solutes of interest in the development of ALSS (e.g. FK506 and other drugs used post transplantation surgery, bile acids and other metabolites that accumulate in blood during liver failure, and drugs found to cause liver failure such as acetaminophen), and provides a method for rapid and reproducible assessment of solutes for which no binding data is available. Albumin was chosen in this study because it is the principal adsorbent in both the most studied artificial

liver support system (MARS) and the most cost effective and readily available method of artificial liver support (single pass albumin dialysis, SPAD). Drugs and metabolytes are frequently bound to a significant degree to albumin or other binding agents in blood. FK506, for example, is principally bound to red blood cells, and a significant portion of the drug that is not bound to red blood cells is bound by albumin.[66] This does not however rule out using SPR to determine the ability of other compounds (e.g. lipid based carriers, artificial resins, or antibodies) to bind a target small molecules for removal.

5.0 SPECIFIC AIM 2: IMPROVED MATHEMATICAL DESCRIPTION OF BSD

Albumin dialysis, and more generally bound solute dialysis (BSD) has the potential to improve the care of patients in liver failure. The current methods of BSD, the Molecular Adsorbent Recirculating System (MARS) and single pass albumin dialysis (SPAD) were heuristically designed, and have not been well characterized. The development of a mathematical model that is able to predict the performance of a BSD system can be used to better define the aspects of the system that can be exploited to make BSD a more effective therapy for the treatment of liver failure. Patzer and Bane (2003) presented a model for the removal of albumin bound solutes by dialysis with a sweep fluid containing a binder.[18] The model describes the concentration profile in the dialysis cartridge for solutes that have fast binder-solute binding/unbinding reactions when compared to the rate of transport of the solute across the dialysis membrane. In the Patzer model of BSD, the binder-solute binding reactions in both the patient's blood and in the dialysis sweep fluid were assumed to be at equilibrium throughout the dialysis cartridge. The assumption of reaction equilibrium is not necessarily correct. The equilibrium assumption was a reasonable simplification considering the paucity of information on the kinetics of small and middle weight solutes (such as bilirubin, bile acids, middle and long chain fatty acids, phenol red, and salicylic acid, to name a few) binding to albumin, and the slow rates of removal that are seen in bound solute dialysis (BSD). Recent advances in biosensor technology have made it possible to determine the reaction rate constants for albumin-solute binding reactions with

relative ease. Incorporating the reaction rates into the model allows the equilibrium assumption built into the Patzer model of BSD to be relaxed. A mathematical model with an improved description of the kinetics and mass transport involved in BSD treatment can be used to further describe what is necessary for BSD to become a cost effective and available treatment for patients with liver function insufficiencies. The equilibrium model of BSD may be giving us an incomplete picture of the interaction between the kinetics of binding and unbinding and the mass transport of solutes across the dialysis membrane.

Dialysis is generally performed with the therapeutic goal of removing a set of solutes that are present in the blood. The solutes generally considered are those that are building up due to metabolic processes or acute intoxication (for example urea and salts in renal failure and bilirubin, drugs, or drug metabolites in liver failure). Although many of the solutes that are of interest in liver and renal failure are not necessarily toxic, they may have the potential to cause damage by persisting in higher than typical concentrations. High concentrations of albumin bound solutes in the blood of patients in liver failure prevents albumin from performing it's normal function as a solute carrier in blood by saturating albumin's binding sites. The original equilibrium model presented by Patzer and the model presented here incorporating the albumin-solute binding kinetics consider the case of solutes that are bound by albumin in the blood and dialysate streams, but both models are equally applicable to binders other than albumin as well as different binders on the blood and dialysate sides with little additional mathematical complexity.

5.1 METHODS

5.1.1 Albumin-solute binding reactions

The diffusive flux of a bound solute being removed from a patient's blood by BSD is a three step process (Figure 5.1). As blood passes through the dialyzer, free binder (albumin), *A*, and free solute, *S*, in the blood (subscript *B*) associate to form the solute-binder complex, *S*●*A*, and the complex dissociates into free binder and solute:

$$(S \bullet A)_B \underset{k_d}{\overset{k_a}{\rightleftarrows}} (A)_B + (S)_B \qquad \textbf{Equation 5.1}$$

Molecules that are smaller than the molecular weight cutoff of the membrane being used will diffuse down their concentration gradient into the dialysate (subscript *D*):

$$(S)_B \rightarrow (S)_D \qquad \textbf{Equation 5.2}$$

k_a (L mol^{-1} s^{-1}) and k_d (s^{-1}) are the reaction rate constants of association and dissociation, respectively, of the solute binder complex. Likewise, any molecule that has a higher concentration in the dialysate will diffuse down its concentration gradient into the blood. Free binder present on the dialysate side will react with solute crossing the membrane.

$$(A)_D + (S)_D \underset{k_d}{\overset{k_a}{\rightleftarrows}} (S \bullet A)_D \qquad \textbf{Equation 5.3}$$

The “cleaned blood” that exits the dialyzer is then returned to the patient.

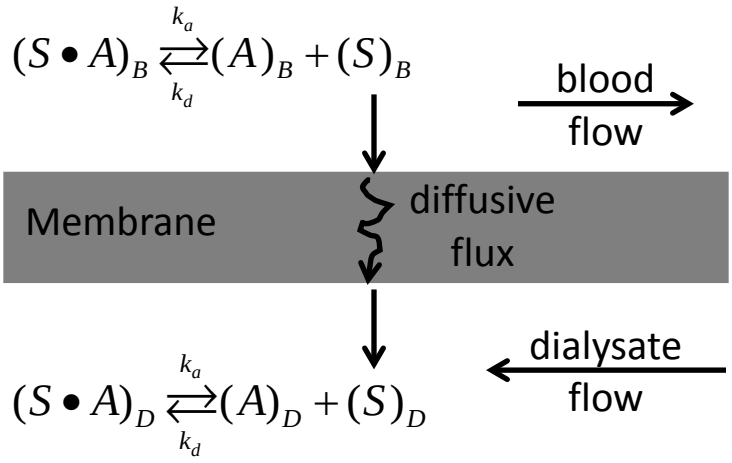

Figure 5.1. Schematic of the binder-solute binding reactions and diffusive solute transport in a countercurrent dialyzer. As blood passes through the dialyzer, free binder, *A*, and free solute, *S*, in the blood (subscript *B*) associate to form the solute-binder complex, *S•A*, and the complex dissociates into free binder and solute. Molecules that are smaller than the molecular weight cutoff of the membrane being used will diffuse down their concentration gradient into the dialysate (subscript *D*). k_a (L mol^{-1} s^{-1}) and k_d (s^{-1}) are the reaction rate constants of association and dissociation, respectively, of the solute binder complex. Free binder present on the dialysate side will react with solute crossing the membrane.

5.1.2 Single solute dialyzer concentration profile

A series of non-linear first order ordinary differential equations (ODEs) were derived to describe the reactions and removal of the solute and solute-albumin complex on both the blood and dialysate sides. The complete derivation and non-dimensionalization scheme for the equations presented in this section can be found in Appendix C. Mass balances on the blood side, subscript

B, yield non-dimensional equations describing the normalized concentration of solute, $(\tilde{C}_S)_B$, and the normalized solute binder complex, $(\tilde{C}_{SA})_B$, as a function of position ($\tilde{z}$) in the dialyzer.

$$\frac{d(\tilde{C}_S)_B}{d\tilde{z}} = \kappa\left((\tilde{C}_S)_D - (\tilde{C}_S)_B\right) + Da_1(\tilde{C}_{SA})_B - Da_2(\tilde{C}_S)_B(\varepsilon - (\tilde{C}_{SA})_B) \quad \textbf{Equation 5.4}$$

$$\frac{d(\tilde{C}_{SA})_B}{d\tilde{z}} = Da_2(\tilde{C}_S)_B(\varepsilon - (\tilde{C}_{SA})_B) - Da_1(\tilde{C}_{SA})_B \quad \textbf{Equation 5.5}$$

Symbol definitions are provided in Table 5.1. κ is a dimensionless mass transport constant (the dialyzer area-mass transport constant normalized to blood flow rate, kA/Q_B), Da_1, the dissociation Damkohler number, is the ratio of the complex dissociation rate constant to the rate of convective throughput ($V_B k_d/Q_B$), Da_2, the association Damkohler number, is the ratio of the complex association rate constant to the rate of convective throughput of solute ($V_B k_a/Q_B[(C_{S,total})_B]_{in}$), and ε is molar ratio of albumin to bilirubin at the blood stream inlet ($(C_{A,total})_B/[(C_{S,total})_B]_{in}$). A mass balance on the dialysate side, subscript *D*, yields

$$\frac{d(\tilde{C}_S)_D}{d\tilde{z}} = \frac{\kappa}{-\alpha}\left((\tilde{C}_S)_B - (\tilde{C}_S)_D\right) + \frac{\gamma\, Da_1}{-\alpha}(\tilde{C}_{SA})_D - \frac{\gamma\, Da_2}{-\alpha}(\tilde{C}_S)_D(\beta\varepsilon - (\tilde{C}_{SA})_D)) \quad \textbf{Equation 5.6}$$

$$\frac{d(\tilde{C}_{SA})_D}{d\tilde{z}} = \frac{\gamma\, Da_2}{-\alpha}(\tilde{C}_S)_D(\beta\varepsilon - (\tilde{C}_{SA})_D) - \frac{\gamma\, Da_1}{-\alpha}(\tilde{C}_{SA})_D \quad \textbf{Equation 5.7}$$

where γ is the ratio of the blood side volume to the dialysate side volume (V_D/V_B), α is the ratio of the dialysate side flow rate to the blood side flow rate (Q_D/Q_B), and β is the molar ratio of the binder (albumin) concentration in the dialysate to the concentration in the dialysate

($(C_{A,total})_D/(C_{A,total})_B$). The boundary values for the blood side inlet are set to the equilibrium concentrations and the dialysate side inlet has clean dialysate,

$$(\tilde{C}_S)_B = [(\tilde{C}_S)_B]_{in} \ @ \ \tilde{z} = 0 \qquad \textbf{Equation 5.8}$$

$$(\tilde{C}_{SA})_B = [(\tilde{C}_{SA})_B]_{in} \ @ \ \tilde{z} = 0 \qquad \textbf{Equation 5.9}$$

$$(\tilde{C}_S)_D = 0 \ @ \ \tilde{z} = 1 \qquad \textbf{Equation 5.10}$$

$$(\tilde{C}_{SA})_D = 0 \ @ \ \tilde{z} = 1 \qquad \textbf{Equation 5.11}$$

Table 5.1. Symbol and dimensionless parameter definitions for kinetic model of bound solute dialysis.

Parameter	Meaning	Range
$\tilde{C}_A$	Dimensionless concentration of binder	
$\tilde{C}_S$	Dimensionless concentration of solute	
$\tilde{C}_{S\bullet A}$	Dimensionless concentration of the solute-binder complex	
$\kappa = kA / Q_B$	Dialyzer mass transfer/blood flow rate ratio	0.5 – 3.0
$\alpha = Q_D / Q_B$	Dialysate/blood flow rate ratio	0.1 – 2.5
$Da_1 = V_B k_d / Q_B$	Dissociation reaction rate/blood flow rate ratio	0.33 – 600
$Da_2 = V_B k_a / (Q_B[(C_{S,total})_B]_{in})$	Association reaction rate/blood flow rate ratio	$1.0\text{x}10^2 – 1.8\text{x}10^6$
$\varepsilon = (C_{A,total})_B / [(C_{S,total})_B]_{in}$	Blood total albumin/incoming total solute concentration ratio	1.1
$\gamma = V_D / V_B$	Dialysate side/blood side volume ratio	1
$\beta = (C_{A,total})_D / (C_{A,total})_B$	Dialysate/blood total albumin concentration ration	0.01 – 0.5
$K_B = k_a / k_d$	Equilibrium binding constant	$1 – 10^6$ L mol^{-1}

The value of the incoming, subscript *in*, blood side solute and complex concentrations, $[(\tilde{C}_S)_B]_{in}$ and $[(\tilde{C}_{SA})_B]_{in}$, respectively, are calculated from the equilibrium binding constant, total solute concentration, and total albumin concentration at the blood side inlet. For the one to one binding model presented here, the association equilibrium binding constant, K_B (L mol^{-1}), is defined as

$$K_B = \frac{k_a}{k_d} = \frac{C_{S\bullet A,eq}}{C_{S,eq}C_{A,eq}}$$ **Equation 5.12**

The concentration of the complex, $C_{S\bullet A,eq}$ (mol L^{-1}), the solute, $C_{S,eq}$, and the albumin concentration, $C_{A,eq}$, are the concentrations at equilibrium (subscript *eq*). The total solute and albumin concentrations (regardless of whether the reactions are at equilibrium) are given by

$$C_{S,total} = C_S + C_{SA}$$ **Equation 5.13**

$$C_{A,total} = C_A + C_{SA}$$ **Equation 5.14**

Equation 5.4 through Equation 5.7 with boundary conditions (Equation 5.8 through Equation 5.11) were solved with boundary value problem solver (bvp4c) in the software package MATLAB (The MathWorks, Inc.,Natick, MA). The blood side inlet conditions are determined from the blood total concentrations of albumin and solute and the equilibrium binding constant.

5.2 RESULTS

In order to reduce the number of permutations of parameters to explore, the models (the original Patzer model of BSD and the extended kinetic description presented here) were solved at constant values of the total blood side albumin concentration, $(C_{A,\,total})_B$ = 40 g L^{-1} = 6.06x10^{-4} mol L^{-1}, the blood total albumin/incoming total solute concentration ratio, ε = 1.1, and the

dialysate side/blood side volume ratio, $\gamma = 1$. A choice of Da_1, K_B, $(C_{A,\,total})_B$, and ε also defines Da_2 according to the equation

$$Da_2 = Da_1 K_B \varepsilon (C_{A,total})_B \qquad \textbf{Equation 5.15}$$

For lightly bound solutes ($K_B = 10^0$), the dissociation Damkohler number, Da_1, is three orders of magnitude greater than the association Damkohler number, Da_2, ($Da_1/Da_2 = 1500$); for moderately bound solutes ($K_B = 10^4$) the value of the dissociation Damkohler number is one order of magnitude smaller than the association Damkohler number ($Da_1/Da_2 = 0.15$); and for tightly bound solutes ($K_B = 10^6$) the value of the dissociation Damkohler number is three orders of magnitude smaller than association Damkohler number ($Da_1/Da_2 = 0.0015$) (Figure 5.2).

The solute concentration profile through the dialysis cartridge was solved for pairings of high (+) and low (-) values of the clinical range for the dialysate/blood flow rate ratio, α, and mass transport/blood flow rate ratio parameter, κ. High and low values for parameters used for modeling are provided in Table 5.2. For each flow rate ratio/mass transport parameter pairing, the models were solved for a range of the dialysate/blood albumin concentration ratios, β, and binding constants, K_B, and for each K_B value the models were solved for a range of dissociation Damkohler number, Da_1, values (Figure 5.3, Figure 5.4, Figure 5.5, and Figure 5.6).

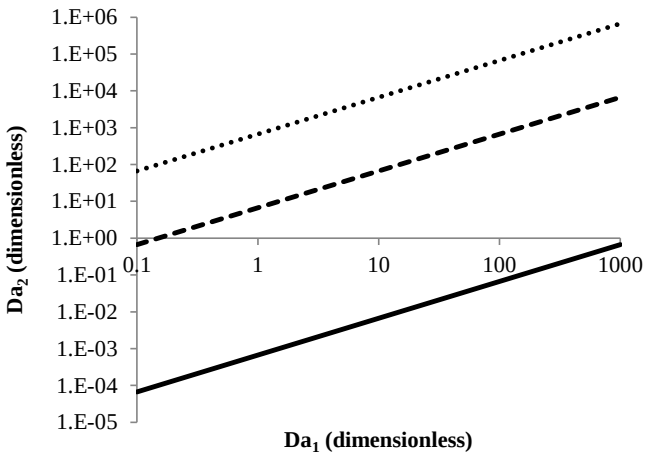

Figure 5.2. For a given value of the equilibrium constant, K_B (L mol^{-1}), the value of Da_1 was chosen and the value of Da_2 changes according to Equation 5.15. For $K_B = 10^0$ (solid line), the value of the Damkohler number for dissociation, Da_1, is three orders of magnitude greater than the value of the Damkohler number for association, Da_2, ($Da_1/Da_2 = 1500$), for $K_B = 10^4$ the value of Da_1 is one order of magnitude smaller than Da_2 ($Da_1/Da_2 = 0.15$), and for $K_B = 10^6$ the value of Da_1 is three orders of magnitude smaller than Da_2 ($Da_1/Da_2 = 0.0015$).

Table 5.2. Values of parameters used for kinetic modeling of bound solute dialysis. The values for each parameter are chosen to reflect current CVVHD and albumin dialysis practices. $(C_{A,total})_B$ and γ are held constant for all simulations.

Parameter	Units	Low (-)	High (+)
$(C_{A,total})_B$	g L^{-1}	40	40
β		0.01	0.5
ε		1.1	1.1
α		0.1	2.5
κ		0.5	2.0
γ		1	1
K_B	L mol^{-1}	1	10^6
Da_1		0.1	1000

The single pass fractional removal, F, can be used as a metric of the removal effectiveness for a given set of conditions, and is defined as

$$F = \frac{[(C_{S,total})_B]_{in} - [(C_{S,total})_B]_{out}}{[(C_{S,total})_B]_{in}} = 1 - [(\tilde{C}_{S,total})_B]_{out} \qquad \textbf{Equation 5.16}$$

The behavior of the equilibrium BSD model as a function of the dialysate side/blood side albumin concentration ratio, β, the relative flow rates of the dialysate to blood streams, α, and the mass transport rate/blood side flow rate ratio, κ, was explored in detail by Patzer *et. al*. The fractional removals of solute for the conditions tested in this study are presented in Table 5.3, Table 5.5, Table 5.4, and Table 5.6. Although the results are presented here in terms of the fractional removal (not the fractional removal normalized to the fractional removal under high flow rate dialysis without albumin present as presented by Patzer *et. al.*), the results obtained for the equilibrium model mirror those obtained by Patzer *et. al*. Maximal removal was seen for maximum dialysate/blood flow rate ratio, α+, and maximum mass transport rate/blood flow rate ratio, κ+, regardless of the dialysate side/blood side albumin concentration ratio, β, present in the dialysate. At the minimum dialysate/blood flow rate ratio, α-, there is a negligible difference in the fractional removal (< 2%) for changes in the value of the mass transport rate/blood flow rate ratio, κ, in the range tested. Increasing the dialysate/blood flow rate ratio, α, regardless of the value of the mass transport rate/blood flow rate ratio, resulted in a large increase to the fractional removal. For any given flow rate ratio/mass transport parameter pairing, the maximum removal was always seen for lightly bound solutes ($K_B = 10^0$), and the lowest removals were seen for tightly bound solutes ($K_B = 10^6$). For lightly bound solutes ($K_B = 10^0$) there was negligible improvement in the removal rate of bound solutes with the addition of albumin to the dialysate,

and for moderately bound solutes ($K_B = 10^4$) or tightly bound solutes ($K_B = 10^6$) removal rates are increased with increasing dialysate side albumin concentrations. Although in general higher removal is seen at high dialysate/blood flow rate ratios, for tightly bound solutes ($K_B > 10^6$) at high dialysate/blood albumin ratios ($\beta \geq 0.5$), the system becomes insensitive to flow rate and becomes a function of the mass transport parameter only.

The difference between the results obtained using the original equilibrium model of BSD and the results obtained using the expanded model accounting for the kinetics of the binding reactions can be quantified by defining the deviation, D, between the solutions of the two models in terms of the percent difference in the fractional removal

$$D = 100\left[\frac{(F)_{Equilibrium} - (F)_{Da_1}}{(F)_{Equilibrium}}\right]_{K_B,\beta,\alpha,\kappa,\varepsilon,(C_{A,total})_B} \qquad \textbf{Equation 5.17}$$

For determining the deviation, D, the equilibrium binding constant, K_B, the dialysate/blood albumin ratio, β, the dialysate/blood flow rate ratio, α, and the mass transport rate/blood flow rate ratio, κ, were chosen, and the values of the Damkohler numbers for dissociation, Da_1, and association, Da_2, were chosen around those values. For a given value of the equilibrium constant, the value of dissociation Damkohler number was chosen and the value of association Damkohler number is found using Equation 5.15. Positive values of deviation indicate that the equilibrium model is overestimating the single pass fractional removal, and negative values indicate the equilibrium model underestimating single pass fractional removal. As the value of deviation approaches zero, the solution of the kinetic model approaches the solution to the

equilibrium model. The deviation for each condition tested can be found in Table 5.3, Table 5.5, Table 5.4, and Table 5.6.

Regardless of the condition tested, the equilibrium model overestimated the single pass fractional removal. The equilibrium model assumes that the rate of dissociation of the solute-albumin complex on the blood side is fast compared to the rate that solute can transit the dialysis membrane and that the solute on the dialysate side is then bound at an infinitely fast rate. In other words the reactions are always at equilibrium. This is a best case scenario in that, as long as solute is being removed from the blood side, finite reaction rates require that the blood side is always free solute depleted and the dialysate side is always free solute enriched compared to when the binding reactions are at equilibrium (the opposite is of course true for solutes that are in higher concentrations on the dialysate side than on the blood side).

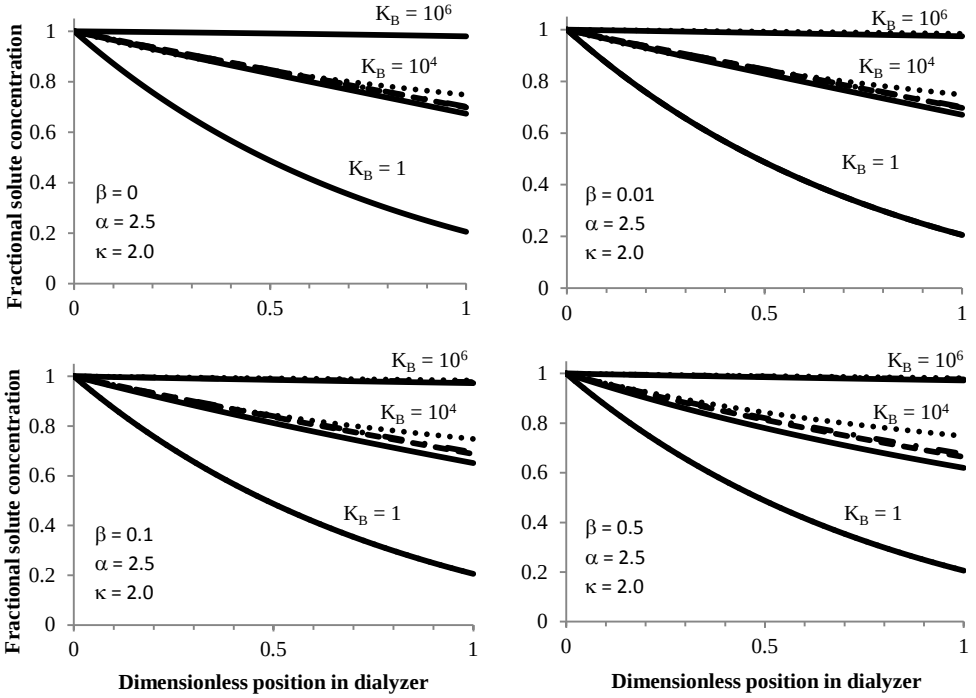

Figure 5.3. Fractional concentration of solute as a function of dimensionless position on the blood path side of a countercurrent dialyzer for α=2.5 and κ=2.0 (α+ κ+) at K_B =10^0, 10^4, and 10^6 (separated by groupings on the plots). The solution to the Patzer equilibrium BSD model (solid line) over estimates the removal of solute compared to the kinetic model regardless of the choice of reaction rate constants (Da_1=0.1 [dotted line], Da_1=10 [dash/dot line], and Da_1=1000 [dashed line]). For a given equilibrium binding constant the kinetic model solution approaches the equilibrium model solution for increasing values of Da_1 (i.e. the dissociation rate constant, k_d). The kinetic BSD model was unsolvable by the chosen numerical solution method for α=2.5, κ=2.0, and K_B=10^6 for the following combinations of β and Da_1: β=0/Da_1=10, β=0/Da_1=1000, β=0.01/Da_1=10, β=0.01/Da_1=1000, β=0.1/Da_1=1000, β=0.5/Da_1=1000.

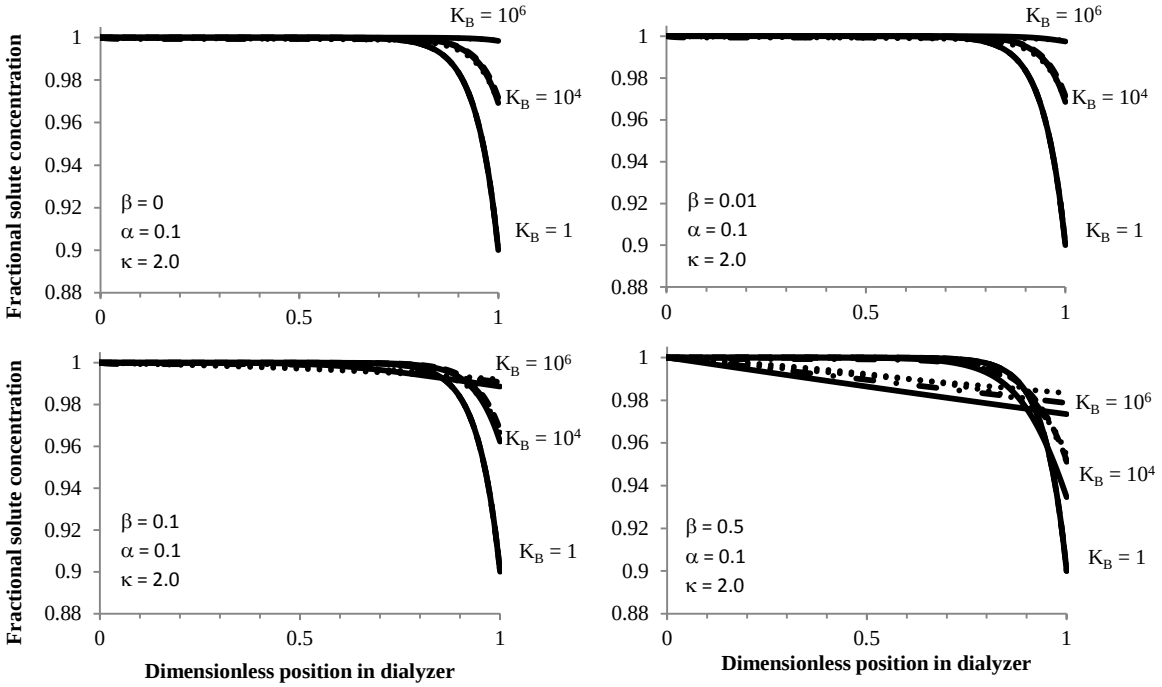

Figure 5.4. Fractional concentration of solute as a function of dimensionless position on the blood path side of a countercurrent dialyzer for α=0.1 and κ=2.0 (α- κ+) at $K_B = 10^0$, 10^4, and 10^6 (separated by groupings on the plots). The solution to the Patzer equilibrium BSD model (solid line) over estimates the removal of solute compared to the kinetic model regardless of the choice of reaction rate constants (Da_1=0.1 [dotted line], Da_1=10 [dash/dot line], and Da_1=1000 [dashed line]). For a given equilibrium binding constant the kinetic model solution approaches the equilibrium model solution for increasing values of Da_1 (i.e. the dissociation rate constant, k_d). The kinetic BSD model was unsolvable by the chosen numerical solution method for α=0.1, κ=2.0, and $K_B=10^6$ for the following combinations of β and Da_1: β=0/Da_1=10, β=0/Da_1=1000, β=0.01/Da_1=10, β=0.01/Da_1=1000, β=0.1/Da_1=1000, β=0.5/Da_1=1000.

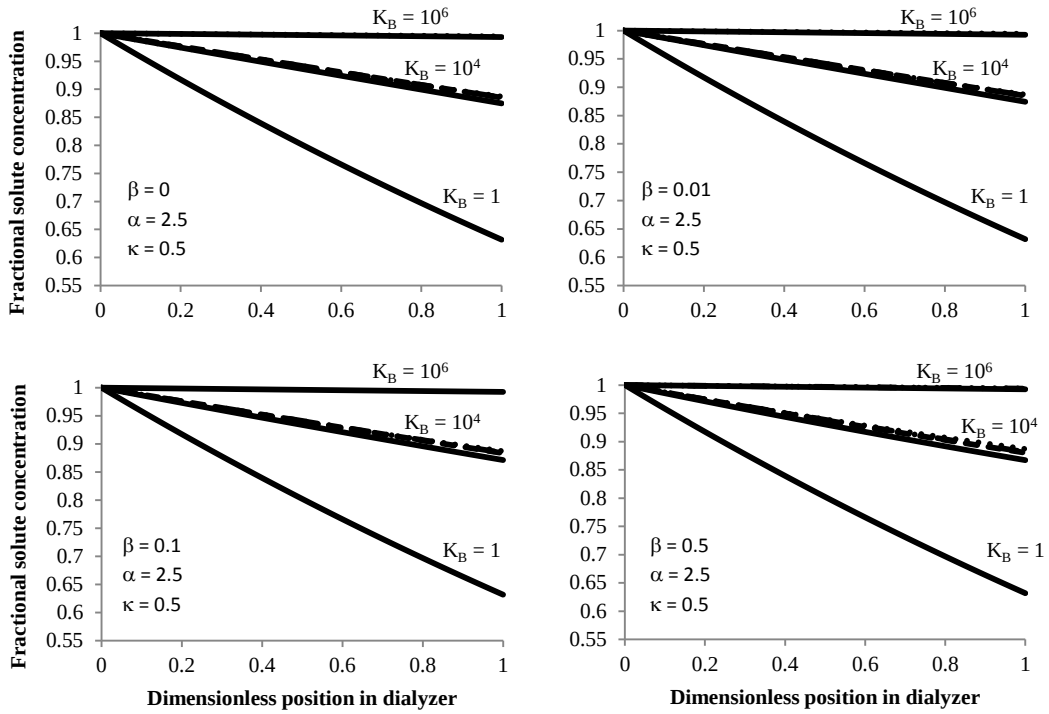

Figure 5.5. Fractional concentration of solute as a function of dimensionless position on the blood path side of a countercurrent dialyzer for α=2.5 and κ=0.5 (α+ κ-) at K_B =10^0, 10^4, and 10^6 (separated by groupings on the plots). The solution to the Patzer equilibrium BSD model (solid line) over estimates the removal of solute compared to the kinetic model regardless of the choice of reaction rate constants (Da_1=0.1 [dotted line], Da_1=10 [dash/dot line], and Da_1=1000 [dashed line]). For a given equilibrium binding constant the kinetic model solution approaches the equilibrium model solution for increasing values of Da_1 (i.e. the dissociation rate constant, k_d). The kinetic BSD model was unsolvable by the chosen numerical solution method for α=2.5, κ=0.5, and K_B=10^6 for the following combinations of β and Da_1: β=0/Da_1=10, β=0/Da_1=1000, β=0.01/Da_1=10, β=0.01/Da_1=1000, β=0.1/Da_1=1000, β=0.5/Da_1=1000.

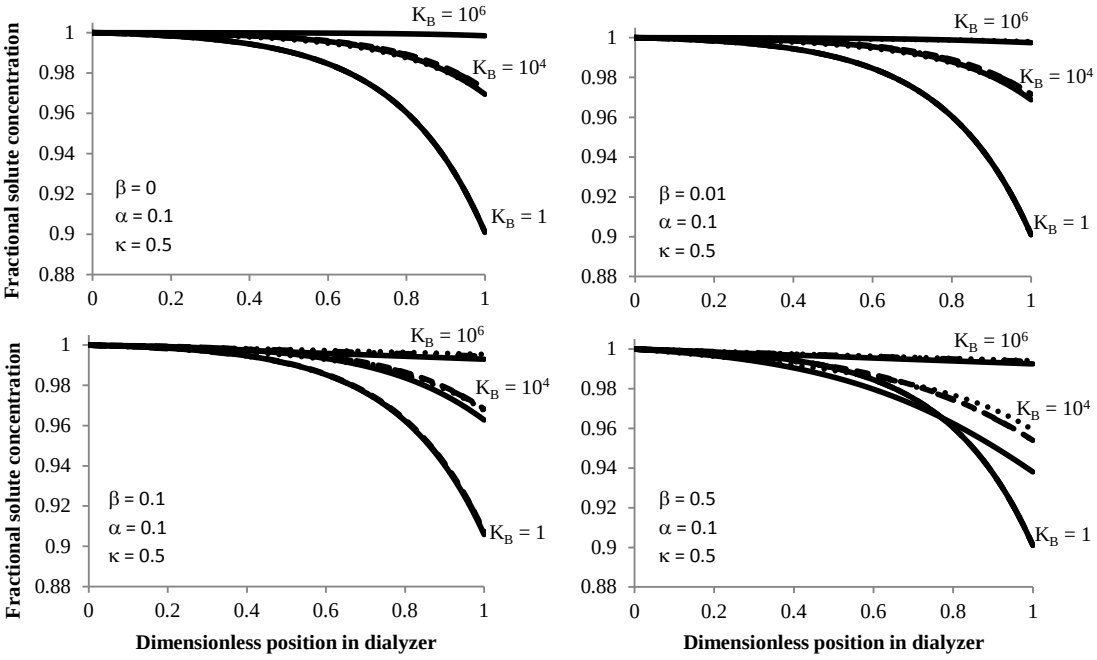

Figure 5.6. Fractional concentration of solute as a function of dimensionless position on the blood path side of a countercurrent dialyzer for α=0.1 and κ=0.5 (α- κ-) at $K_B = 10^0$, 10^4, and 10^6 (separated by groupings on the plots). The solution to the Patzer equilibrium BSD model (solid line) over estimates the removal of solute compared to the kinetic model regardless of the choice of reaction rate constants (Da_1=0.1 [dotted line], Da_1=10 [dash/dot line], and Da_1=1000 [dashed line]). For a given equilibrium binding constant the kinetic model solution approaches the equilibrium model solution for increasing values of Da_1 (i.e. the dissociation rate constant, k_d). The kinetic BSD model was unsolvable by the chosen numerical solution method for α=0.1, κ=0.5, and $K_B=10^6$ for the following combinations of β and Da_1: β=0/Da_1=0.1, β=0/Da_1=10, β=0/Da_1=1000, β=0.01/Da_1=10, β=0.01/Da_1=1000, β=0.1/Da_1=1000, β=0.5/Da_1=1000.

Table 5.3. Fractional removal of blood side solute and percent deviation of the fractional removal for α=2.5 and κ=2.0 (α+ κ+) as predicted by both the kinetic BSD model and the Patzer equilibrium BSD model. Conditions that were unsolvable using the chosen numerical solution method are indicated with n/a. EQ: equilibrium BSD model, n/a: value not available

		Fractional removal				Deviation		
		Da_1				Da_1		
β	K_B	0.1	10	1000	EQ	0.1	10	1000
0	10^0	0.794	0.794	0.794	0.794	0.0	0.0	0.0
0	10^4	0.252	0.299	0.302	0.326	22.9	8.5	7.6
0	10^6	0.016	n/a	n/a	0.020	21.3	n/a	n/a
0.01	10^0	0.794	0.794	0.794	0.794	0.0	0.0	0.0
0.01	10^4	0.252	0.300	0.303	0.329	23.5	9.0	8.1
0.01	10^6	0.016	n/a	n/a	0.025	37.7	n/a	n/a
0.1	10^0	0.794	0.794	0.794	0.794	0.0	0.0	0.0
0.1	10^4	0.252	0.306	0.312	0.349	27.8	12.3	10.5
0.1	10^6	0.017	0.023	n/a	0.027	38.8	15.9	n/a
0.5	10^0	0.794	0.794	0.794	0.794	0.0	0.0	0.0
0.5	10^4	0.252	0.325	0.336	0.380	33.7	14.6	11.6
0.5	10^6	0.019	0.024	n/a	0.028	32.1	14.8	n/a

Table 5.4. Fractional removal of blood side solute and percent deviation of the fractional removal for α=2.5 and κ=0.5 (α+ κ-) as predicted by both the kinetic BSD model and the Patzer equilibrium BSD model. Conditions that were unsolvable using the chosen numerical solution method are indicated with n/a. EQ: equilibrium BSD model, n/a: value not available

		Fractional removal				Deviation		
		Da_1				Da_1		
β	K_B	0.1	10	1000	EQ	0.1	10	1000
0	10^0	0.368	0.368	0.368	0.368	0.0	0.0	0.0
0	10^4	0.113	0.115	0.115	0.125	9.7	8.4	8.2
0	10^6	0.006	n/a	n/a	0.007	16.8	n/a	n/a
0.01	10^0	0.368	0.368	0.368	0.368	0.0	0.0	0.0
0.01	10^4	0.113	0.115	0.115	0.126	10.1	8.6	8.4
0.01	10^6	0.006	n/a	n/a	0.007	22.8	n/a	n/a
0.1	10^0	0.368	0.368	0.368	0.368	0.0	0.0	0.0
0.1	10^4	0.113	0.116	0.117	0.129	12.2	10.1	9.5
0.1	10^6	0.006	0.006	n/a	0.008	22.5	15.8	n/a
0.5	10^0	0.368	0.368	0.368	0.368	0.0	0.0	0.0
0.5	10^4	0.113	0.118	0.120	0.133	14.9	10.8	9.8
0.5	10^6	0.006	0.006	n/a	0.008	19.9	15.5	n/a

Table 5.5. Fractional removal of blood side solute and percent deviation of the fractional removal for α=0.1 and κ=2.0 (α- κ+) as predicted by both the kinetic BSD model and the Patzer equilibrium BSD model. Conditions that were unsolvable using the chosen numerical solution method are indicated with n/a. EQ: equilibrium BSD model, n/a: value not available

		Fractional removal				Deviation		
		Da_1				Da_1		
B	K_B	0.1	10	1000	EQ	0.1	10	1000
0	10^0	0.100	0.100	0.100	0.100	0.0	0.0	0.0
0	10^4	0.031	0.029	0.028	0.031	0.3	6.3	8.4
0	10^6	0.001	n/a	n/a	0.002	5.8	n/a	n/a
0.01	10^0	0.100	0.100	0.100	0.100	0.0	0.0	0.0
0.01	10^4	0.031	0.029	0.029	0.031	1.4	7.1	9.1
0.01	10^6	0.002	n/a	n/a	0.003	11.7	n/a	n/a
0.1	10^0	0.100	0.100	0.100	0.100	0.0	0.0	0.0
0.1	10^4	0.034	0.033	0.032	0.038	10.2	12.9	14.6
0.1	10^6	0.008	0.009	n/a	0.011	29.0	18.7	n/a
0.5	10^0	0.100	0.100	0.100	0.100	0.0	0.0	0.0
0.5	10^4	0.046	0.049	0.048	0.065	29.7	25.3	26.3
0.5	10^6	0.017	0.021	n/a	0.027	37.0	19.7	n/a

Table 5.6. Fractional removal of blood side solute and percent deviation of the fractional removal for α=0.1 and κ=0.5 (α- κ-) as predicted by both the kinetic BSD model and the Patzer equilibrium BSD model. Conditions that were unsolvable using the chosen numerical solution method are indicated with n/a. EQ: equilibrium BSD model, n/a: value not available

		Fractional removal				Deviation		
		Da_1				Da_1		
B	K_B	0.1	10	1000	EQ	0.1	10	1000
0	10^0	0.099	0.099	0.099	0.099	0.0	0.0	0.0
0	10^4	0.030	0.028	0.028	0.031	1.1	7.8	8.4
0	10^6	n/a	n/a	n/a	0.002	n/a	n/a	n/a
0.01	10^0	0.099	0.099	0.099	0.099	0.0	0.0	0.0
0.01	10^4	0.030	0.029	0.028	0.031	2.4	8.5	9.2
0.01	10^6	0.002	n/a	n/a	0.003	19.8	n/a	n/a
0.1	10^0	0.099	0.099	0.099	0.099	0.0	0.0	0.0
0.1	10^4	0.033	0.032	0.032	0.037	12.6	14.1	14.6
0.1	10^6	0.005	0.005	n/a	0.007	34.2	21.8	n/a
0.5	10^0	0.099	0.099	0.099	0.099	0.0	0.0	0.0
0.5	10^4	0.041	0.046	0.046	0.062	34.1	25.5	25.7
0.5	10^6	0.006	0.006	n/a	0.007	21.6	16.6	n/a

Lightly bound solutes ($K_B = 10^0$): There was essentially no deviation (<1%) for lightly bound solutes ($K_B = 10^0$, $Da_1/Da_2 = 1500$) regardless of the other conditions tested. With lightly bound solutes the rate that the solute-albumin complex on the blood side can dissociate is sufficient to keep up with the rate that free solute can be removed from the blood side regardless of the mass transport parameter or dialysate/blood flow rate ratio. As was expected based on the results of Patzer et. al., the addition of albumin to the dialysate side (increasing β) had no practical impact on the rate of solute removal from the blood side. In the case of weakly bound solutes the system is essentially controlled by the mass transport properties of the dialysis membrane and the

convective flow rates of blood and dialysate. Since the binding reactions play such a minor role in the removal, existing dialysis models that do not consider solute-albumin reactions are adequate to describe removal of such weakly bound solutes.

Moderately bound solutes ($K_B = 10^4$): With less albumin in the dialysate than what is required to maximize the removal rate (β = 0, 0.01, or 0.1) the magnitude of the deviation decreases with increasing reaction rates (Da_1 and Da_2) for high dialysate/blood flow rate ratio (regardless of the value of the mass transport parameter), but the value of deviation increases (lower removal rates) with increasing reaction rates (Da_1 and Da_2) for low dialysate/blood flow rate ratio (regardless of the value of the mass transport parameter). This indicates that there is less benefit to higher reaction rates if there is insufficient sweep fluid or albumin present to depress the dialysate side free solute concentration. For cases of either high dialysate albumin concentrations or high dialysate/blood flow rate ratio, deviation decreases with higher reaction rates (Da_1 and Da_2).

Tightly bound solutes ($K_B = 10^6$): All of the simulations performed in this study were solved using a MATLAB boundary value problem solver (bvp4c). All equilibrium (Patzer model) BSD simulations ran and provided a numerical solution without error, but kinetic BSD simulations with tightly bound solutes ($K_B = 10^6$) had an apparent numerical instability. The numerical solution diverged from the boundary conditions at higher values of the Damkohler numbers (Da_1 and Da_2). Although this instability may be related to the initial guess used in the simulation, attempts to use the solution to simulations performed at low vales of Da_1 and Da_2 as the initial guess for simulations at higher Da_1 and Da_2 did not result in an improved ability for the solver to reach a stable solution.

General trends for tightly bound solutes were difficult to establish given that the simulations were unstable and would not solve at higher values of reaction rates (Da_1 and Da_2)

or low values of the dialysate/blood albumin concentration ratio, β. Overall, deviation was higher for tightly bound solutes (K_B=10^6, Da_1/Da_2 = 0.0015) than for less tightly bound solutes (K_B=10^4, Da_1/Da_2 = 0.15). The higher deviation is slightly misleading however in that fractional removal values are so low for tightly bound solutes. For tightly bound solutes the deviation ranged from 6% to 39% with a difference in fractional removal ranging from 0.0001 to 0.01, respectively, as opposed to deviation for moderately bound solutes ranging from 0.3% to 34% with a difference in fractional removal ranging from 0.0001 to 0.13 (a much bigger difference in the actual removal rate), respectively. For higher dialysate side albumin concentrations, β=0.1 or 0.5, the deviation decreased with increasing reaction rates (Da_1=0.1 to 10) for all flow rate/mass transport parameter (α and κ) pairs. At slow reaction rates (Da_1=0.1) the deviation was highest for high flow rates and high mass transport parameter (α+ κ+), but at higher reaction rates (Da_1=10) the value of deviation was higher for low dialysate/blood flow rate ratios (α-) regardless of the value of the mass transport parameter, κ.

5.3 DISCUSSION

A model of BSD that accurately represents the physics of the system is important to developing an understanding of what impact system properties and operating parameters have on the removal rates that can be achieved. Models of BSD have been published describing the effect of the addition of a binding agent to the dialysate stream on bound solute removal, the effect of convection (ultrafiltration) on bound solute removal, and the use of solid adsorbents to remove bound solutes. The model presented here explores the reaction kinetics of BSD. The kinetic model of BSD also provides a platform for the comparison of the original Patzer model of BSD

that makes the assumption of reaction equilibrium with a kinetic model that relaxes the equilibrium assumption, when it comes to BSD performance.

The dimensionless parameters governing removal in the kinetic description of BSD are: the membrane mass transport/blood flow rate ratio, κ; the dialysate/blood flow rate ratio, α; the dialysate side/blood side volume ratio, γ; the dialysate/blood total albumin concentration ratio, β; the dissociation reaction rate/blood flow rate ratio, Da_1; and the association reaction rate/blood flow rate ratio, Da_2. The first four parameters, κ, α, γ, and β, are either dialysis operating parameters or can be controlled to some degree by dialyzer choice. Since the blood flow rate is chosen based on the clinical situation the Damkohler numbers for dissociation and association, Da_1 and Da_2 respectively, are determined by the solute-binder system being considered. In the blood the main carrier of solutes that are of interest in liver failure is albumin, but the binder on the dialysate side could potentially be chosen based on the target solute. Removal was found to be insensitive to changes in the dialysate/blood compartment volume ratio, γ, regardless of other parameters tested. The equilibrium models presented by Patzer include a term describing the ratio of the binding constants on the blood and dialysate sides to account for a different binder in the blood and dialysate. As the model is described here, the same binder is considered on both sides and there is only one binding reaction considered, so the values of Da_1 and Da_2 are the same for the blood side and the dialysate side. The addition of different binders on the dialysate and blood sides would necessitate having different Da_1 and Da_2 values for the equations describing the blood and dialysate sides to reflect the binder-solute interaction on the respective sides with no additional mathematical complexity. The addition of multiple binders or multiple solutes would add additional equations and terms in the equations describing the new interactions. Multiple solutes interacting with the binding agent would add two ODEs on both

the blood and dialysate sides for each additional solute to describe the free and bound solute concentration on each side, but, assuming the solute-binder interaction is still a 1:1 reaction as described in the introduction, wouldn't add additional terms to the equations. Multiple binders with one solute would add one ODE on each side to describe the concentration profile of the solute complex with the second binder, and would add loss and generation by reaction terms to the equations describing the free concentration to describe the reactions with the second binder.

Initial attempts to obtain a numerical solution to the system of nonlinear ODEs derived to describe the kinetic model of BSD were performed using the MATLAB ODE solvers used previously (ode45, ode15s, ode23, and ode23s). The numerical solvers included ones that are meant for "stiff" and other difficult to solve system of ODEs. Although the original Patzer model of BSD would solve using any of the older solvers, the normalized kinetic model would not. When the dimensional kinetic model was used (as opposed to the normalized model) some cases would solve. Since these solvers are for initial value problems (as opposed to boundary value problem solvers), additional steps need to be taken to pose the boundary conditions as initial values at one end and then match the output to the boundaries on the other side. The boundary value problem solvers, bvp4c and bvp5c (included in MATLAB 6.0 and later), solved most cases of the kinetic model, and did so in considerably less time than the older ODE solvers. A description of the numerical methods used in this solver can be found at the MATLAB website, www.mathworks.com. Both bvp4c and bvp5c are of forth order accuracy, and only differ in the method used for residual control. Both bvp4c and bvp5c were used to solve several cases of the kinetic BSD model, and when no practical difference was found in the solution provided or the solution time needed, bvp4c was chosen arbitrarily for the rest of the simulations.

In all cases tested, the fractional removal found using the equilibrium model was the same as or higher than fractional removal found using the kinetic description. This makes sense when one considers that a depletion effect on the blood side always exists as the concentration is reduced and time is needed for the dissociation of the solute-binder complex. Conversely there will always be a higher free concentration in the dialysate than will be indicated by the equilibrium model since the association step always takes a finite time to occur. The equilibrium model can therefore be taken as an upper bound for the removal rate.

For lightly bound solutes (K_B=10^0), no difference was seen between the removal found using either the equilibrium model or the kinetic model. No improvement to removal rates were seen with the addition of binder to the dialysate stream, and no change in removal rates were seen with faster kinetics (higher Da_1 and Da_2). For such lightly bound solutes, the assumption can be made that the total concentration (as opposed to the free or unbound concentration) is the driving force for solute removal and the removal rates can be assumed to follow descriptions for conventional aqueous dialysis.

For moderately bound solutes (K_B = 10^4, Da_1/Da_2 = 0.15) the situation arises that for low end dialysate flow rates and high end blood side flow rates, α-, with less binder than is required to approach maximum removal, the deviation increases with faster kinetics (lower removal), but for higher sweep fluid flow rates, α+, and high dialysate side albumin concentrations,β, the deviation decreases with faster kinetics (increased removal). For α- with low β, faster kinetics will result in the blood side producing free solute at a higher rate, but the dialysate side carrying capacity (the amount of solute that can be carried out of the system by the dialysate, roughly proportional to the product $Q_D(C_{A,total})_D$) is insufficient to keep up with the rate that solute transits the membrane.

It is not possible based on these simulations to determine general trends for tightly bound solutes (K_B=10^6) given that the simulations were unstable and would not solve at higher values of Da_1 and Da_2 or low values of β. This apparent instability points out a situation where the original Patzer equilibrium model of BSD is the better model even when it is not as good a representation of the actual removal rates. It will do no good to use a more complete (and complicated) model for the removal if it can't be solved, even if the alternative over estimates the removal by almost 40%.

5.4 CONCLUSION

Hemodialysis, whether only hemodialysis (diffusive flux), hemofiltration (convective flux), or hemodiafiltration (both diffusion and convection), is performed with the therapeutic goal of removing a set of solutes that are present in the blood at higher concentrations than are desirable and the removal of bulk fluid. In liver failure the solutes that build up in the patient's blood tend to be albumin bound and sparingly soluble. A typical hemodialysis membrane has a sieving coefficient of <1% for albumin, meaning that, whether by diffusion or by convection, <1% of the albumin present in the blood will transit the membrane, and the same is true for albumin bound solutes. For a solute such as bilirubin where the majority is bound to albumin (or any large carrier) in the blood the removal is limited to the free fraction, and the free solute concentration is very low. This small driving force for diffusion makes the removal of tightly bound solutes, whether to albumin or other carriers such as red blood cells, by dialysis to slow to provide an effective therapy. Once a small amount of solute has passed into the dialysate stream the removal is further slowed by the reduction in the free solute concentration gradient across the

membrane, the driving force for the diffusion of bound solutes. The addition of a binding agent, such as albumin, to the dialysate stream to bind solute as it transits the membrane is one proposed method to increase the rate of removal of tightly bound solutes by hemodialysis.

For the simple 1:1 solute-binder interaction that is described here, the additional mathematical complexity and numerical stability problems with the kinetic description of BSD certainly reduces its potential utility. While the equilibrium model overestimated removal by almost 40%, it provides a reasonable estimate of the removal potential based on the equilibrium binding constant. The utility of the equilibrium model becomes more obvious when considering the lack of good information describing the kinetics of albumin solute interactions. A more significant difference may be seen between the equilibrium and kinetic descriptions of BSD when additional binder-solute interactions (multiple binders with one solute, one binder and multiple solutes, or multiple binders with multiple solutes) are considered.

6.0 SPECIFIC AIM 3: EXAMINING THE PENETRATION OF ALBUMIN INTO COMMERCIAL DIALYSIS FIBERS

While studies in our lab have shown different commercial dialysis membranes, of the same nominal surface area, to have different rates of removal of the tightly albumin bound solute bilirubin (data not published), the reason for the difference on removal rates is not clear why. Possible explanations for the differences in removal rates that are seen between commercial dialyzer types (after correcting for area) include dialysis membrane and solute charge effects, polarity of the solute and the membrane, the thickness of the membrane walls, and the tortuosity of the pore network to name a few. Dialysis membranes are typically considered to be impermeable to large proteins, like albumin, but the ability of albumin to enter or bind to the surface of the dialysis membrane or the pore walls could, for better or worse, impact the removal of tightly albumin bound solutes. The designers of the MARS artificial liver support system (ALSS) advocated the use of the MARSFlux dialysis membrane. The claim was that the properties of this particular membrane, a polyethersulfone (PES) high flux dialysis membrane, allows albumin to penetrate into the membrane pores. PES membranes typically have a fine pored inner lumen for sieving and an open fingerlike support layer. Albumin penetration into the membrane could contribute to the removal of solutes by binding the solutes directly and by contributing additional transport mechanisms (surface diffusion, decreased diffusional distance, or decreased free solute concentration). The relatively open pore structure of PES membranes

also expose more surface area for high molecular weight proteins to adsorb directly to the membrane surface. The equivalent dialyzer produced by Gambro, who currently owns the MARS technology, has a similar pore structure as do other membranes produced by thermally induced phase separation.[67-69]

The designers of the MARS prescribe a 1 hour cartridge pretreatment with a 10% albumin solution before it is used with a patient.[1] Their claim is that this pretreatment impregnates the membrane with albumin. When a solution containing high concentrations of protein is run across a filter (especially in the case of perpendicular or dead end ultrafiltration) a polarization layer develops close to the membrane, and generally a protein cake or gel layer forms on the membrane surface.[55] Although the cross flow configuration of a dialysis cartridge minimizes the gel layer formation, several studies have shown a significant amount of albumin and other proteins will penetrate into conventional dialysis membranes during clinical use.[67, 70] Clark *et. al.* investigated the adsorption of the small protein β_2-microglobulin and of bovine serum albumin to the surface of polyacrylonitrile (PAN) and cellulose triacetate (CT) dialysis membranes. Polyacrylonitrile and cellulose triacetate dialysis membranes were incubated in solutions containing radiolabeled β_2-microglobulin or bovine serum albumin. Significantly more β_2-microglobulin adsorbed to the surface than albumin. The higher β_2-microglobulin adsorption was taken by the authors as indication of β_2-microglobulin adsorption to the inner surface of the pores but the exclusion of the larger albumin molecule from the pore network.[71] Fujimori *et. al.* measured the adsorption of several proteins, including albumin, to CT, polymethylmethacrylate (PMMA), and PAN clinical dialyzer membranes. After use in the renal dialysis clinic, the dialysis membranes were washed with saline and fixed using 2% paraformaldehyde. The proteins were then labeled using fluorescently tagged antibodies. The

fluorescence of the labeled proteins was measured using confocal laser microscopy. A qualitative assessment of the albumin concentration showed adsorption to the outer surfaces of the CTA membrane, little adsorption to the PMMA, and albumin adsorption to the inner and outer surfaces as well as the pore network of the PAN membrane.[72]

Early experiments by Patzer on the removal of bilirubin during albumin dialysis using a Cobe Centrysystem 300 HG dialyzer (second GmbH, Dransfeld, Germany) show what could be a shift to a higher order removal rate after about 180 min of contact time with 40 g L^{-1} BSA in PBS on the patient side and >4 g L^{-1} BSA in PBS on the dialysate side (Figure 6.1).[18] This phenomena was never explained, but we have speculated that it may have to do with an adsorbed albumin layer building up and reaching a critical concentration where additional transport mechanisms may begin to contribute to removal.

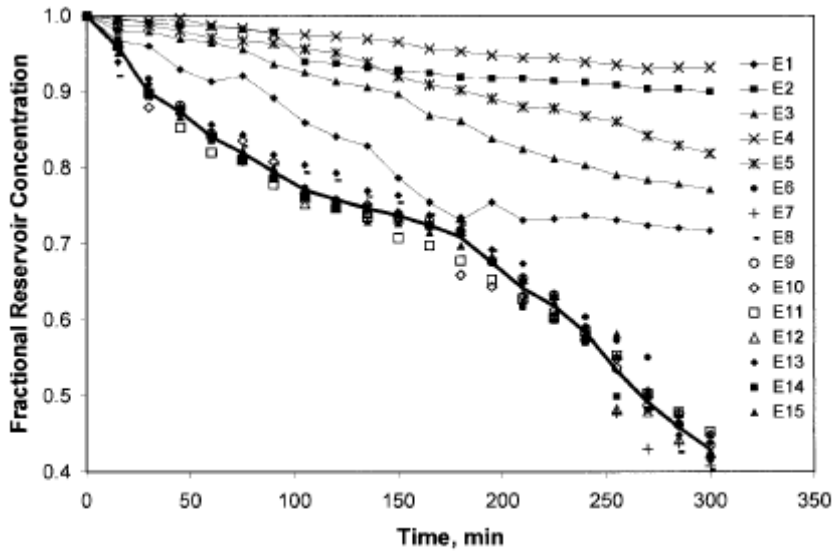

Figure 6.1. ***In vitro*** **patients consisting of BSA (40 g L^{-1}) in PBS spiked with unconjugated bilirubin were dialyzed against PBS (E1-E5) or PBS containing BSA (E6-E15) using pediatric cellulose acetate membranes. Removal for experiments using albumin containing dialysate all had essentially the same removal rate regardless of dialysate albumin concentration. The removal rate of bilirubin shows a distinctly different removal rate after 180 minutes of contact time. The change to a different removal rate was never explained, but the change in removal rate may be due to albumin penetrating the membrane and contributing additional removal mechanisms.**

The ability of albumin to bind to and enter the dialysis membrane may be one of the factors determining the rate of removal during an albumin dialysis procedure, and may be an important consideration in the choice of a dialyzer for use in albumin dialysis therapies. The goal of this work is to improve our understanding of the mechanism of removal during albumin dialysis by developing small scale hollow fiber dialyzers using commercial dialysis fibers to allow for the direct imaging of protein penetration into the fiber in real time. Small dialyzers designed for use in a microscopy facility also have potential as a platform for the examination of the Fahraeus-Lindquist effect (change in fluid viscosity with changes in capillary diameter as a

result of near wall cell free layer formation) in dialysis membranes and platelet margination in capillaries.

6.1 MATERIALS AND METHODS

Alexa 488 labeled BSA used was from Invitrogen (Carlsbad, CA). Dialysis fibers were excised from Exeltra cellulose triacetate (Baxter Healthcare Corporation, Deerfield, IL), Multiflow 60 AN69 (HOSPAL Industrie, Meyzieu, France), and Polyflux 11S polyarylethersulfone (Gambro Dialysatoren GmbH & Co. KG, Hechingen, Germany) commercial dialyzers (Figure 6.2 and Figure 6.3).

Figure 6.2. The commercial dialyzers used in our lab include (from left to right) Multiflow 60 AN69*, the pediatric Cobe Centrysystem 300 HG, the Gambro 500 HG hemophane, the Polyflux 11S polyarylethersulfone*, and the Exeltra cellulose triacetate dialyzers*. Dialyzer used in this experimentation are marked with *.

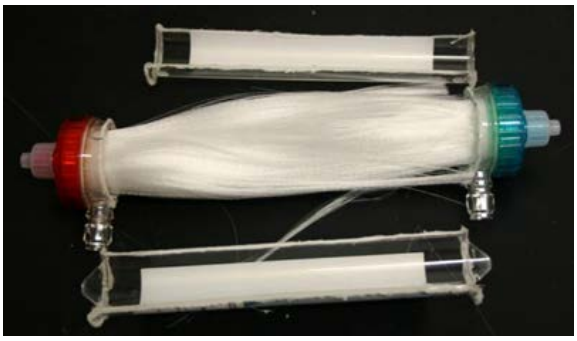

Figure 6.3. A high speed rotary tool was used to cut the shell off of the dialyzer to expose the membranes. The rotary tool was set to a high speed to melt the polycarbonate as it was cut to reduce the amount of dust generated.

Plastic shim stock (PETG, 0.03" thickness) (McMaster-Carr, Robbinsville, NJ) was cut to fit on the microscope stage (80x100 mm) and a 15 mm hole was cut to accommodate the microscope objective. A 45x50 mm coverslip (1.5 thickness) (Fisher Scientific, was affixed over the hole using general purpose (thick, non-flowable) silicone sealant (RTV sealant, 732 Multi-Purpose Sealant, Dow Corning Corporation, Midland, MI). Ten fibers were evenly spaced across the cover slip, and were affixed to the cover slip using general purpose silicone sealant. The fibers were gently pressed into the silicone so that they were in contact with the cover slip. Two lengths of microbore tygon tubing (2" length, 0.040" ID, 0.070" OD) (Saint-Gobain, Granville, NY), were positioned at the edge of the cover slip perpendicular to the fibers to create a cross flow configuration through the extracapillary space of the slide. A 50x50 mm (~0.03" thickness) borosilicate slide glass (Eastman Kodak Company, Rochester, NY) was placed on top of the slide to create a flow chamber around the fibers, and the glass was sealed in place using general purpose silicone sealant. The portion of the fibers outside of the glass chamber was then wetted with general purpose silicone sealant, gently gathered together, and allowed to dry overnight. A 4 cm piece of silicone tubing (0.125" ID, 0.188" OD) (Cole-Parmer, Vernon Hills,

IL) was slid over the fibers on both sides of the slide dialyzer, and the tubing was backfilled with flowable silicone sealant (RTV sealant, 734 Multi-Purpose Sealant, Dow Corning Corporation, Midland, MI) to encase the fibers. A razor blade was used to cut the tubing housing the fibers, opening the fibers to flow. A female to female luer lock connector (Value Plastics, Fort Collins, CO) with one side bored out to the OD of the tubing used to house the fibers was glued in place with flowable RTV silicone sealant. The area around the fibers and the edge of the slide glass was covered with flowable silicone to seal any leaks and gaps. After allowing the silicone to fully cure, the slides were connected to a syringe pump at a flow rate of 1.0 ml min^{-1} to test for leaks. A more complete procedure and diagrams are provided in Appendix D.

6.2 RESULTS

6.2.1 Slide dialyzer prototypes

Nine slide prototypes (four with AN69 membranes, four with Exeltra CTA membranes, and one with 100 kDa CTA albumin permeable membranes (expired research bioreactor hollow fiber cartridge provided by Excorp Medical) were created. During flow testing at 1 ml min^{-1}, prototype 1 (AN69-1, Figure 6.4) had several leaks around the sides of the slide glass and where the fiber bundle enters the luer fittings. After sealing the leaks with silicone grease (High vacuum grease, Dow Corning Corporation, Midland, MI) the slide maintained flow for 1hr without leaking, but was not used on a microscope owing to the risk of leaking. For the second generation device (prototype 2, AN69-2, Figure 6.5), the diameter of the shell space tubing was

reduced (from 0.063” ID, 0.125” OD to 0.040” ID, 0.070 OD) and flowable RTV sealant was used to seal the area around the slide and where the fiber bundle enters the luer fittings. The device was flow tested at 1 ml min^{-1} (fibers and shell in series) for approximately 5 minutes before the bottom cover slip burst (Figure 6.6).

The rest of the prototypes were already under construction when prototype 2 failed, and no changes were made in the design of prototypes 3-9 (Figure 6.7). Prototype 3 and prototype 4 were both flow tested for 1 hr at 1 ml/min flow rate (fibers and shell in series). Prototypes 5 through 8 were not flow tested, and prototype 9 was not completed.

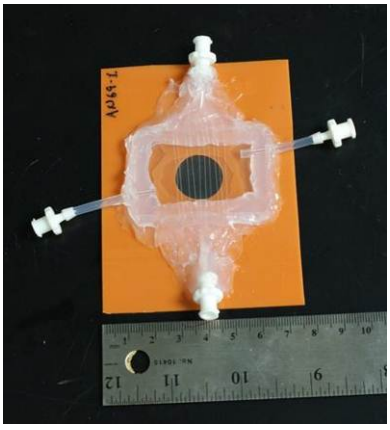

Figure 6.4. Prototype 1 (AN69-1) was the first attempt to create a slide dialyzer using fibers excised from a commercial dialyzer. The slide dialyzer was made using membranes from an AN69 commercial dialyzer. Flow testing was performed using a syringe pump at 0.25 ml min^{-1}. Leaks were found at several points around the slide and at the luer fitting encasing the fibers. Silicone grease was used to seal leaks, allowing the slide to hold a sustained flow of 1 ml min^{-1} for one hour during flow testing.

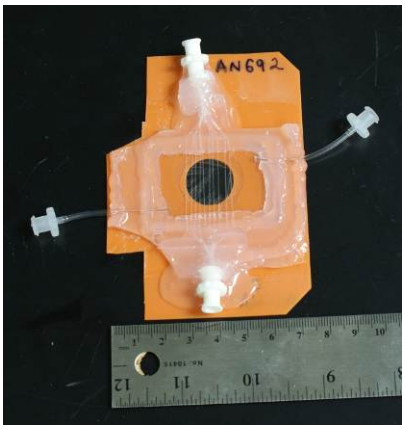

Figure 6.5. Prototype 2 (AN69-2) was the second prototype produced. Changes in the second generation prototype were smaller tubing for the extracapillary space and flowable RTV silicone sealant used to seal the space around the slide glass and the luer fitting with the fiber bundle. The notches in the plastic support are to accommodate the shape of the stage on the Leica confocal microscope used. Flow testing at 0.25 ml min^{-1} produced enough pressure in the shell space to burst the coverslip.

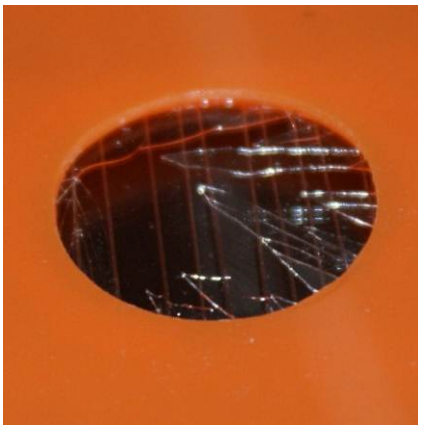

Figure 6.6. Prototype 2 (AN69-2) shown here from underneath. Once hooked up to a syringe pump at 0.25 ml min^{-1} pressure build up in the extra capillary space burst the coverslip.

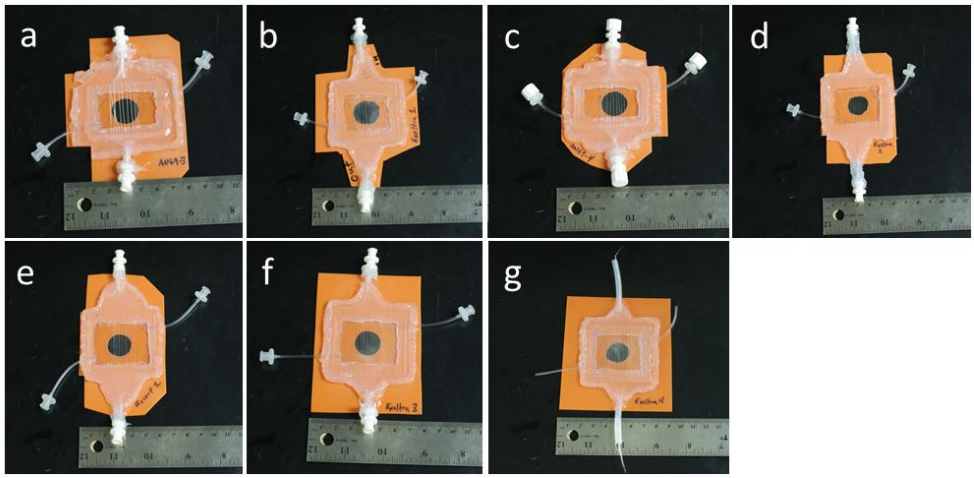

Figure 6.7. Prototype slide dialyzers. a: prototype 3 (AN69-3), b: prototype 4 (Exeltra-1), c: prototype 5 (AN69-4), d: prototype 6 (Exeltra-2), e: prototype 7 (Excorp-1), f: prototype 8 (Exeltra-3), and g: prototype 9 (Exeltra 4).

6.2.2 Fiber auto-fluorescence and fluorophore choice

Three fiber types were tested during these experiments, AN69, polysulfone (PS), and cellulose-triacetate (CTA). Dialysis membranes made from AN69 and cellulose triacetate are transparent, and the polysulfone membranes are opaque. The AN69 and polysulfone fibers tested in these experiments exhibit broad range autofluorescence, absorbing and emitting over the range of commonly used fluorescent tags (Figure 6.8 and Figure 6.9). Although the PS fibers tested are opaque, attempts were made to use 2-photon microscopy to image the fibers. Only the outer skin and proximate interior of the larger pores of the PS membrane could be seen. The inside of the PS fiber wall and the inner surface of the fiber could not be imaged.

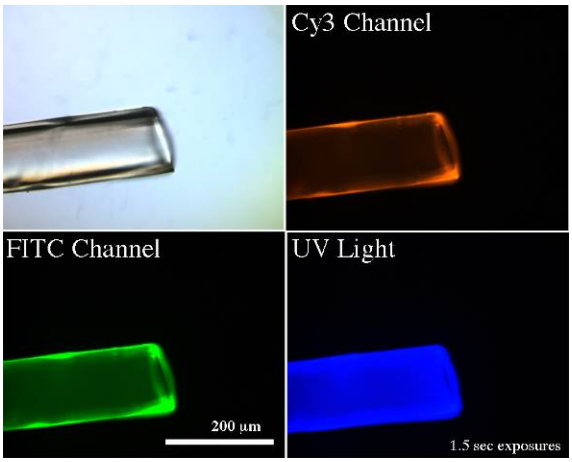

Figure 6.8. AN69 polyacylonitrile dialysis membranes exhibit broad range auto fluorescence. The fiber is shown here under bright field (top left), Cy3 channel (550 nm excitation, 570 nm emission), FITC channel (495 nm excitation, 520 nm emission), and unfiltered mercury vapor lamp UV excitation and unfiltered autofluoresence.

.

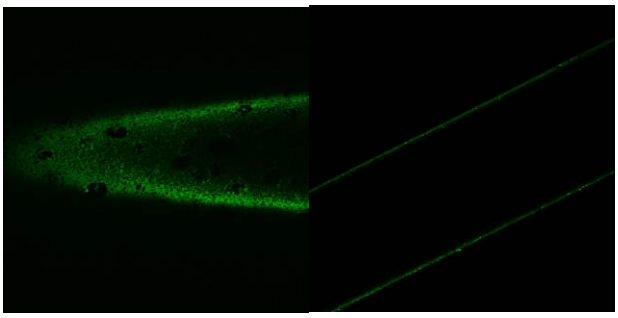

Figure 6.9. Polyethersulphone membranes (outer diameter=265 µm) are opaque, but have broad range autofluorescence over a broad range of excitation wavelengths. The membrane is shown here in its autofluorescence (excitation=488 nm, emission=520 nm) showing the pores at the surface (left) and at half depth (right).

Prototype 3 (AN69-3) was imaged on a Leica DMI 4000 B confocal microscope (Leica Microsystems Inc., Buffalo Grove, IL). Despite best efforts during fabrication to have the entire fiber length lie flat on the cover slip surface, all but one of the fibers were too far from the cover slip to image. A syringe was used to fill both the fiber lumen and the shell space with PBS, and

a cross section of the dialysis fiber at half depth was imaged (Figure 6.10). Without repositioning the slide, the fiber lumen was then filled with Alexa 488 labeled BSA. The fiber was again imaged at half depth. The labeled BSA can be clearly seen in the fiber lumen. No fluorescent signal was seen in the shell space indicating that there were no leaks from the fiber lumen flow path to the shell space of the slide dialyzer.

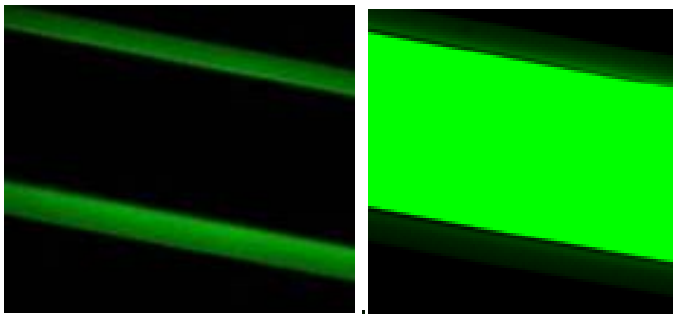

Figure 6.10. AN69-3 slide cartridge with polyacylonitrile dialysis membranes is shown here at half depth in its autofluorescence (excitation=488 nm, emission=520 nm) filled with PBS (left). A syringe was used to fill the lumen of the fiber with Alexa 488 labeled bovine albumin (Invitogen, Carlsbad, CA).

6.3 DISSCUSION AND CONCLUSIONS

The choice of an appropriate dialyzer for use in an albumin dialysis system could have a significant impact on its removal effectiveness. Although we know from experimentation done in our lab that significant differences exist in the removal capability of commercial dialyzers of the same nominal surface area when they are used for albumin dialysis, the reason for the difference is not clear. Slide dialyzers like those presented here have the potential to provide a platform to study some of the differences between optically transparent dialysis membranes, and

have the potential to provide real time concentration profiles of compounds passing through the dialysis membrane.

Although I was able to provide proof of concept, no information on the albumin penetration into the dialysis membranes was elucidated through this project. The slide dialyzers presented are a viable design, but the design has several flaws. The risk of breaking the cover slip from the pressure required to drive flow through the extra-capillary space was seen with the second device made. The cover slip breakage can be addressed in several ways. A slower flow rate will reduce the pressure in the extra-capillary space. The use of larger tubing for the extra-capillary space will reduce the pressure, but would increase the volume of the extra-capillary space. A thicker cover slip could be used, but that would require the use of longer working-distance microscope objectives than were available on the microscope used. In the tests done on the slide dialyzers the flow was driven using a syringe pump. Driving the extra-capillary space flow using suction will also mitigate the leakage that would be caused in the case of a break by stopping the flow as soon as suction is lost.

The auto-fluorescence that is seen with the dialysis fibers tested interferes with the signal that would be seen from the labeled albumin as it enters the fiber wall. In order to make accurate measurements of the concentration of the labeled protein, the noise from the fiber autofluorescence signal needs to be minimized. The fiber autofluorescence needs to be mapped to find an excitation/emission that minimally interferes with available fluorescent tags. This can be done by scanning the autofluorescence emission at the available laser wavelengths and choosing a fluorescent tag that will fall into a region of low background.

The use of small scale slide dialyzers has the potential to provide a method by which the interaction between commercial dialysis membranes and proteins during use without the need for

fixing the proteins and sectioning the fibers after use. In addition to the intended use of examining the penetration of albumin into the fiber wall, a slide dialyzer like those presented here could be used to examine the cell free layer formation that occurs in commercial dialysis fiber, platelet margenation in blood flow, and the interaction between the dialysis membrane with any type of cells in flow (red blood cells, leukocytes, or platelets).

APPENDIX A

SYMBOL DEFINITIONS

Symbol	Units	Definition
L	Liter	Volume in liters
mol	mole	Mass in moles
s	second	Time in seconds
g	gram	Mass in grams
dL	deciliter	Volume in deciliters (1 dL = 0.1 L)
m	meter	Length in meters
m^2	square meter	Area in square meters
°C	degree Celsius	Temperature in degrees Celsius
K	Kelvin	Temperature in Kelvin
J	Joule	Energy in Joules
nm	nanometer	Length in nanometers
RU	relative response units	Dimensionless relative response units
µg	microgram	Mass in microgram
mmol	millimole	Mass in millimoles
mL	milliliter	Volume in milliliters
µmol	micromole	Mass in micromoles
min	minutes	Time in minutes
mm	millimeters	Length in millimeters
"	inch	Length in inches

APPENDIX B

SPECIFIC AIM 1

B.1 Derivation of SPR curve fitting equations

The reaction at the surface of a sensor chip can be described as a reaction between a solute that is free in solution (*A*) and a reacting site on a molecule that has been bound to the surface (*B*) to form the complex AB (Figure B.1).

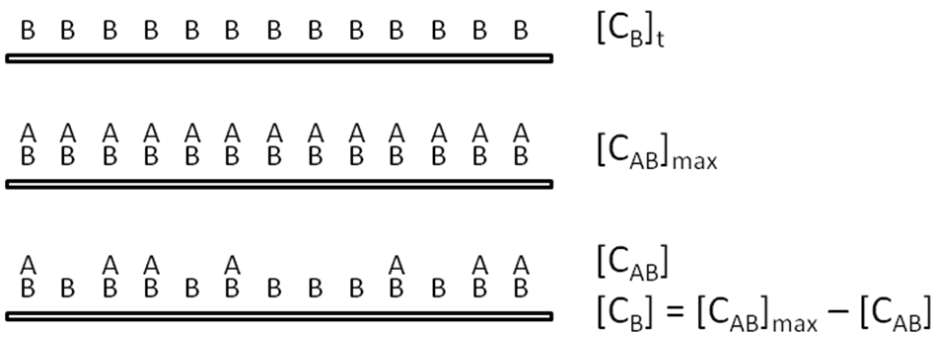

Figure B.1. Reactant B is bound to the sensor chip surface to form reacting sites, $[C_B]_t$ (top). If all of the available sites are occupied, the complex concentration reaches its theoretical maximum, $[C_{AB}]_{max}$ (middle). The concentrations of occupied and free sites are C_{AB} and C_B, respectively (bottom).

Biacore SPR tracks the rate of formation of the *AB* complex at the sensor chip surface. The formation of the complex proceeds according to the 1:1 reaction

$$A + B \underset{k_d}{\overset{k_a}{\rightleftharpoons}} AB$$ **Equation B.1**

Where k_a and k_d are the reaction rates of association and dissociation respectively. In the case that there is more than one type of binding site on the surface, the reactions are considered to be independent and the SPR response is additive. The rate of formation of the complex at the chip surface is

$$\frac{dC_{AB}}{dt} = k_a C_A C_B - k_d C_{AB}$$ **Equation B.2**

Where t is time and the C_i are the solute solution concentration, the concentration of free sites, and the concentration of the complex (subscripts A, B, and AB respectively). If the maximum concentration of the complex is $[C_{AB}]_{max}$, then the number of free sites, C_B, is

$$C_B = [C_{AB}]_{\max} - C_{AB}$$ **Equation B.3**

The mass balance (Equation B.3) can be substituted into Equation B.2

$$\frac{dC_{AB}}{dt} = k_a C_A ([C_{AB}]_{\max} - C_{AB}) - k_d C_{AB}$$ **Equation B.4**

The SPR response is considered to be proportional to the concentration of the complex at the sensor chip surface, and that proportionality is constant with changes in the complex concentration.

$$R = aC_{AB} \rightarrow R_{\max} = a[C_{AB}]_{\max} \qquad \textbf{Equation B.5}$$

where R is the SPR response, a is an arbitrary proportionality constant, and R_{max} is the theoretical maximum signal that is obtained is all of the sites on the surface are occupied. Using the relation in Equation B.5, Equation B.4 can now be put in terms of SPR response.

$$\frac{d(aR)}{dt} = k_a C_A(aR_{\max} - aR) - k_d aR$$
$$\downarrow \qquad \textbf{Equation B.6}$$
$$\frac{dR}{dt} = k_a C_A(R_{\max} - R) - k_d R$$

Equilibrium response analysis (determining K_B): When the reaction at the sensor chip's surface is at equilibrium, the rate of change of the SPR signal is zero.

$$\frac{dR}{dt} = 0 = k_a C_A(R_{\max} - R) - k_d R \qquad \textbf{Equation B.7}$$

The equilibrium binding constant (K_B) is the ratio of the rate of association (k_a) to the rate of dissociation (k_d) of the AB complex (Equation 4.2). Equation B.7 can now be put in terms of the equilibrium binding constant instead of the reaction rate constants by dividing through by k_d.

$$0 = \frac{k_a}{k_d} C_A R_{\max} - \frac{k_a}{k_d} C_A R - R$$

$$\downarrow$$

$$0 = K_B C_A R_{\max} - K_B C_A R - R$$

Equation B.8

The right hand side of Equation B.8 can now be solved for the equilibrium response value, R.

$$R = \frac{K_B C_A R_{\max}}{1 + K_B C_A}$$

Equation B.9

The scrubber software package fits Equation B.9 to the equilibrium SPR response data using a nonlinear least squares fitting method with K_B and R_{max} as the adjustable parameters. For a given solute-binder pair, Equation B.9 is globally fit to all of the data sets simultaneously

Transient response analysis (determining k_a *and* k_d*)*: To determine the reaction rate constants during the association phase of the experiment, Equation B.6 can be integrated and the transient response can be fit to the integrated equation.

$$\frac{dR}{dt} = k_a C_A (R_{\max} - R) - k_d R$$

$$\downarrow$$

$$\frac{dR}{dt} = \underbrace{k_a C_A R_{\max}}_{a} + R\underbrace{(-k_a C_A - k_d)}_{b}$$

Equation B.10

$$\downarrow$$

$$\int \frac{dR}{a + bR} = \int dt, \quad i.c: R\big|_{t=0} = 0$$

Integrating Equation B.10 with its initial conditions yields the equation for the response during the association phase as a function of time.

$$R = \frac{k_a C_A R_{\max}}{k_a C_A + k_d}(1 - e^{-(k_a C_A + k_d)t}) \qquad \textbf{Equation B.11}$$

Equation B.11 is fit to the association phase of the SPR response data by the Scrubber software package using a nonlinear least squares fitting method with k_a, k_d, and R_{max} as the adjustable parameters. For a given solute-binder pair, Equation B.11 is globally fit to all of the data sets simultaneously.

During the dissociation phase of the experiment k_a =0, making the rate of change of the SPR response curve

$$\frac{dR}{dt} = -k_d R \qquad \textbf{Equation B.12}$$

To determine the reaction rate constants during the dissociation phase of the experiment, Equation B.12 can be integrated and the transient response can be fit to the integrated rate equation.

$$\int \frac{dR}{R} = \int -k_d dt, \; i.c. \; R\big|_{t=t_0} = R_0 \qquad \textbf{Equation B.13}$$

where R_0 is the SPR response at t_0, which is the beginning of the dissociation phase. Integrating Equation B.13 with its initial condition yields the equation for the response during the dissociation phase as a function of time.

$$R = R_0 e^{-k_d (t - t_0)} \qquad \textbf{Equation B.14}$$

B.2 SPR response curves with curve fits

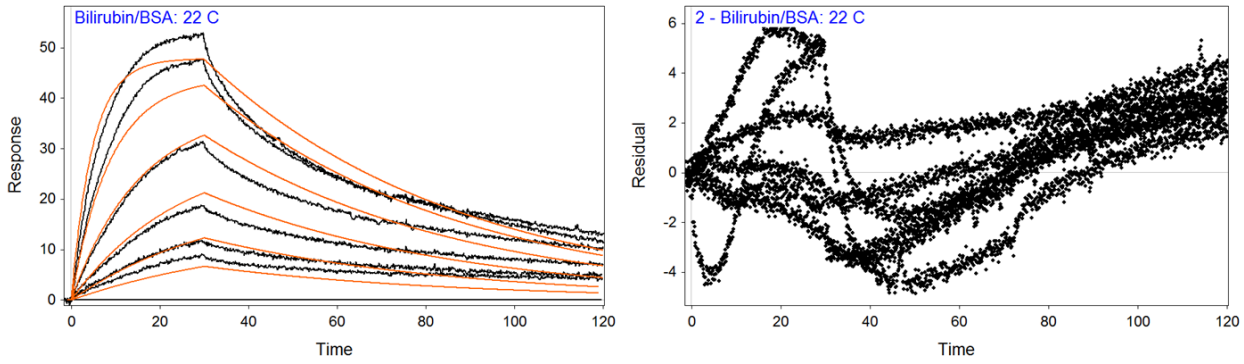

Figure B.2. SPR response (jagged curves) for bilirubin binding to BSA at 22°C (left) with rate equation curve fits (smooth lines, Equation 4.5 and Equation 4.6) using the non-linear curve fitting methods built into SCRUBBER-2. The association (k_a = 1.010(6)x10^5 L mole^{-1} s^{-1}) and dissociation (k_d = 0.175(2) s^{-1}) rates and maximal response (R_{max} = 52.21(6)) were the adjustable parameters in the fit. The residuals (residual=(data value)-(model fit value)) of the curve fit are shown at right. The SPR curves used for determining kinetic rate constants have the high concentration curves removed to restrict the binding reaction to the higher affinity binding site. Numbers in parentheses denote the error associated with the last significant digit.

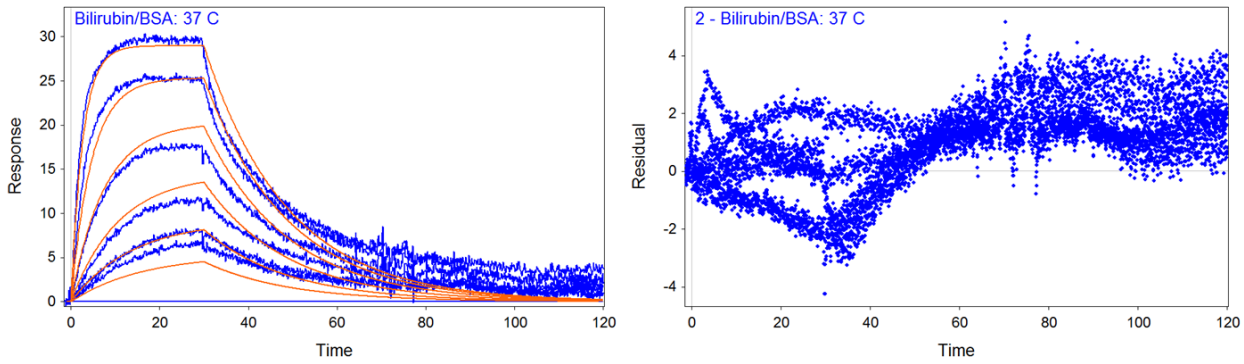

Figure B.3. SPR response (jagged curves) for bilirubin binding to BSA at 37°C (left) with rate equation curve fits (smooth lines, Equation 4.5 and Equation 4.6) using the non-linear curve fitting methods built into SCRUBBER-2. The association (k_a = 1.70(2)x10^5 L mol^{-1} s^{-1}) and dissociation (k_d = 0.535(8) s^{-1}) rates and maximal response (R_{max} = 33.81(8)) were the adjustable parameters in the fit. The residuals (residual=(data value)-(model fit value)) of the curve fit are shown at right. The SPR curves used for determining kinetic rate constants have the high concentration curves removed to restrict the binding reaction to the higher affinity binding site. Numbers in parentheses denote the error associated with the last significant digit.

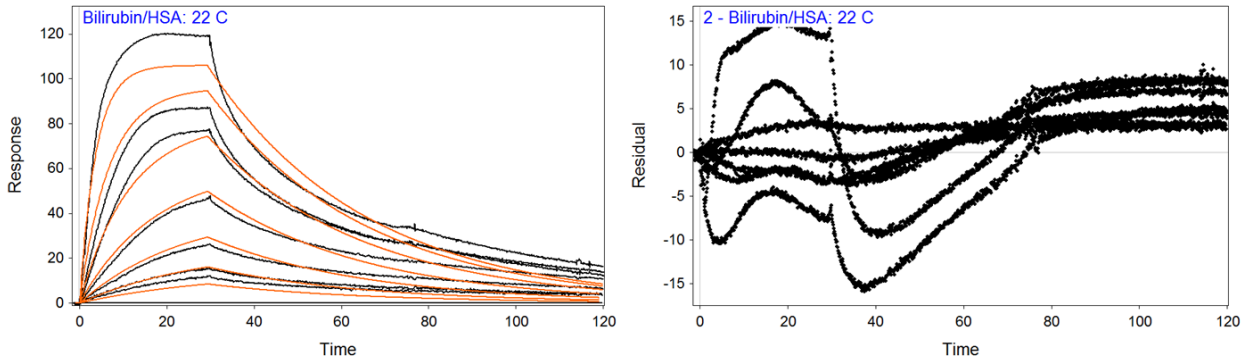

Figure B.4. SPR response (jagged curves) for bilirubin binding to HSA at 22°C (left) with rate equation curve fits (smooth lines, Equation 4.5 and Equation 4.6) using the non-linear curve fitting methods built into SCRUBBER-2. The association (k_a = 6.55(5)x10^4 L mole^{-1} s^{-1}) and dissociation (k_d = 0.0282(3) s^{-1}) rates and maximal response (R_{max} = 118.3(3)) were the adjustable parameters in the fit. The residuals (residual=(data value)-(model fit value)) of the curve fit are shown at right. The SPR curves used for determining kinetic rate constants have the high concentration curves removed to restrict the binding reaction to the higher affinity binding site. Numbers in parentheses denote the error associated with the last significant digit.

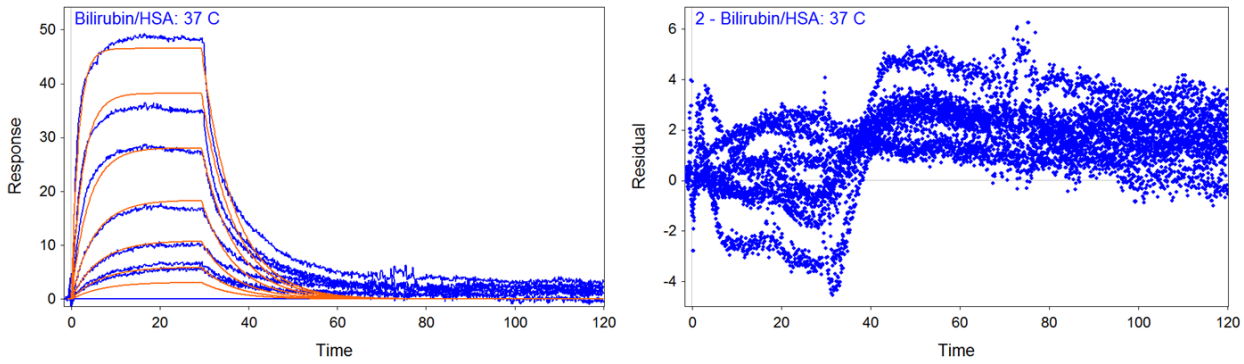

Figure B.5. SPR response (jagged curves) for bilirubin binding to HSA at 37°C (left) with rate equation curve fits (smooth lines, Equation 4.5 and Equation 4.6) using the non-linear curve fitting methods built into SCRUBBER-2. The association (k_a = 1.60(4)x10^5 L mol^{-1} s^{-1}) and dissociation (k_d = 0.128(3) s^{-1}) rates and maximal response (R_{max} = 59.6(5)) were the adjustable parameters in the fit. The residuals (residual=(data value)-(model fit value)) of the curve fit are shown at right. The SPR curves used for determining kinetic rate constants have the high concentration curves removed to restrict the binding reaction to the higher affinity binding site. Numbers in parentheses denote the error associated with the last significant digit.

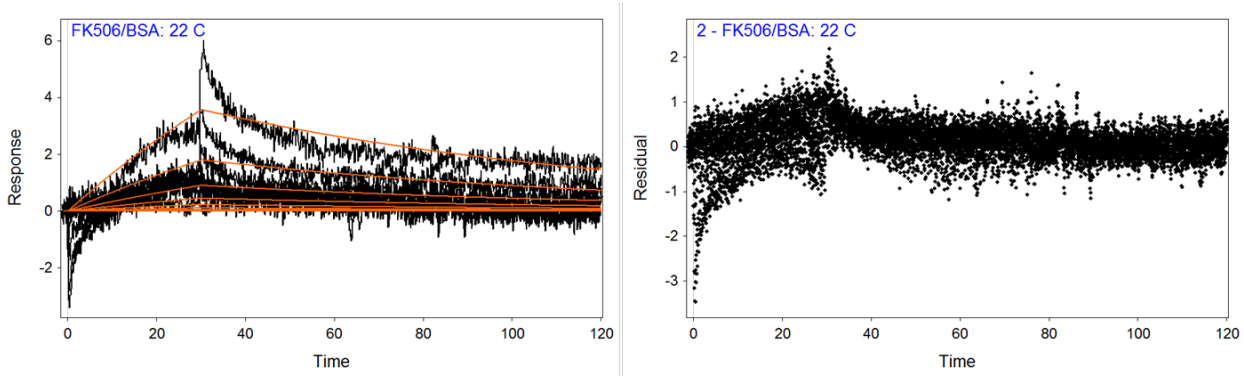

Figure B.6. SPR response (jagged curves) for FK506 binding to BSA at 22°C (left) with rate equation curve fits (smooth lines, Equation 4.5 and Equation 4.6) using the non-linear curve fitting methods built into SCRUBBER-2. The association (k_a = 94.4(6) L mol^{-1} s^{-1}) and dissociation (k_d = 0.0100(1) s^{-1}) rates and maximal response (R_{max} = 99(1)) were the adjustable parameters in the fit. The residuals (residual=(data value)-(model fit value)) of the curve fit are shown at right. The SPR curves used for determining kinetic rate constants have the high concentration curves removed to restrict the binding reaction to the higher affinity binding site. Numbers in parentheses denote the error associated with the last significant digit.

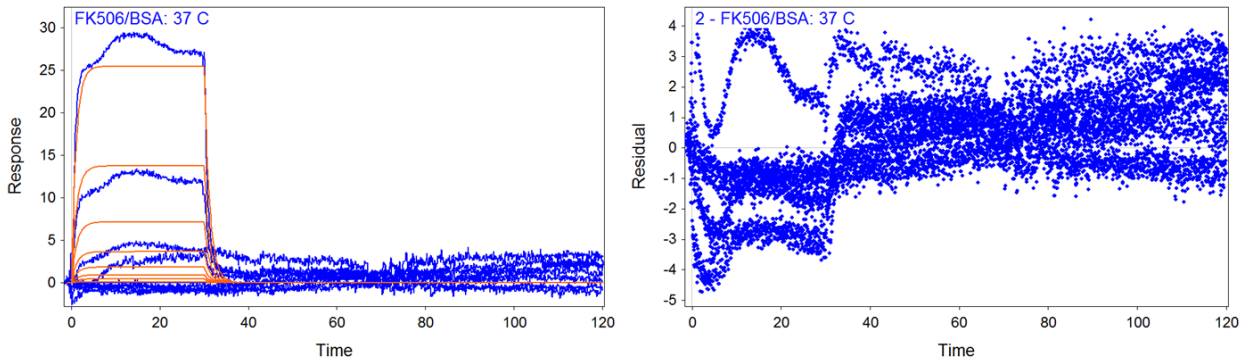

Figure B.7. SPR response (jagged curves) for FK506 binding to BSA at 37°C (left) with rate equation curve fits (smooth lines, Equation 4.5 and Equation 4.6) using the non-linear curve fitting methods built into SCRUBBER-2. The association (k_a = 9.3(2)x10^3).1 L mol^{-1} s^{-1}) and dissociation (k_d = 0.81(1) s^{-1}) rates and maximal response (R_{max} = 172.3(4)) were the adjustable parameters in the fit. The residuals (residual=(data value)-(model fit value)) of the curve fit are shown at right. The SPR curves used for determining kinetic rate constants have the high concentration curves removed to restrict the binding reaction to the higher affinity binding site. Numbers in parentheses denote the error associated with the last significant digit.

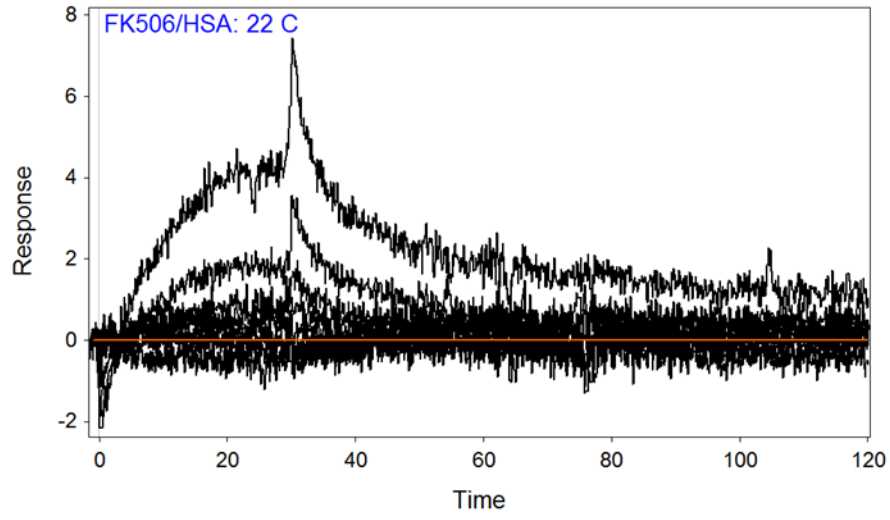

Figure B.8. The SPR response for FK506 binding to HSA at 22°C could not be used for curve fitting with the rate equations (Equation 4.5 and Equation 4.6) using the non-linear curve fitting methods built into SCRUBBER-2. The fit tolerances could not be met by the software solvers.

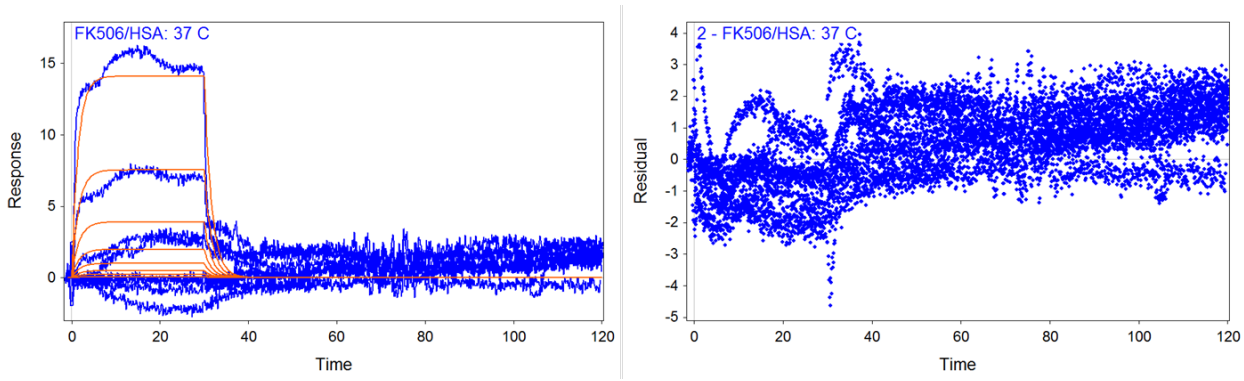

Figure B.9. SPR response (jagged curves) for FK506 binding to HSA at 37°C (left) with rate equation curve fits (smooth lines, Equation 4.5 and Equation 4.6) using the non-linear curve fitting methods built into SCRUBBER-2. The association (k_a = 6.0(5)x10^3 L mol^{-1} s^{-1}) and dissociation (k_d = 0.60(1) s^{-1}) rates and maximal response (R_{max} = 108.2(3)) were the adjustable parameters in the fit. The residuals (residual=(data value)-(model fit value)) of the curve fit are shown at right. The SPR curves used for determining kinetic rate constants have the high concentration curves removed to restrict the binding reaction to the higher affinity binding site. Numbers in parentheses denote the error associated with the last significant digit.

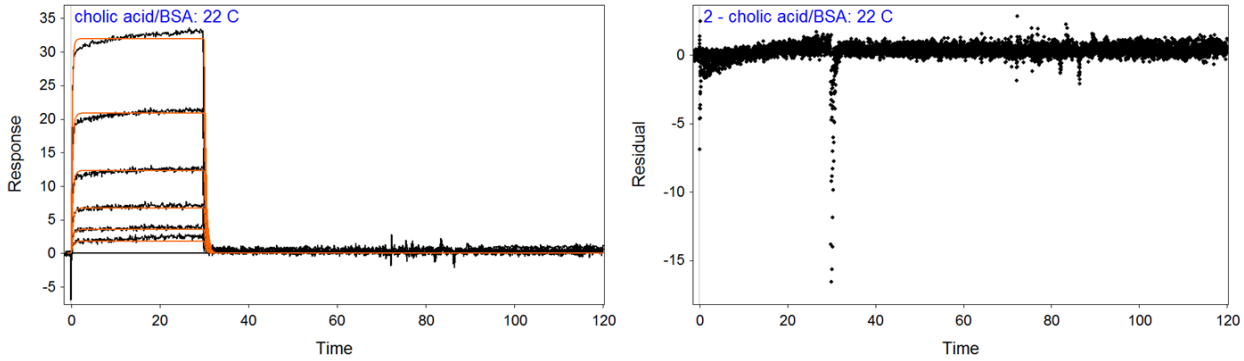

Figure B.10. SPR response (jagged curves) for cholic acid binding to BSA at 22°C (left) with rate equation curve fits (smooth lines, Equation 4.5 and Equation 4.6) using the non-linear curve fitting methods built into SCRUBBER-2. The association (k_a = 1.09(3)x10^5 L mol^{-1} s^{-1}) and dissociation (k_d = 2.33(6) s^{-1}) rates and maximal response (R_{max} = 68.5(1)) were the adjustable parameters in the fit. The residuals (residual=(data value)-(model fit value)) of the curve fit are shown at right. The SPR curves used for determining kinetic rate constants have the high concentration curves removed to restrict the binding reaction to the higher affinity binding site. Numbers in parentheses denote the error associated with the last significant digit.

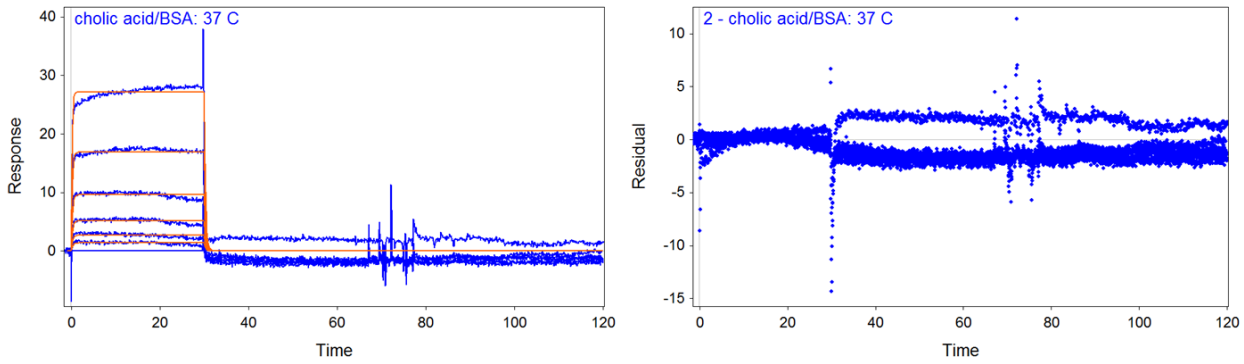

Figure B.11. SPR response (jagged curves) for cholic acid binding to BSA at 37°C (left) with rate equation curve fits (smooth lines, Equation 4.5 and Equation 4.6) using the non-linear curve fitting methods built into SCRUBBER-2. The association (k_a = 1.10(4)x10^5 L mol^{-1} s^{-1}) and dissociation (k_d = 3.2(1) s^{-1}) rates and maximal response (R_{max} = 69.4(1)) were the adjustable parameters in the fit. The residuals (residual=(data value)-(model fit value)) of the curve fit are shown at right. The SPR curves used for determining kinetic rate constants have the high concentration curves removed to restrict the binding reaction to the higher affinity binding site. Numbers in parentheses denote the error associated with the last significant digit.

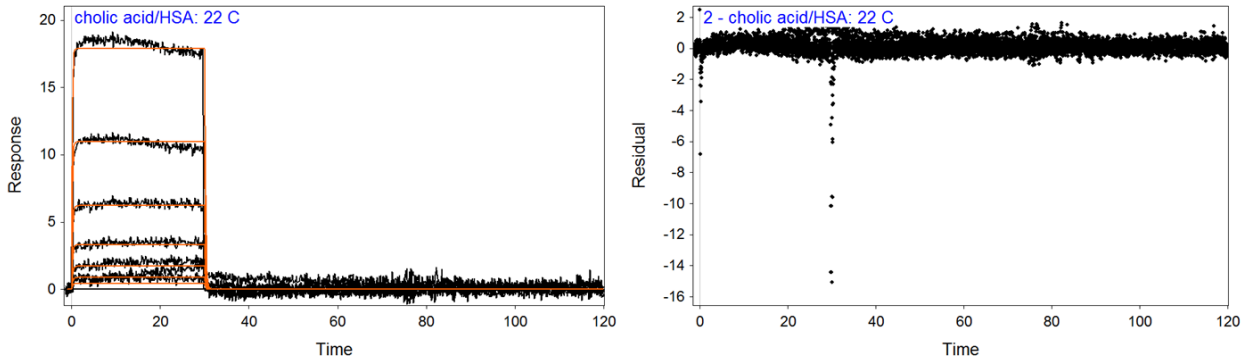

Figure B.12. SPR response (jagged curves) for cholic acid binding to HSA at 22°C (left) with rate equation curve fits (smooth lines, Equation 4.5 and Equation 4.6) using the non-linear curve fitting methods built into SCRUBBER-2. The association (k_a = 7.2(3)x10^4 L mol^{-1} s^{-1}) and dissociation (k_d = 4.5(2) s^{-1}) rates and maximal response (R_{max} = 47.70(9)) were the adjustable parameters in the fit. The residuals (residual=(data value)-(model fit value)) of the curve fit are shown at right. The SPR curves used for determining kinetic rate constants have the high concentration curves removed to restrict the binding reaction to the higher affinity binding site. Numbers in parentheses denote the error associated with the last significant digit.

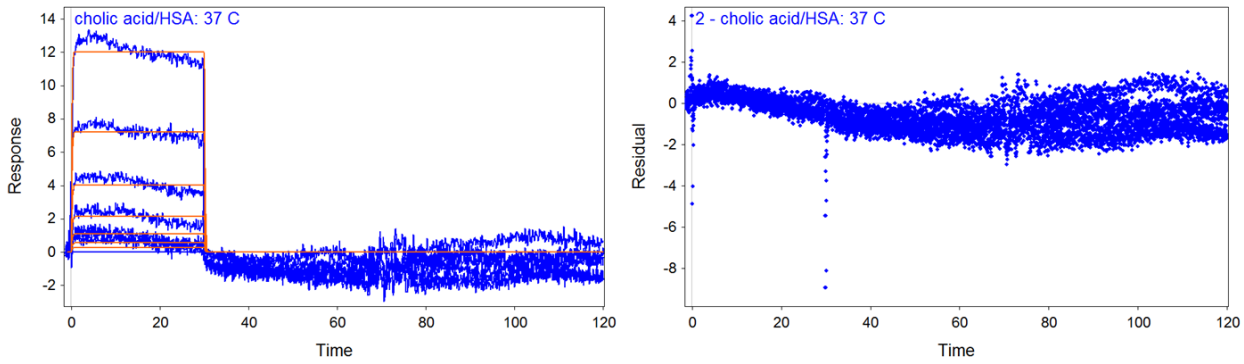

Figure B.13. SPR response (jagged curves) for cholic acid binding to HSA at 37°C (left) with rate equation curve fits (smooth lines, Equation 4.5 and Equation 4.6) using the non-linear curve fitting methods built into SCRUBBER-2. The association (k_a = 8.7(7)x10^4 L mol^{-1} s^{-1}) and dissociation (k_d = 6.4(5) s^{-1}) rates and maximal response (R_{max} = 35.6(1)) were the adjustable parameters in the fit. The residuals (residual=(data value)-(model fit value)) of the curve fit are shown at right. The SPR curves used for determining kinetic rate constants have the high concentration curves removed to restrict the binding reaction to the higher affinity binding site. Numbers in parentheses denote the error associated with the last significant digit.

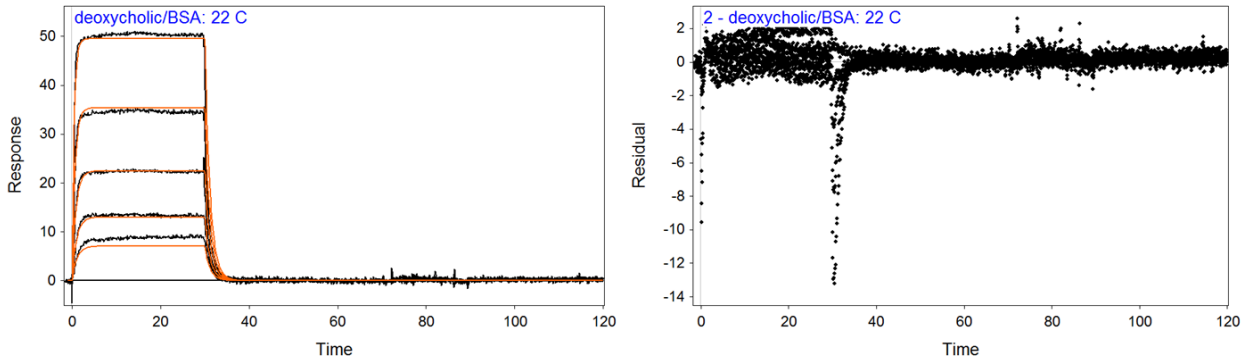

Figure B.14. SPR response (jagged curves) for deoxycholic acid binding to BSA at 22°C (left) with rate equation curve fits (smooth lines, Equation 4.5 and Equation 4.6) using the non-linear curve fitting methods built into SCRUBBER-2. The association (k_a = 1.35(1)x10^5 L mol^{-1} s^{-1}) and dissociation (k_d = 0.845(8) s^{-1}) rates and maximal response (R_{max} = 82.57(8)) were the adjustable parameters in the fit. The residuals (residual=(data value)-(model fit value)) of the curve fit are shown at right. The SPR curves used for determining kinetic rate constants have the high concentration curves removed to restrict the binding

reaction to the higher affinity binding site. Numbers in parentheses denote the error associated with the last significant digit.

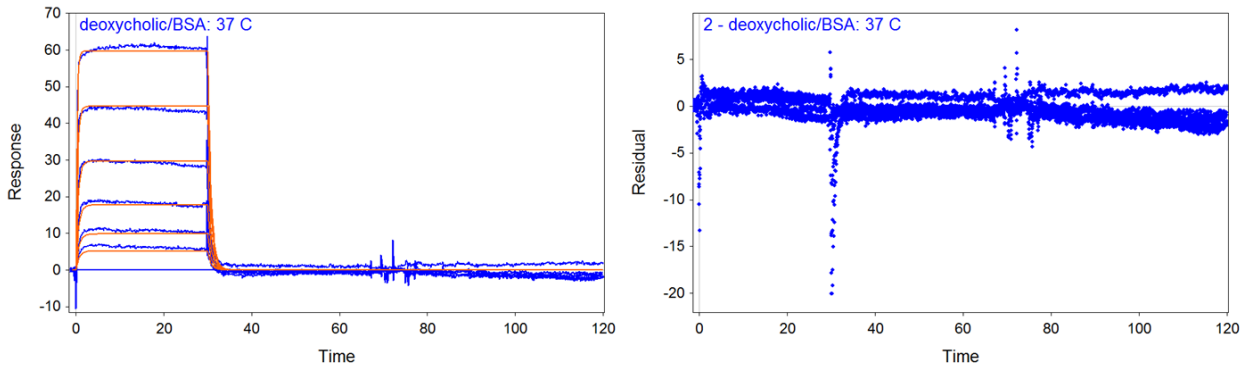

Figure B.15. SPR response (jagged curves) for deoxycholic acid binding to BSA at 37°C (left) with rate equation curve fits (smooth lines, Equation 4.5 and Equation 4.6) using the non-linear curve fitting methods built into SCRUBBER-2. The association (k_a = 1.41(1)x10^5 L mol^{-1} s^{-1}) and dissociation (k_d = 1.35(1) s^{-1}) rates and maximal response (R_{max} = 90.25(7)) were the adjustable parameters in the fit. The residuals (residual=(data value)-(model fit value)) of the curve fit are shown at right. The SPR curves used for determining kinetic rate constants have the high concentration curves removed to restrict the binding reaction to the higher affinity binding site. Numbers in parentheses denote the error associated with the last significant digit.

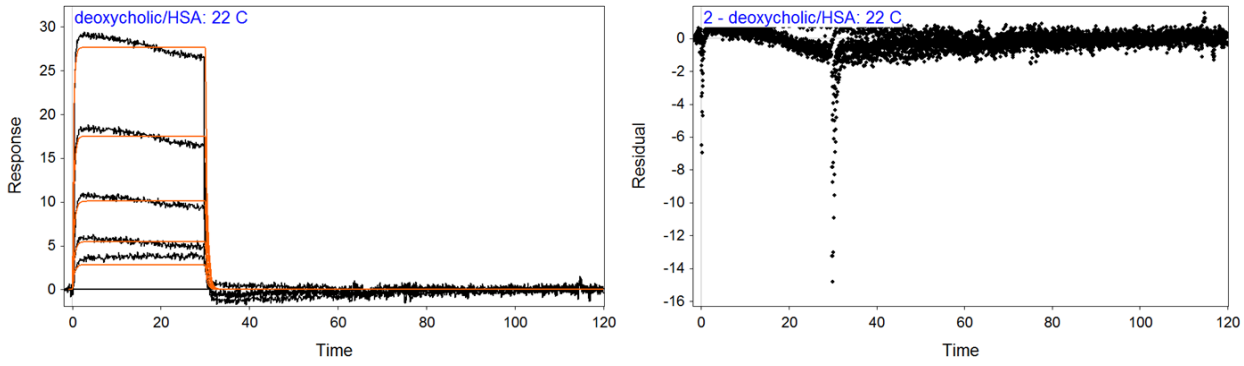

Figure B.16. SPR response (jagged curves) for deoxycholic acid binding to HSA at 22°C (left) with rate equation curve fits (smooth lines, Equation 4.5 and Equation 4.6) using the non-linear curve fitting methods

built into SCRUBBER-2. The association (k_a = 1.62(3)x10^5 L mol^{-1} s^{-1}) and dissociation (k_d = 2.09(4) s^{-1}) rates and maximal response (R_{max} = 65.74(9)) were the adjustable parameters in the fit. The residuals (residual=(data value)-(model fit value)) of the curve fit are shown at right. The SPR curves used for determining kinetic rate constants have the high concentration curves removed to restrict the binding reaction to the higher affinity binding site. Numbers in parentheses denote the error associated with the last significant digit.

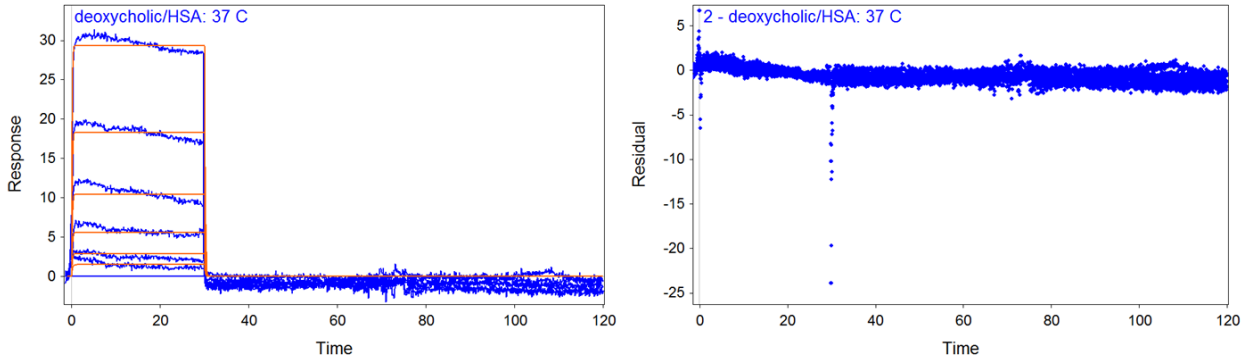

Figure B.17. SPR response (jagged curves) for deoxycholic acid binding to HSA at 37°C (left) with rate equation curve fits (smooth lines, Equation 4.5 and Equation 4.6) using the non-linear curve fitting methods built into SCRUBBER-2. The association (k_a = 2.13(7)x10^5 L mol^{-1} s^{-1}) and dissociation (k_d = 6.1(2) s^{-1}) rates and maximal response (R_{max} = 74.2(1)) were the adjustable parameters in the fit. The residuals (residual=(data value)-(model fit value)) of the curve fit are shown at right. The SPR curves used for determining kinetic rate constants have the high concentration curves removed to restrict the binding reaction to the higher affinity binding site. Numbers in parentheses denote the error associated with the last significant digit.

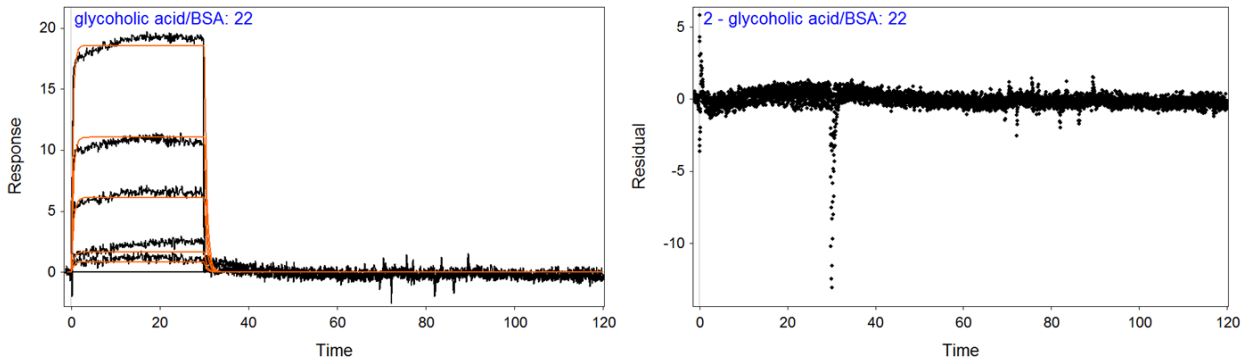

Figure B.18. SPR response (jagged curves) for glycocholic acid binding to BSA at 22°C (left) with rate equation curve fits (smooth lines, Equation 4.5 and Equation 4.6) using the non-linear curve fitting methods built into SCRUBBER-2. The association (k_a = 4.4(2)x10^4 L mol^{-1} s^{-1}) and dissociation (k_d = 1.77(6) s^{-1}) rates and maximal response (R_{max} = 58.5(2)) were the adjustable parameters in the fit. The residuals (residual=(data value)-(model fit value)) of the curve fit are shown at right. The SPR curves used for determining kinetic rate constants have the high concentration curves removed to restrict the binding reaction to the higher affinity binding site. Numbers in parentheses denote the error associated with the last significant digit.

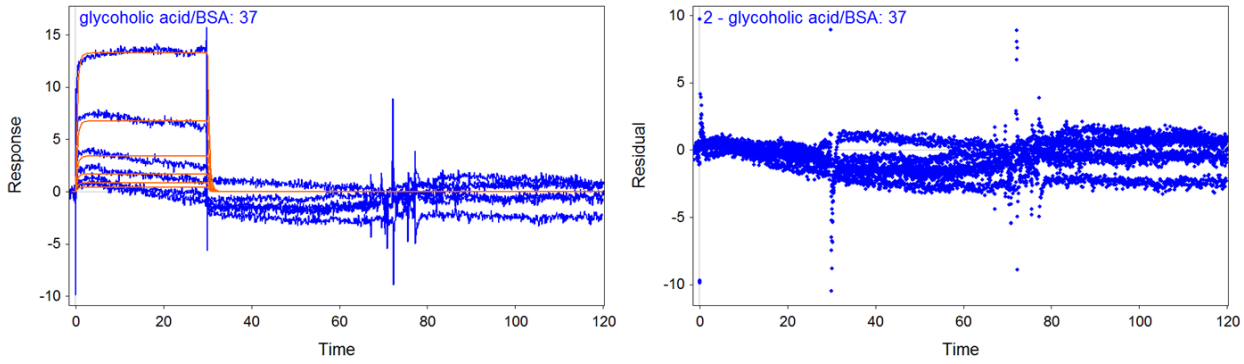

Figure B.19. SPR response (jagged curves) for glychoic acid binding to BSA at 37°C (left) with rate equation curve fits (smooth lines, Equation 4.5 and Equation 4.6) using the non-linear curve fitting methods built into SCRUBBER-2. The association (k_a = 4(2)x10^3 L mol^{-1} s^{-1}) and dissociation (k_d = 2.4(1) s^{-1}) rates and maximal response (R_{max} = 438(2)) were the adjustable parameters in the fit. The residuals (residual=(data value)-(model fit value)) of the curve fit are shown at right. The SPR curves used for determining kinetic rate

constants have the high concentration curves removed to restrict the binding reaction to the higher affinity binding site. Numbers in parentheses denote the error associated with the last significant digit.

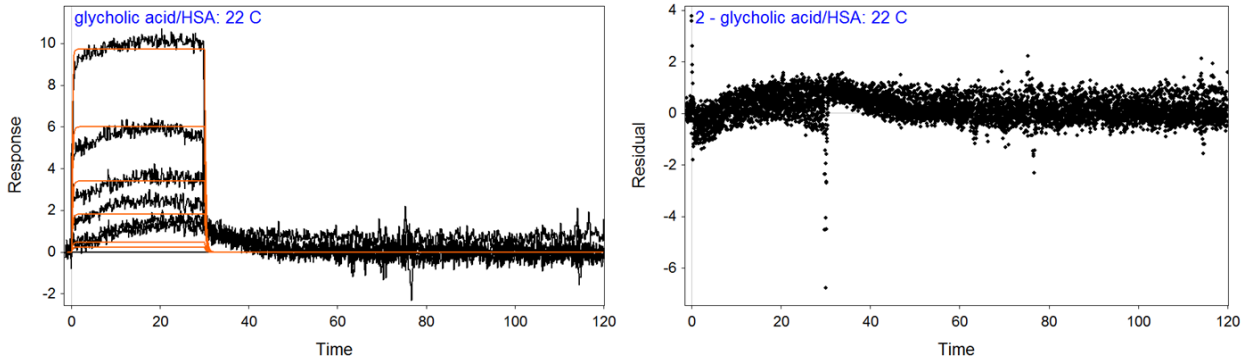

Figure B.20. SPR response (jagged curves) for glycocholic acid binding to HSA at 22°C (left) with rate equation curve fits (smooth lines, Equation 4.5 and Equation 4.6) using the non-linear curve fitting methods built into SCRUBBER-2. The association (k_a = 6.1(5)x10^4 L mol^{-1} s^{-1}) and dissociation (k_d = 3.7(3) s^{-1}) rates and maximal response (R_{max} = 25.45(9)) were the adjustable parameters in the fit. The residuals (residual=(data value)-(model fit value)) of the curve fit are shown at right. The SPR curves used for determining kinetic rate constants have the high concentration curves removed to restrict the binding reaction to the higher affinity binding site. Numbers in parentheses denote the error associated with the last significant digit.

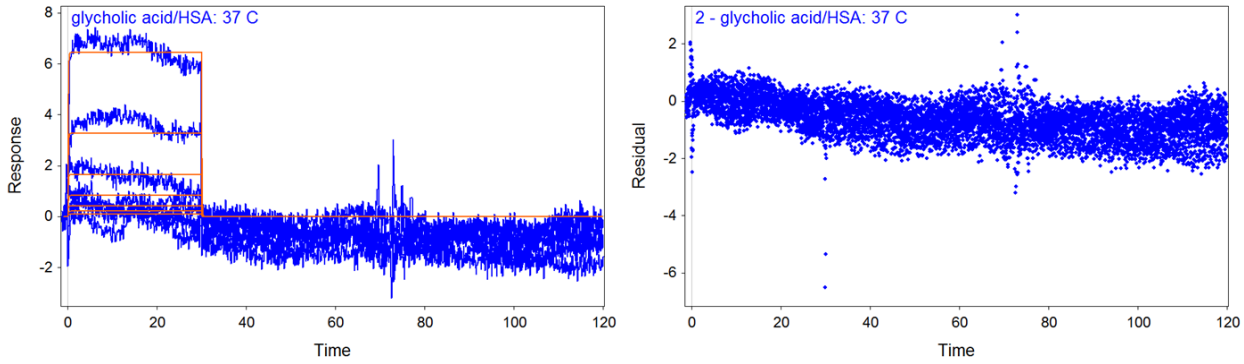

Figure B.21. SPR response (jagged curves) for glycocholic acid binding to HSA at 37°C (left) with rate equation curve fits (smooth lines, Equation 4.5 and Equation 4.6) using the non-linear curve fitting methods

built into SCRUBBER-2. The association (k_a = 1.1(8)x10^4 L mol^{-1} s^{-1}) and dissociation (k_d = 13(2) s^{-1}) rates and maximal response (R_{max} = 213(1)) were the adjustable parameters in the fit. The residuals (residual=(data value)-(model fit value)) of the curve fit are shown at right. The SPR curves used for determining kinetic rate constants have the high concentration curves removed to restrict the binding reaction to the higher affinity binding site. Numbers in parentheses denote the error associated with the last significant digit.

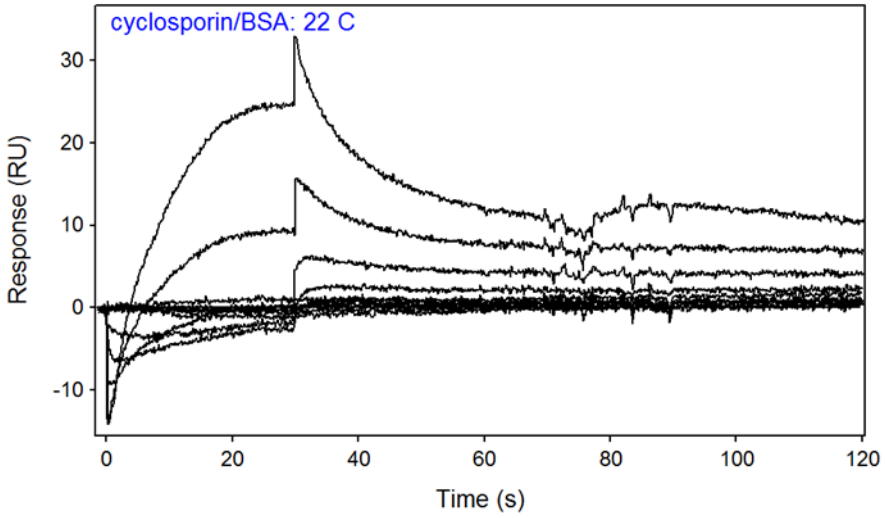

Figure B.22. The SPR response for cyclosporin A binding to BSA at 22°C could not be used for curve fitting with the rate equations (Equation 4.5 and Equation 4.6) using the non-linear curve fitting methods built into SCRUBBER-2. The fit tolerances could not be met by the software solvers.

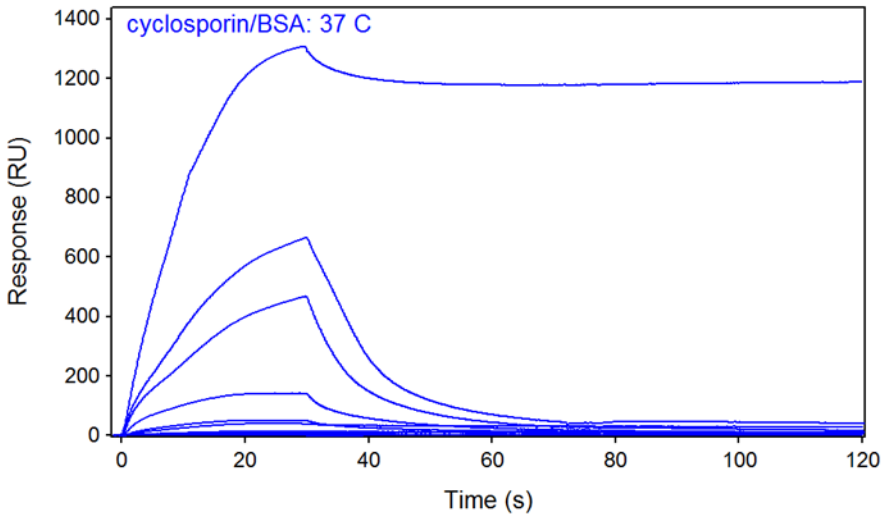

Figure B.23. The SPR response for cyclosporin A binding to BSA at 37°C could not be used for curve fitting with the rate equations (Equation 4.5 and Equation 4.6) using the non-linear curve fitting methods built into SCRUBBER-2. The unusually high response for the size of the cyclosporine A molecule is indicative of aggregates of the solute binding with the surface.

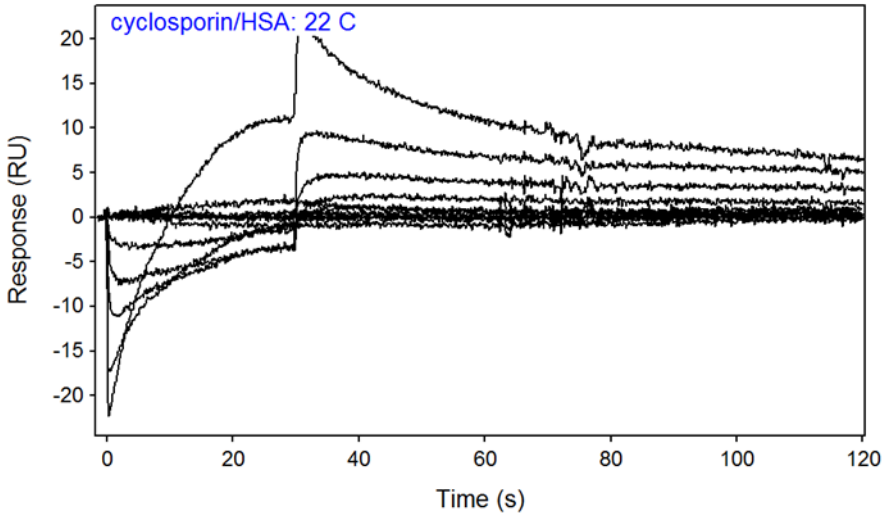

Figure B.24. The SPR response for cyclosporin A binding to HSA at 22°C could not be used for curve fitting with the rate equations (Equation 4.5 and Equation 4.6) using the non-linear curve fitting methods built into SCRUBBER-2. The fit tolerances could not be met by the software solvers.

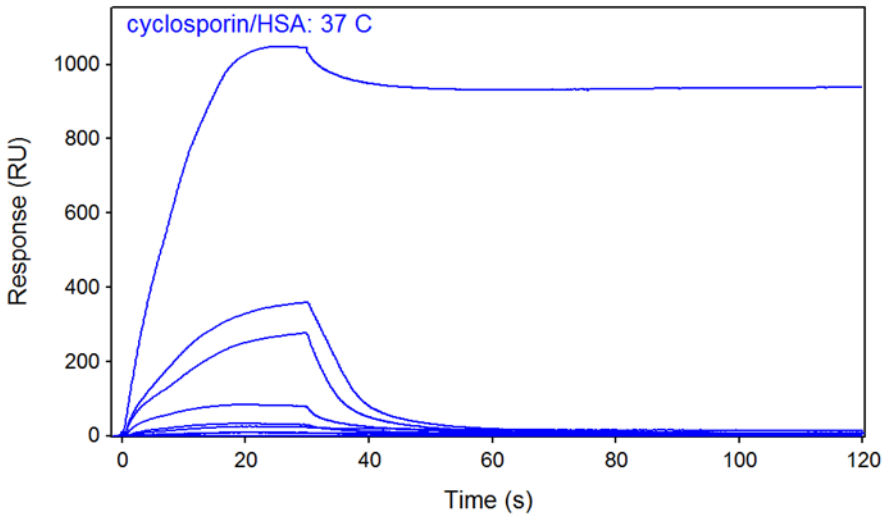

Figure B.25. The SPR response for cyclosporin A binding to BSA at 37°C could not be used for curve fitting with the rate equations (Equation 4.5 and Equation 4.6) using the non-linear curve fitting methods built into SCRUBBER-2. The unusually high response for the size of the cyclosporine A molecule is indicative of aggregates of the solute binding with the surface.

B.3 Binding constant detailed results

Table B.1. BSA/small molecule equilibrium dissociation constants (K_D, mol L^{-1}) obtained by fitting the equilibrium portion of SPR response curves for a binding pair at a given temperature to Equation 4.5. K_{D1}, K_{D2}, and the R_{max} values (K_{D1} and K_{D2} have separate R_{max} values associated with them) were the adjustable parameters in the curve fits. The number in the parentheses is the error associated with the last digit. For example for bilirubin at 22°C $K_{D1}=970x10^{-9} \pm 20x10^{-9}$.

		K_{D1}	% error	Rmax	K_{D2}	% error	Rmax
Bilirubin	22°C	970(20) nM	2.1	89.8(7)	----	----	----
	37°C	1.19(4) µM	3.4	55.0(6)	----	----	----
FK506	22°C	960(70) µM	7.3	200	----	----	----
	37°C	75.2(7) uM	0.9	200	----	----	----
Colic acid	22°C	11.4(3) uM	0.7	32.1(6)	168(3) uM	1.8	117.3(3)
	37°C	19.1(3) uM	1.6	44.6(7)	370(20) uM	5.4	102(1)
Deoxycholic acid	22°C	6.9(1) uM	1.4	79.0(9)	330(10) uM	3.0	259(3)
	37°C	7.4(1) uM	1.4	67.8(8)	320(10) uM	3.1	242(3)
Glycocholic acid	22°C	41(4) uM	9.8	39(6)	350(50) uM	14.3	123.19
	37°C	60(5) uM	8.3	40(3)	620(60) uM	9.7	123.19

Table B.2. HSA/small molecule equilibrium dissociation constants (K_D, mol L^{-1}) obtained by fitting the equilibrium portion of SPR response curves for a binding pair at a given temperature to Equation 4.5. K_{D1}, K_{D2}, and the R_{max} values (K_{D1} and K_{D2} have separate R_{max} values associated with them) were the adjustable parameters in the curve fits. The number in the parentheses is the error associated with the last digit. For example for bilirubin at 22°C $K_{D1}=1.00\text{x}10^{-6} \pm 0.02\text{x}10^{-6}$.

		KD1	% error	Rmax	KD2	% error	Rmax
Bilirubin	22°C	1.00(2) uM	2.0	144.4(8)	----	----	----
	37°C	2.08(6) uM	2.9	80.4(8)	----	----	----
FK506	22°C	730(20) uM	2.7	200	----	----	----
	37°C	158(1) uM	0.6	200	----	----	----
Colic acid	22°C	42(2) uM	4.8	17(2)	280(20) uM	7.1	92.32
	37°C	64.2(9) uM	1.4	17	503(2) uM	0.4	92.32
Deoxycholic acid	22°C	11.6(1) uM	0.9	54.4(4)	550(10) uM	1.8	270(3)
	37°C	18.9(3) uM	1.6	42.1(6)	640(20) uM	3.1	327(4)
Glycocholic acid	22°C	81(2) uM	2.5	20	4(1) mM	25.0	400(1)
	37°C	166(5) uM	3.0	20	5(1) mM	20.0	400(1)

APPENDIX C

SPECIFIC AIM 2

C.1 Equation derivations

A schematic of the shell balance used in deriving equations is provided in Figure C.1. For dimensional consistency parameters are presented with SI units. A conventional dialysis cartridge consists of several thousand semipermeable hollow fibers encased in a plastic shell. Blood flows through the inner lumens of the fibers, and sweep fluid (called dialysate) flows outside of the fibers countercurrent to the blood stream. The “cleaned blood” that exits the dialyzer is then returned to the patient.

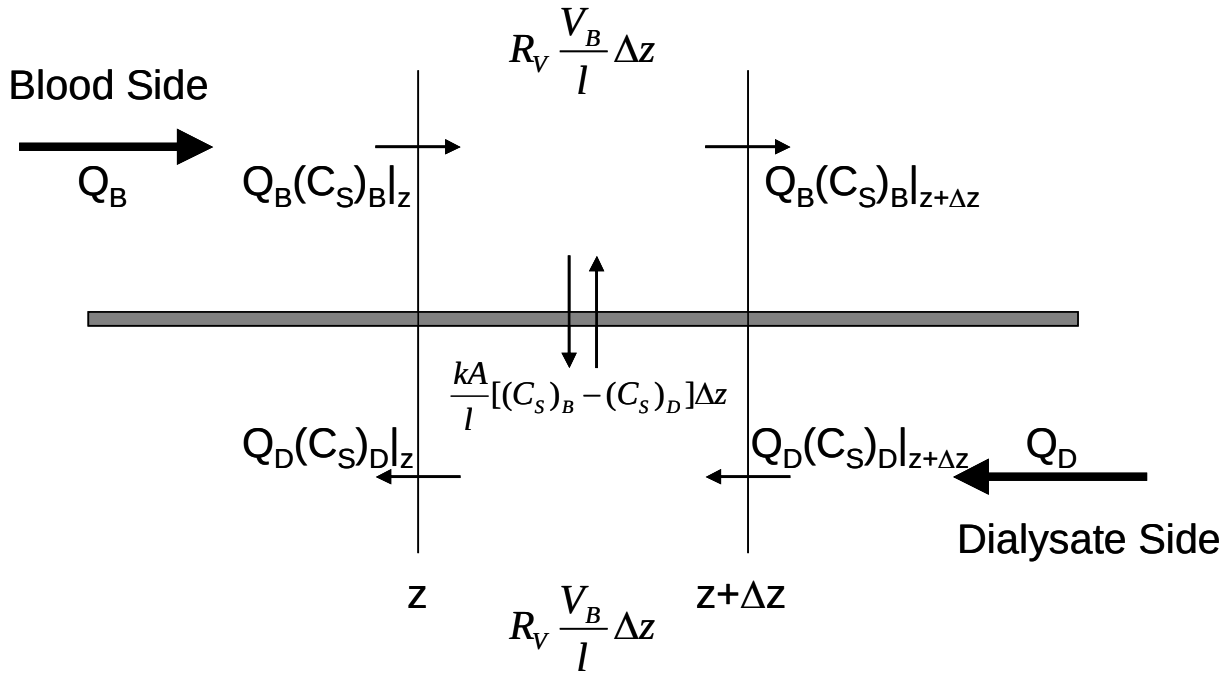

Figure C.1. A typical dialyzer consists of two countercurrent flow paths with volumes of V_B and V_D with flow rates of Q_B and Q_D for blood and dialysate respectively. The flow paths are segregated by a membrane of length l that can be separated into finite segments of size Δz. The free solute concentrations ($(C_S)_B$ and $(C_S)_D$ for blood and dialysate respectively) change along the length, *l*, of the membrane as solute diffuses across the membrane at a rate proportional to the difference in concentrations on each side of the membrane and the membrane area/mass transport rate constant *(kA)* that is dependent on the solute and membrane that are being used. Albumin-solute volumetric binding reactions occur at the rate R_V that is dependent on the binder and solute involved.

As blood passes through the dialyzer, free binder (albumin), *A*, and free solute, *S*, in the blood (subscript *B*) associate to form the solute-binder complex, *S*•*A*, and the complex dissociates into free binder and solute:

$$(S \bullet A)_B \underset{k_d}{\overset{k_a}{\rightleftarrows}} (A)_B + (S)_B \qquad \textbf{Equation C.1}$$

where k_a (m^3 mol^{-1} s^{-1}) and k_d (s^{-1}) are the reaction rate constants of association and dissociation, respectively, of the solute binder complex. Molecules in the blood that are smaller than the molecular weight cutoff of the membrane being used will diffuse down their concentration gradient into the dialysate (subscript *D*). Likewise, any molecule that has a higher concentration in the dialysate than in the blood stream will diffuse down its concentration gradient into the blood.

$$(S)_B \rightleftarrows (S)_D$$ **Equation C.2**

It is being assumed that the binder molecules are not able to cross the dialysis membrane. Free binder present on the dialysate side will react with solute crossing the membrane.

$$(A)_D + (S)_D \underset{k_d}{\overset{k_a}{\rightleftarrows}} (S \bullet A)_D$$ **Equation C.3**

For the one-to-one binding scheme presented here, the association equilibrium binding constant, K_B (m^3 mol^{-1}), is defined as

$$K_B = \frac{k_a}{k_d} = \frac{C_{S \bullet A,eq}}{C_{S,eq} C_{A,eq}}$$ **Equation C.4**

The concentrations of the complex, $C_{S \bullet A,eq}$, the solute, $C_{S,eq}$, and the binder, $C_{A,eq}$, are the concentrations at equilibrium (subscript eq). The total solute and binder concentrations (whether the reactions are at equilibrium or not) are given by

$$C_{S,total} = C_S + C_{SA}$$ **Equation C.5**

$$C_{A,total} = C_A + C_{SA}$$ **Equation C.6**

A mass balance on the free solute on the blood side yields the ordinary differential equation

$$Q_B \frac{d(C_S)_B}{dz} = \frac{kA}{l}\left((C_S)_D - (C_S)_B\right) + R_V^{SB}\frac{V_B}{l}$$ **Equation C.7**

where Q_B ($m^3\ s^{-1}$) is the volumetric flow rate of the blood side, $(C_S)_D$ (mol m^{-3}) is the free solute concentration on the dialysate side, $(C_S)_B$ (mol m^{-3}) is the concentration of free solute on the blood side, z (m) is the axial coordinate, k (m s^{-1}) is the mass transfer coefficient, A (m^2) is the membrane surface area for transport, l (m) is the axial length of the membrane, $R^{SB}{}_V$ (mol $m^{-3}\ s^{-1}$) is the volumetric production rate of solute on the blood side, and V_B (m^3) is the volume of the blood side. The equilibrium model described by Patzer was presented in terms of the total solute concentration as a function of axial position in the cartridge, but the kinetic model presented here is in terms of free solute concentration. The volumetric production rate of free solute, $R^S{}_V$, is the sum of the production of free solute from the dissociation of the binder-solute complex and the loss of free solute resulting from the association of free solute with free binder

$$R_V^S = k_d C_{SA} - k_a C_S C_A = k_d C_{SA} - k_a C_S (C_{A,total} - C_{SA})$$ **Equation C.8**

Here the superscript *S* on the volumetric production rate denotes that it is the production of solute. The *B* in Equation C.7 denotes the blood side. Substituting Equation C.8 into Equation C.7 yields

$$Q_B \frac{d(C_S)_B}{dz} = \frac{kA}{l}\left((C_S)_D - (C_S)_B\right) + \frac{V_B}{l}\left(k_d (C_{SA})_B - k_a (C_S)_B ((C_A)_B^t - (C_{SA})_B)\right) \qquad \textbf{Equation C.9}$$

Similarly on the dialysate side

$$-Q_D \frac{d(C_S)_D}{dz} = \frac{kA}{l}\left((C_S)_B - (C_S)_D\right) + \frac{V_D}{l}\left(k_d (C_{SA})_D - k_a (C_S)_D ((C_A)_D^t - (C_{SA})_D)\right) \qquad \textbf{Equation C.10}$$

Here the subscript *D*, denoting the dialysate side, replaces the subscript *B* used for the blood side. The negative on Q_D denotes the direction of flow as counter to the direction of increasing *z*. Countercurrent flow is the norm in dialysis.

In the original paper describing BSD, to define these equations as functions of C_S only, the fraction of albumin binding a solute molecule, Ψ (dimensionless), was introduced.

$$\Psi = \frac{C_{SA}}{C_A + C_{SA}} \qquad \textbf{Equation C.11}$$

The fraction of binder associating with a solute molecule, Ψ, was also described as a function of the equilibrium binding constant, K_B. The equations can no longer be described in terms of C_S only since it can no longer be assumed that the reactions are at equilibrium. Two additional

ODEs must be introduced to keep track of the amount of bound solute (C_{SA}) on both the blood and dialysate sides. It is assumed that no binder passes through the membrane.

$$Q_B \frac{d(C_{SA})_B}{dz} = \frac{V_B}{l}\left(k_a (C_S)_B ((C_A)_{B,total} - (C_{SA})_B) - k_d (C_{SA})_B\right) \quad \textbf{Equation C.12}$$

$$-Q_D \frac{d(C_{SA})_D}{dz} = \frac{V_D}{l}\left(k_a (C_S)_D ((C_A)_{D,total} - (C_{SA})_D) - k_d (C_{SA})_D\right) \quad \textbf{Equation C.13}$$

These equations can be normalized by introducing scaling relations

$$\tilde{z} = \frac{z}{l} \quad \textbf{Equation C.14}$$

$$(\tilde{C}_S)_B = \frac{(C_S)_B}{[(C_S)_{B,total}]_{in}} \quad \textbf{Equation C.15}$$

$$(\tilde{C}_{SA})_B = \frac{(C_{SA})_B}{[(C_S)_{B,total}]_{in}} \quad \textbf{Equation C.16}$$

$$(\tilde{C}_S)_D = \frac{(C_S)_D}{[(C_S)_{B,total}]_{in}} \quad \textbf{Equation C.17}$$

$$(\tilde{C}_{SA})_D = \frac{(C_{SA})_D}{[(C_S)_{B,total}]_{in}} \quad \textbf{Equation C.18}$$

When those substitutions are made we get

$$\frac{d([(C_S)_{B,total}]_{in}(\tilde{C}_S)_B)}{d(\tilde{z}l)} = \frac{kA}{Q_B l}\left([(C_S)_{B,total}]_{in}(\tilde{C}_S)_D - [(C_S)_{B,total}]_{in}(\tilde{C}_S)_B\right) + \frac{V_B}{Q_B l}\left(k_d[(C_S)_{B,total}]_{in}(\tilde{C}_{SA})_B - k_a[(C_S)_{B,total}]_{in}(\tilde{C}_S)_B((C_A)_{B,total} - [(C_S)_{B,total}]_{in}(\tilde{C}_{SA})_B)\right)$$

Equation C.19

$$\frac{d([(C_S)_{B,total}]_{in}(\tilde{C}_S)_D}{d(\tilde{z}l)} = \frac{kA}{-Q_D l}\left([(C_S)_{B,total}]_{in}(\tilde{C}_S)_B - [(C_S)_{B,total}]_{in}(\tilde{C}_S)_D\right) + \frac{V_D}{-Q_D l}\left(k_d[(C_S)_{B,total}]_{in}(\tilde{C}_{SA})_D - k_a[(C_S)_{B,total}]_{in}(\tilde{C}_S)_D((C_A)_{D,total} - [(C_S)_{B,total}]_{in}(\tilde{C}_{SA})_D)\right)$$

Equation C.20

$$\frac{d([(C_S)_{B,total}]_{in}\tilde{C}_{SA})_B)}{d(\tilde{z}l)} = \frac{V_B}{Q_B l}\left(k_a[(C_S)_{B,total}]_{in}(\tilde{C}_S)_B((C_A)_{B,total} - [(C_S)_{B,total}]_{in}(\tilde{C}_{SA})_B) - k_d[(C_S)_{B,total}]_{in}(\tilde{C}_{SA})_B\right)$$

Equation C.21

$$\frac{d([(C_S)_{B,total}]_{in}(\tilde{C}_{SA})_D)}{d(\tilde{z}l)} = \frac{V_D}{-Q_D l}\left(k_a[(C_S)_{B,total}]_{in}(\tilde{C}_S)_D((C_A)_{D,total} - [(C_S)_{B,total}]_{in}(\tilde{C}_{SA})_D) - k_d[(C_S)_{B,total}]_{in}(\tilde{C}_{SA})_D\right)$$

Equation C.22

Simplifying the equations

$$\frac{d(\tilde{C}_S)_B}{d\tilde{z}} = \frac{kA}{Q_B}\left((\tilde{C}_S)_D - (\tilde{C}_S)_B\right) + \frac{V_B}{Q_B}\left(k_d(\tilde{C}_{SA})_B - k_a(\tilde{C}_S)_B((C_A)_{B,total} - [(C_S)_{B,total}]_{in}(\tilde{C}_{SA})_B)\right)$$

Equation C.23

$$\frac{d(\tilde{C}_S)_D}{d\tilde{z}} = \frac{kA}{-Q_D}\left((\tilde{C}_S)_B - (\tilde{C}_S)_D\right) + \frac{V_D}{-Q_D}\left(k_d(\tilde{C}_{SA})_D - k_a(\tilde{C}_S)_D((C_A)_{D,total} - [(C_S)_{B,total}]_{in}(\tilde{C}_{SA})_D)\right)$$

Equation C.24

$$\frac{d(\tilde{C}_{SA})_B}{d\tilde{z}} = \frac{V_B}{Q_B}\left(k_a(\tilde{C}_S)_B((C_A)_{B,total} - [(C_S)_{B,total}]_{in}(\tilde{C}_{SA})_B) - k_d(\tilde{C}_{SA})_B\right)$$

Equation C.25

$$\frac{d(\tilde{C}_{SA})_D}{d\tilde{z}} = \frac{V_D}{-Q_D}\left(k_a(\tilde{C}_S)_D((C_A)_{D,total} - [(C_S)_{B,total}]_{in}(\tilde{C}_{SA})_D) - k_d(\tilde{C}_{SA})_D\right)$$

Equation C.26

The equations can be further simplified by introducing the following dimensionless groups

$$\kappa = \frac{kA}{Q_B}$$ **Equation C.27**

$$\alpha = \frac{Q_D}{Q_B}$$ **Equation C.28**

$$Da_1 = \frac{V_B k_d}{Q_B}$$ **Equation C.29**

$$Da_2 = \frac{V_B k_a}{Q_B[(C_S)_{B,total}]_{in}}$$ **Equation C.30**

$$\varepsilon = \frac{(C_A)_{B,total}}{[(C_S)_{B,total}]_{in}}$$ **Equation C.31**

$$\gamma = \frac{V_D}{V_B}$$ **Equation C.32**

$$\beta = \frac{(C_A)_{D,total}}{(C_A)_{B,total}}$$ **Equation C.33**

Substitution of Equation C.27- Equation C.33 into the mass balance equations yields

$$\frac{d(\tilde{C}_S)_B}{d\tilde{z}} = \kappa\left((\tilde{C}_S)_D - (\tilde{C}_S)_B\right) + Da_1(\tilde{C}_{SA})_B - Da_2(\tilde{C}_S)_B(\varepsilon - (\tilde{C}_{SA})_B)$$ **Equation C.34**

$$\frac{d(\tilde{C}_{SA})_B}{d\tilde{z}} = Da_2(\tilde{C}_S)_B(\varepsilon - (\tilde{C}_{SA})_B) - Da_1(\tilde{C}_{SA})_B$$ **Equation C.35**

$$\frac{d(\tilde{C}_S)_D}{d\tilde{z}} = \frac{\kappa}{-\alpha}\left((\tilde{C}_S)_B - (\tilde{C}_S)_D\right) + \frac{\gamma\, Da_1}{-\alpha}(\tilde{C}_{SA})_D - \frac{\gamma\, Da_2}{-\alpha}(\tilde{C}_S)_D(\beta\varepsilon - (\tilde{C}_{SA})_D))$$ **Equation C.36**

$$\frac{d(\tilde{C}_{SA})_D}{d\tilde{z}} = \frac{\gamma\, Da_2}{-\alpha}(\tilde{C}_S)_D(\beta\varepsilon - (\tilde{C}_{SA})_D) - \frac{\gamma\, Da_1}{-\alpha}(\tilde{C}_{SA})_D$$ **Equation C.37**

with the initial conditions

$$(\tilde{C}_S)_D = 0 \ @ \ \tilde{z} = 1$$

$$(\tilde{C}_{AS})_D = 0 \ @ \ \tilde{z} = 1$$

$$(\tilde{C}_S)_B = [(\tilde{C}_S)_B]_{in} \ @ \ z = 0$$

$$(\tilde{C}_{SA})_B = [(\tilde{C}_{SA})_B]_{in} \ @ \ z = 0$$ **Equation C.38**

C.2 Symbol definitions

System parameters	Units	Meaning	Definition
Q_B	L s^{-1}	Blood volumetric flow rate	
Q_D	L s^{-1}	Dialysate volumetric flow rate	
$(C_S)_B$	mol L^{-1}	Concentration of unbound solute in the blood	
$(C_S)_D$	mol L^{-1}	Concentration of unbound solute in the dialysate	
C_{SA}	mol L^{-1}	Concentration of the albumin solute complex	
C_A	mol L^{-1}	Concentration of free albumin	
C_S	mol L^{-1}	Concentration of free solute	
C_A^t	mol L^{-1}	Total concentration of albumin (the sum of the concentrations of free albumin and the albumin solute complex)	
$(C_{AS})_B$	mol L^{-1}	Concentration of the albumin solute complex on the blood side of the dialysis cartridge	
$(C_{AS})_D$	mol L^{-1}	Concentration of the albumin solute complex on the dialysate side of the dialysis cartridge	
$(C_A)_D^t$	mol L^{-1}	Total concentration of albumin on the dialysate side of the dialysis membrane	
$(C_A)_B^t$	mol L^{-1}	Total concentration of albumin on the blood side of the dialysis membrane	

System parameters	Units	Meaning	Definition
$[(C_S)_B]_{in}$	mol L^{-1}	Concentration of unbound solute in the blood at the entrance to the dialysis cartridge	
$[(C_S)_B^t]_{in}$	mol L^{-1}	Total concentration of solute in the blood at the entrance to the dialysis cartridge (scaling factor for concentrations)	
$(C_S)_D^t$	mol L^{-1}	Total concentration of solute in the dialysate	
$(C_S)_B^t$	mol L^{-1}	Total concentration of solute in the blood	
$[(C_S)^t]_{res}$	mol L^{-1}	Total concentration of solute in the single compartment patient	
$[(C_A)^t]_{res}$	mol L^{-1}	Total albumin concentration in the single compartment patient	
$[(C_S)^t]_{out}$	mol L^{-1}	Total concentration of solute leaving the dialysis cartridge	
z	m	Axial coordinate in the dialysate cartridge	
l	m	Axial length of the dialysis cartridge (scaling factor for axial coordinate)	
kA	L s^{-1}	Lumped surface area/mass transfer rate	
R_V^{SB}	mol s^{-1} L^{-1}	Volumetric production rate of free solute on the blood side of the dialysis membrane	
R_V^S	mol s^{-1} L^{-1}	Volumetric production rate of free solute	
k_d	s^{-1}	Rate of dissociation of the albumin solute complex (first order reaction)	
k_a	L mol^{-1} s^{-1}	Rate of association of the albumin solute complex (second order reaction)	
K_B	L mol^{-1}	Equilibrium binding constant	C_{AS} $(C_A C_S)^{-1}$

System parameters	Units	Meaning	Definition
V_D	L	Volume of the dialysate side of the dialysis cartridge	
V_B	L	Volume of the blood side of the dialysis cartridge	
Ψ		Fraction of albumin that has a solute molecule bound to it (at equilibrium)	$C_{AS}(C_A + C_{AS})^{-1}$ $K_B C_S (1+K_B \cdot C_S)^{-1}$
$\tilde{z}$		Dimensionless axial coordinate	$z\ l^{-1}$
$(\tilde{C_S})_B$		Dimensionless free solute concentration on the blood side	$(C_S)_B([(C_S)_B^t]_{in})^{-1}$
$(\tilde{C_{SA}})_B$		Dimensionless albumin/solute complex concentration on the blood side	$(C_{AS})_B([(C_S)_B^t]_{in})^{-1}$
$(\tilde{C_S})_D$		Dimensionless free solute concentration on the dialysate side	$(C_S)_D([(C_S)_B^t]_{in})^{-1}$
$(\tilde{C_{SA}})_D$		Dimensionless albumin/solute complex concentration on the dialysate side	$(C_{AS})_D([(C_S)_B^t]_{in})^{-1}$
κ		Dimensionless mass transfer rate	$kA\ Q_B^{-1}$
α		Dimensionless flow rate	$Q_D\ Q_B^{-1}$
Da_1		Dimensionless reaction rate of dissociation of the albumin solute complex	$V_B k_d\ Q_B^{-1}$
Da_2		Dimensionless reaction rate of association of the albumin solute complex	$Vbka\ (Q_B[(C_S)_B^t]_{in})^{-1}$
ε		Dimensionless total albumin (binder) concentration	$(C_A)_B^t([(C_S)_B^t]_{in})^{-1}$
γ		Ratio of volumes in the dialysate and blood sides of the dialysis cartridge	$V_D\ V_B^{-1}$
β		Ratio of the concentrations of albumin on the dialysate and blood sides	$(C_A)_D^t\ ((C_A)_B^t)^{-1}$

C.3 MATlab programs

Subsection titles are the file names that were used for the programs. All of the programs need to be in the same folder for MATlab to use them the way they are written.

C.3.1 kinetic_BSD_model.m

```
%%%%%%%%%%%%%%%%%%%%%%%%%%%%%%%%%%%%%%%%%%%%%%%%%%%%%%%%%%%%%%%%%%%%%%%%%%%%%%%%%%%%%%%%%%%%%
%
% Richard H. Miller
% University of Pittsburgh
% Department of Chemical and Petroleum Engineering
%
%%%%%%%%%%%%%%%%%%%%%%%%%%%%%%%%%%%%%%%%%%%%%%%%%%%%%%%%%%%%%%%%%%%%%%%%%%%%%%%%%%%%%%%%%%%%%
%
% kinetic_BSD_model.m
% This program solves the system of odes that were derived to describe
% the concentration profile in a dialysis cartridge used for BSD.  This
% is the system of equations derived for and presented in my
% dissertation.
%
%    REQUIRES THE FOLLOWING PROGRAMS IN THE SAME FOLDER AS THIS PROGRAM:
%       poly_solv_kin_BSD.m
%       bvp_bc_eq.m
%       bvp_bc_kin.m
%       bvp_init_eq.m
%       bvp_init_kin.m
%       equations_equilibrium_BSD.m
%       equations_kinetic_BSD.m
%
%%%%%%%%%%%%%%%%%%%%%%%%%%%%%%%%%%%%%%%%%%%%%%%%%%%%%%%%%%%%%%%%%%%%%%%%%%%%%%%%%%%%%%%%%%%%%

%Clear all variables/global variables/functions
clear all
clc
disp('start')

%DECLARE GLOBAL VARIABLES
%so that I don't have to pass a ton of variables into functions
  global C_alb_tot_bl
  global C_alb_tot_dial
  global C_solute_tot_in_bl
  global Cs_free_bl
  global Cas_bl
```

```
   global Cs_free_bl_DL
   global Cas_bl_DL
   global Ca_free_bl_DL
   global KB
   global alpha
   global kappa
   global gamma
   global Da1
   global Da2
   global epsilon
   global beta

%DECLARE/DEFINE VARIABLES
   C_alb_tot_bl  = 40/66000*1000 %moles/m^3
   beta  = 0.1
   KB  = .001 %m^3/mole
   alpha  = 0.1
   kappa  = 0.5
   epsilon  = 1.1
   Da1  = 0.1
   Da2  = Da1*KB*epsilon*C_alb_tot_bl
   gamma  =1;
   C_alb_tot_dial  = beta*C_alb_tot_bl %moles/m^3
   C_solute_tot_in_bl  = C_alb_tot_bl/epsilon

%%%%%%%%%%%%%%%%%%%%%%%%%%%%%%%%%%%%%%%%%%%%%%%%%%%%%%%%%%%%%%
%%%%%%%%%%%%%%%%%%%%

%DETERMINE INITIAL CONDITIONS
   %Uses the function poly_solv_kin_BSD to create an array for the
   %incoming concentrations on the blood side
      conc = poly_solv_kin_BSD(C_solute_tot_in_bl, C_alb_tot_bl, KB);

   %split up the solution into its indavidual concentrations
      Cs_free_bl = conc(1);
      Cas_bl = conc(2);
      Ca_free_bl = conc(3);

   %Convert to dimensionless concentrations.  Dimensionless quantities are
   %denoted by _DL at the end of the variable name
      Cs_free_bl_DL = Cs_free_bl/C_solute_tot_in_bl;
      Cas_bl_DL = Cas_bl/C_solute_tot_in_bl;
      Ca_free_bl_DL = Ca_free_bl/C_solute_tot_in_bl;

%ODE SOLVERS
   %INITIAL GUESS FOR BVP SOLVER
   %create an array for initial guess values for the BVP solver
   %(initial guess array returned by bvpinit) =
   %bvpinit(define mesh points, @handle for function defining the guess
   %at each point)
      %kinetic BSD guess
      solinit_kin = bvpinit(linspace(0,1,101),@bvp_init_kin);
      %equilibrium BSD guess
      solinit_eq  = bvpinit(linspace(0,1,101),@bvp_init_eq);
```

```
    %BVP SOLVERS
    %Use the boundry value problem solver bvp4c to solve the equations
    %defined in @equiations_functionname, with the boundary values
    %defined by @bvp_bc_name, with the initial guess vector solinit_name
       %kinetic BSD solution
       sol_kin = bvp4c(@equations_kinetic_BSD,@bvp_bc_kin,solinit_kin);
       %equilibrium solution (solves dimensional concentrations)
       sol_eq  = bvp4c(@equations_equilibrium_BSD,@bvp_bc_eq,solinit_eq);

    %Split the solution into concentrations for the free solute in the
    %blood and the albumin solute complex to get the total concentration
    %of solute
       %kinetic BSD solution
       Csfb_solution_kin = sol_kin.y(1,:);
       Casb_solution_kin = sol_kin.y(2,:);
       Cs_tot_sol_kin = Csfb_solution_kin + Casb_solution_kin;
       Cs_tot_sol_kin_DL = Cs_tot_sol_kin./C_solute_tot_in_bl;

       %equilibrium solution
       Csfb_sol_eq  = sol_eq.y(1,:);
       KBCs = KB.*Csfb_sol_eq;
       Cs_tot_sol_eq = Csfb_sol_eq + C_alb_tot_bl.*(KBCs./(1+KBCs));
       %convert to dimensionless concentrations
       Cs_tot_sol_eq_DL = Cs_tot_sol_eq./C_solute_tot_in_bl;

%PLOT RESULTS
    %clear figure
    clf reset
    %Hold the figure so that multiple plot commands can be made
    hold on

    plot(sol_kin.x,Cs_tot_sol_kin_DL,':','Color','k','LineWidth',1);
    plot(sol_eq.x,Cs_tot_sol_eq_DL,'-','LineWidth',1)
    legend('C~st kin','C~st eq');
    ylabel('Cs~ total');xlabel('z~');xlim([0 1]);ylim([0 1.005]);

    CS_TOTAL_KIN_COPY = Cs_tot_sol_kin_DL';
    POSSITION_KIN_COPY = sol_kin.x';
    CS_TOTAL_EQ_COPY = Cs_tot_sol_eq_DL';
    POSSITION_EQ_COPY = sol_eq.x';
    COPY_KIN = [POSSITION_KIN_COPY CS_TOTAL_KIN_COPY];
    COPY_EQ = [POSSITION_EQ_COPY CS_TOTAL_EQ_COPY];

disp('end');
```

C.3.2 poly_solv_kin_BSD.m

```
function [concentration_array] = poly_solv_kin_BSD(Cst, Cat, Keq)
%Determines the incoming concentrations to be used as the initial values
%in the BVP solver.  Uses the total binder, total solute, and binding
%constant to determine the concentrations of free solute, free binder,
%and binder solute complex for the reaction:
%binder + solute <---> binder solute complex

%INPUTS:
   %Cst = total incoming solute concentration
   %Cat = total incoming binder concentration
   %Keq = equilibrium binding constant of the reaction

%DEFINE the objective function A*Cs^2 + B*Cs + C = 0
   A = Keq;
   B = 1 + (Keq*Cat) - (Keq*Cst);
   C = -Cst;

   obj_fun = @(x) (A*(x^2))+B*x + C;

%DEFINE SEARCH RANGE for the root finding routine
   search_range_low = 0;
   search_range_high = Cst;
   search_range = [search_range_low, search_range_high];

%DEFINE SOLVER TOLERENCE
   x_tol = 0.00000001;

%FIND ROOT OF OBJECTIVE FUNCTION
   root_value = fzero(obj_fun, search_range, optimset('TolX', x_tol));

   Csf = root_value;  %Free solute concentration
   Cas = Cst - Csf;  %binder solute complex concentration
   Caf = Cat - Cas;  %free albumin concentration

%RETURN ARRAY
concentration_array = [Csf Cas Caf];
```

C.3.3 bvp_bc_eq.m

```
function res = bvp_bc_eq(ya,yb)
global Cs_free_bl

%Defines boundary conditions for the BVP solver in terms of the residuals
%for the equilibrum BSD solver
%formatted as [possition(array #)]-[value at possition]
%ya: blood side at z_DL = 0
%yb: dialysate at z_DL = 1

res = [ ya(1)-Cs_free_bl
        yb(2)];
```

C.3.4 bvp_bc_kin.m

```
function res = bvp_bc_kin(ya,yb)

global Cs_free_bl
global Cas_bl

%Defines boundary conditions for the BVP solver in terms of the residuals
%for the kinetic BSD solver
%formatted as [possition(array #)]-[value at possition]
%ya: blood side at z_DL = 0
%yb: dialysate at z_DL = 1

res = [ ya(1)-Cs_free_bl
        ya(2)-Cas_bl
        yb(3)
        yb(4)];
```

C.3.5 bvp_init_eq.m

```
function guess_vector = bvp_init_eq(x)
global Cs_free_bl

%Defines an initial guess starting point for the boundary value problem %solver for the equilibrium BSD model

guess_vector = [ -Cs_free_bl/2*x+Cs_free_bl
                 -0.1*Cs_free_bl/2*x+0.1*Cs_free_bl];
```

C.3.6 bvp_init_kin.m

```
function guess_vector = bvp_init_kin(x)

global Cs_free_bl
global Cas_bl

%Defines an initial guess starting point for the boundary value problem %solver for the kinetic BSD model

guess_vector = [ -Cs_free_bl/2*x+Cs_free_bl
                 -Cas_bl/2*x+Cas_bl
                 -0.1*Cs_free_bl/2*x+0.1*Cs_free_bl
                 -0.1*Cas_bl/2*x+0.1*Cas_bl];
```

C.3.7 equations_equilibrium_BSD.m

```
function [rhs_eq] = equations_equilibrium_BSD(ind_eq,dep_eq)
%Defines the right hand side of the ODEs describing the equilibrium model
%of BSD.

global kappa
global C_alb_tot_bl
global KB
global alpha
global C_alb_tot_dial

%Create some shortened local variable names for print formatting purposes
CAB = C_alb_tot_bl;
CAD = C_alb_tot_dial;
kap = kappa;
al = alpha;
K = KB;
ka=kap/al;

rhs_eq = [1;2];
rhs_eq(1)=(kap)*(dep_eq(2)-dep_eq(1))*((1+CAB*(K/((1+K*dep_eq(1))^2)))^-1);
rhs_eq(2)=(ka)*(dep_eq(2)-dep_eq(1))*((1+CAD*(K/((1+K*dep_eq(2))^2)))^-1);
```

C.3.8 equations_kinetic_BSD.m

```
function [rhs_kin] = equations_kinetic_BSD(ind_vec_kin,dep_vec_kin)
%Defines the right hand side of the ODEs describing the kinetic model of
%BSD.

global kappa
global Da1
global Da2
global alpha
global gamma
global C_solute_tot_in_bl
global C_alb_tot_bl
global C_alb_tot_dial

%shorten variable names for print formatting purposes
a=dep_vec_kin(1);%Csb
b=dep_vec_kin(2);%Csab
c=dep_vec_kin(3);%Csd
d=dep_vec_kin(4);%Csad
CS = C_solute_tot_in_bl;
CD = C_alb_tot_dial;
ga = gamma/alpha;

rhs_kin1=(kappa*(c-a))+(Da1*b)-((Da2/CS)*a*(C_alb_tot_bl-b));
rhs_kin2=((Da2/C_solute_tot_in_bl)*a*(C_alb_tot_bl-b))-(Da1*b);
rhs_kin3=((-kappa/alpha)*(a-c))+((-ga)*Da1*d)-((-ga)*(Da2*CS)*c*(CD-d));
rhs_kin4=((-ga)*(Da2*CS)*c*(CD-d))-((-ga)*Da1*d);
rhs_kin = [rhs_kin1; rhs_kin2; rhs_kin3; rhs_kin4];
```

APPENDIX D

SPECIFIC AIM 3

D.1 Slide dialyzer prototyping

Dialysis fibers were excised from Exeltra cellulose triacetate (Baxter Healthcare Corporation, Deerfield, IL), Multiflow 60 AN69 (HOSPAL Industrie, Meyzieu, France), and Polyflux 11S polyarylethersulfone (Gambro Dialysatoren GmbH & Co. KG, Hechingen, Germany) commercial dialyzers. A high speed rotary tool with a cutting wheel was used to remove the polycarbonate housing from the dialyzer. The rotary tool was used at high speed in an attempt to melt the plastic housing as it was being cut to reduce the amount of saw dust getting into the fiber bed, and a vacuum was used to remove saw dust at the cut site as the cutting was performed (Figure 6.3). Small bundles of ~50 fibers about 90-100 mm long were cut from the fiber bed with surgical scissors. Polysulfone membranes kink easily, are very brittle, dry, and push away from each other due to static charge once the fiber bed is removed from the shell. Cellulose triacetate fiber are quite thin (diameter), easily kinked, and easily broken. AN69 membranes are on the larger side, and are somewhat robust to handling when compared to the other two membrane types used. The AN69 and cellulose triacetate membranes are both packed wet with

glycerin.[73] Attempts to use an albumin permeable cellulose triacetate bioreactor membrane were unsuccessful due to the fragility of the fibers during handling.

Plastic shim stock (PETG, 0.03" thickness) (McMaster-Carr, Robbinsvile, NJ) was cut to fit on the microscope stage (80x100 mm) and a 15 mm hole was cut to accommodate the microscope objective. A 45x50 mm coverslip (1.5 thickness) was affixed over the hole using general purpose (thick, non-flowable) silicone sealant (RTV sealant, 732 Multi-Purpose Sealant, Dow Corning Corporation, Midland, MI) (Figure D.1).

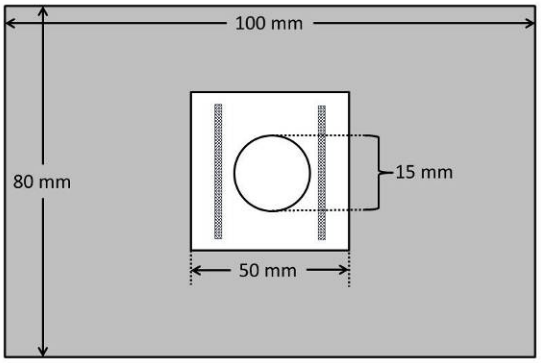

Figure D.1. Plastic shim stock was cut to 80x100 mm. A 15 mm hole was cut in the middle to accommodate a microscope objective. A 45x50 mm cover slip was glued in place over the hole. A bead of silicon was placed on either side of the hole to affix the dialysis fibers.

A small bead of general purpose silicone sealant was laid about 1 mm from the edge on two opposing sides. Ten fibers were evenly spaced across the cover slip, and the fibers were gently pressed into the silicone so that they were in contact with the cover slip. A new bead of general purpose silicone sealant was laid to cover the outside 1 mm of the coverslip. Two lengths of microbore tygon tubing (2" length, 0.040" ID, 0.070 OD) (Saint-Gobain, Granville, NY), were positions perpendicular to the fibers with the end of the tube just inside the silicone

bead to create a cross flow configuration through the extracapillary space of the slide. A second 1 mm bead of general purpose silicone sealant was laid around the outside of the coverslip on top of the first bead to sandwich the tubing. A 50x50 mm (~0.03" thickness) borosilicate slide glass (Eastman Kodak Company, Rochester, NY) was placed on top and gently pressed to seat the coverslip and slide glass onto the tubing. A small beaker was placed on top of the slide glass and the silicone was allowed to cure overnight (Figure D.2).

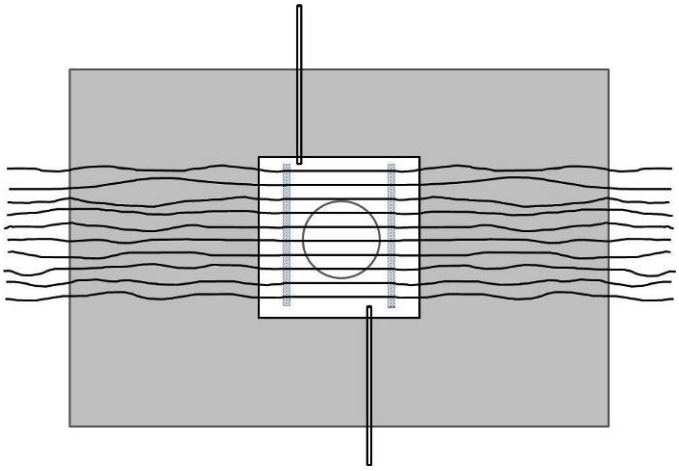

Figure D.2. The dialysis fibers were evenly spaced across the coverslip, and were gently pressed into the silicone. Two pieces of tubing (2" length, 0.040" ID, 0.070 OD) were placed at the edge of the cover slip perpendicular to the dialysis fibers.

The fibers were then wetted with general purpose silicone sealant, gently gathered together, and allowed to dry overnight. This silicone coating served the purpose of sealing the membrane to prevent leaking and to gather the fibers to allow them to be inserted into a piece of tubing. A 4 cm piece of silicone tubing (0.125" ID, 0.188" OD) (Cole-Parmer, Vernon Hills, IL) was slid over the fibers on both sides of the slide dialyzer. A bead of general purpose silicone sealant was laid around the outside of the slide that was just higher than the top of the slide glass and tubing

housing the fibers to create a dam that can be backfilled with silicone to encase and seal the fibers, the edge of the glass sandwich, and the bottom of the tubing housing the fibers. The silicone was allowed to cure overnight. The tubing housing the fibers was filled with flowable silicone sealant (RTV sealant, 734 Multi-Purpose Sealant, Dow Corning Corporation, Midland, MI) from the side toward the glass outward, and the dam around the edge of the slide was back filled with the flowable silicone from the edge of the glass outward. A razor blade was used to cut back several millimeters up the tubing with the fibers, opening the fibers to flow but leaving a stub long enough to place a fitting over the tubing (Figure D.3).

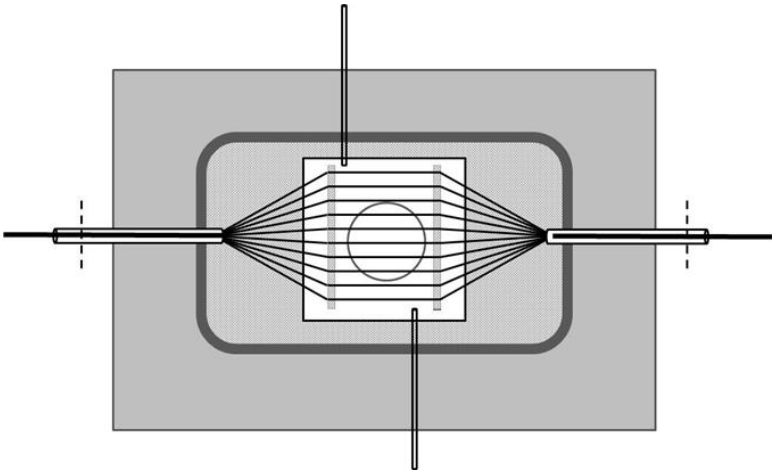

Figure D.3. The fibers were bundled together and slid into a piece of tubing (0.125" ID, 0.188" OD). Silicone sealant was used to fill the tubing, seal the area around the glass, and cover the fibers. After the silicone had cured, the tubing housing the dialysis fibers was cut to expose the open fibers.

The fittings I used were female-female luer lock connectors with one side bored out to the OD of the tubing used to house the fibers. The fitting was placed just over the end of the tubing, and a bead of flowable RTV silicone sealant was put on the tubing at the front edge of the fitting. The fitting was pushed the rest of the way onto the tubing, and additional silicone was allowed to

flow over the fitting to completely seal against leaks. Barbed luer fitting were inserted into the tubing going into the extracapillary space (Figure D.4). After an additional two days to allow all of the silicone to fully cure, the slides were connected to a syringe pump at a flow rate of 0.25 ml/min to test for leaks.

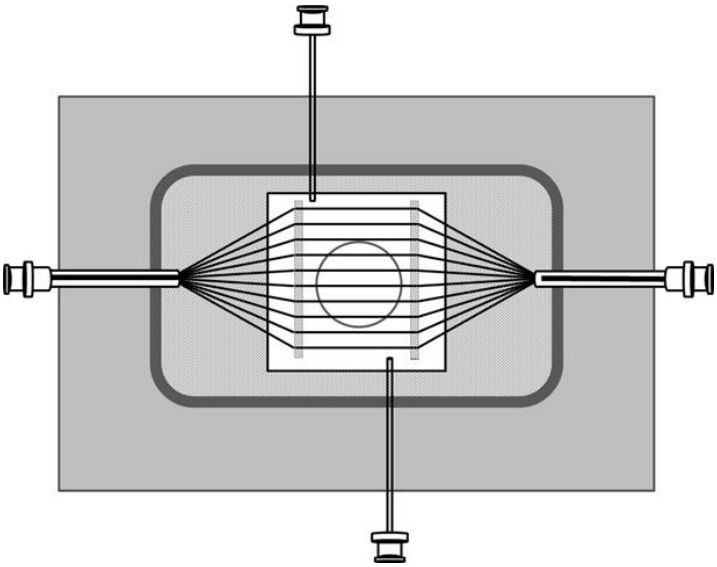

Figure D.4. Female luer fittings were affixed to the tubing housing the fibers and entering the extracapillary space.

BIBLIOGRAPHY

1. Awad, S.S., et al., *Results of a phase I trial evaluating a liver support device utilizing albumin dialysis.* Surgery, 2001. **130**(2): p. 354-62.

2. Campli, C.D., et al., *Successful MARS treatment in severe cholestatic patients with acute on chronic liver failure.* Artif Organs, 2003. **27**(6): p. 565-9.

3. Kjaergard, L.L., et al., *Artificial and bioartificial support systems for acute and acute-on-chronic liver failure: a systematic review.* JAMA, 2003. **289**(2): p. 217-22.

4. OPTN. *Organ Procurement and Transportation Network.* [cited 2012 4/19/2012]; Organ Procurement and Transportation Network, US Department of Health and Human Services]. Available from: optn.transplant.hrsa.gov.

5. Catapano, G., J.F. Patzer, 2nd, and J.C. Gerlach, *Transport advances in disposable bioreactors for liver tissue engineering.* Adv Biochem Eng Biotechnol, 2010. **115**: p. 117-43.

6. Gerlach, J.C., K. Zeilinger, and J.F. Patzer Ii, *Bioartificial liver systems: why, what, whither?* Regen Med, 2008. **3**(4): p. 575-95.

7. O'Grady, J., *Personal view: current role of artificial liver support devices.* Aliment Pharmacol Ther, 2006. **23**(11): p. 1549-57.

8. Pless, G. and I.M. Sauer, *Bioartificial liver: current status.* Transplant Proc, 2005. **37**(9): p. 3893-5.

9. Bartolo, L.D. and A. Bader, *Development of a hybrid liver-support device.* Minim Invasive Ther Allied Technol, 2002. **11**(3): p. 123-34.

10. Ash, S.R., *Powdered sorbent liver dialysis and pheresis in treatment of hepatic failure.* Ther Apher, 2001. **5**(5): p. 404-16.

11. Ash, S.R., T.A. Sullivan, and D.J. Carr, *Sorbent suspensions vs. sorbent columns for extracorporeal detoxification in hepatic failure.* Ther Apher Dial, 2006. **10**(2): p. 145-53.

12. Falkenhagen, D., et al., *Fractionated plasma separation and adsorption system: a novel system for blood purification to remove albumin bound substances.* Artif Organs, 1999. **23**(1): p. 81-6.

13. Rifai, K., et al., *Prometheus--a new extracorporeal system for the treatment of liver failure.* J Hepatol, 2003. **39**(6): p. 984-90.

14. Carpentier, B., A. Gautier, and C. Legallais, *Artificial and bioartificial liver devices: present and future.* Gut, 2009. **58**(12): p. 1690-702.

15. McKenzie, T.J., J.B. Lillegard, and S.L. Nyberg, *Artificial and bioartificial liver support.* Semin Liver Dis, 2008. **28**(2): p. 210-7.

16. Chawla, L.S., et al., *Modification of continuous venovenous hemodiafiltration with single-pass albumin dialysate allows for removal of serum bilirubin.* Am J Kidney Dis, 2005. **45**(3): p. e51-6.

17. Kreymann, B., et al., *Albumin dialysis: effective removal of copper in a patient with fulminant Wilson disease and successful bridging to liver transplantation: a new possibility for the elimination of protein-bound toxins.* J Hepatol, 1999. **31**(6): p. 1080-5.

18. Patzer, J.F., 2nd and S.E. Bane, *Bound solute dialysis.* ASAIO J, 2003. **49**(3): p. 271-81.

19. Patzer, J.F., 2nd, S.A. Safta, and R.H. Miller, *Slow continuous ultrafiltration with bound solute dialysis.* ASAIO J, 2006. **52**(1): p. 47-58.

20. Sauer, I.M., et al., *In vitro comparison of the molecular adsorbent recirculation system (MARS) and single-pass albumin dialysis (SPAD).* Hepatology, 2004. **39**(5): p. 1408-14.

21. Seige, M., et al., *Long-term treatment of patients with acute exacerbation of chronic liver failure by albumin dialysis.* Transplant Proc, 1999. **31**(1-2): p. 1371-5.

22. Stange, J., et al., *The molecular adsorbents recycling system as a liver support system based on albumin dialysis: a summary of preclinical investigations, prospective, randomized, controlled clinical trial, and clinical experience from 19 centers.* Artif Organs, 2002. **26**(2): p. 103-10.

23. Mitzner, S.R., et al., *Albumin dialysis MARS: knowledge from 10 years of clinical investigation.* ASAIO J, 2009. **55**(5): p. 498-502.

24. Sen, S., R. Williams, and R. Jalan, *Emerging indications for albumin dialysis.* Am J Gastroenterol, 2005. **100**(2): p. 468-75.

25. Deland, F.H. and W.A. North, *Relationship Between Liver Size and Body Size.* Radiology, 1968. **1**: p. 1196-1198.

26. Maddrey, W.C., *Atlas of the liver*. 3rd ed. 2003, Philadelphia: Current Medicine. p.

27. Martini, F.H., M.J. Timmons, and R.B. Tallitsch, *Human Anatomy*. sixth ed. 2008, San Fransisco, CA: Pearson Benjamin Cummings.

28. Lee, R.G., *Diagnostic liver pathology*. 1st ed. 1994, St. Louis: Mosby. vii, 517 p.

29. Fontana, R.J., *Acute liver failure including acetaminophen overdose.* Med Clin North Am, 2008. **92**(4): p. 761-94, viii.

30. Chun, L.J., et al., *Acetaminophen hepatotoxicity and acute liver failure.* J Clin Gastroenterol, 2009. **43**(4): p. 342-9.

31. Hofmann, A.F., *Cholestatic liver disease: pathophysiology and therapeutic options.* Liver, 2002. **22 Suppl 2**: p. 14-9.

32. Sen, S., R. Williams, and R. Jalan, *The pathophysiological basis of acute-on-chronic liver failure.* Liver, 2002. **22 Suppl 2**: p. 5-13.

33. UNOS. *United Network for Organ Sharing (UNOS).* 2/28/2010]; Available from: www.unos.org.

34. Starzl, T.E., et al., *History of Liver and Multivisceral Transplantation*, in *Transplantation of the Liver*, R.W. Busutill and G.B. Klintmalm, Editors. 2005, Elsevier Saunders: Philadelphia, PA. p. 3-22.

35. Bernal, W., et al., *Intensive care management of acute liver failure.* Semin Liver Dis, 2008. **28**(2): p. 188-200.

36. O'Grady, J., *Modern management of acute liver failure.* Clin Liver Dis, 2007. **11**(2): p. 291-303.

37. Riordan, S.M. and R. Williams, *Perspectives on liver failure: past and future.* Semin Liver Dis, 2008. **28**(2): p. 137-41.

38. Martin, A.P., et al., *Overview of the MELD score and the UNOS adult liver allocation system.* Transplant Proc, 2007. **39**(10): p. 3169-74.

39. Hashikura, Y., *Living donor liver transplantation for patients with fulminant hepatic failure.* Hepatol Res, 2008. **38**(s1The 6 Japan Society of Hepatology Single Topic Conference: Liver Failure: Recent Progress and Pathogenesis to Management. 28-29 September 2007, Iwate, Japan): p. S56-S59.

40. Patzer, J.F., 2nd, *Advances in bioartificial liver assist devices.* Ann N Y Acad Sci, 2001. **944**: p. 320-33.

41. Rifai, K., C. Tetta, and C. Ronco, *Prometheus: from legend to the real liver support therapy.* Int J Artif Organs, 2007. **30**(10): p. 858-63.

42. Patzer, J.F., 2nd, *Thermodynamic considerations in solid adsorption of bound solutes for patient support in liver failure.* Artif Organs, 2008. **32**(7): p. 499-508.

43. Peters, T., *All about albumin : biochemistry, genetics, and medical applications*. 1996, San Diego: Academic Press. xx, 432 p.

44. Patzer, J., *Principles of bound solute dialysis.* Ther Apher Dial, 2006. **10**(2): p. 118-24.

45. Sri Ranjini, A., P.K. Das, and P. Balaram, *Binding constant measurement by hyper-Rayleigh scattering: bilirubin-human serum albumin binding as a case study.* J Phys Chem B, 2005. **109**(12): p. 5950-3.

46. Gambro. *MARS treatment kit product insert*. [cited 2012 March 21, 2012]; Available from: http://www.gambro.com/PageFiles/1918/MARSkit-1112-1.pdf?epslanguage=en.

47. Mitzner, S.R., et al., *Improvement of hepatorenal syndrome with extracorporeal albumin dialysis MARS: results of a prospective, randomized, controlled clinical trial.* Liver Transpl, 2000. **6**(3): p. 277-86.

48. Kantola, T., et al., *Cost-utility of molecular adsorbent recirculating system treatment in acute liver failure.* World J Gastroenterol, 2010. **16**(18): p. 2227-34.

49. Kortgen, A., et al., *Albumin dialysis in liver failure: comparison of molecular adsorbent recirculating system and single pass albumin dialysis--a retrospective analysis.* Ther Apher Dial, 2009. **13**(5): p. 419-25.

50. Awad, S.S., et al., *Characteristics of an albumin dialysate hemodiafiltration system for the clearance of unconjugated bilirubin.* ASAIO J, 1997. **43**(5): p. M745-9.

51. Peszynski, P., et al., *Albumin dialysis: single pass vs. recirculation (MARS).* Liver, 2002. **22 Suppl 2**: p. 40-2.

52. Rich, R.L., et al., *High-resolution and high-throughput protocols for measuring drug/human serum albumin interactions using BIACORE.* Analytical Biochemistry, 2001. **296**(2): p. 197-207.

53. McQuarrie, D.A. and D.S. John, *Physical Chemistry: A Molecular Approach*.

54. Smith, J.M., H.C. Van Ness, and M.M. Abbott, *Introduction to chemical engineering thermodynamics*. 7th ed. McGraw-Hill chemical engineering series. 2005, Boston: McGraw-Hill. xviii, 817 p.

55. Shuler, M.L. and F. Karg*, *Bioprocess engineering*. 2nd ed. Prentice-Hall international series in the physical and chemical engineering sciences. 2002, Upper Saddle River, NJ: Prentice Hall. xx, 553 p.

56. Markey, F., *Interpreting Data.* Biajournal, 1995. **2**(1).

57. Healthcare, G. 11/20/2009]; Available from: www.biacore.com.

58. Myszka, D.G., *Analysis of small-molecule interactions using Biacore S51 technology.* Analytical Biochemistry, 2004. **329**(2): p. 316-323.

59. Roda, A., et al., *Quantitative aspects of the interaction of bile acids with human serum albumin.* J Lipid Res, 1982. **23**(3): p. 490-5.

60. Piekoszewski, W. and W.J. Jusko, *Plasma protein binding of tacrolimus in humans.* J Pharm Sci, 1993. **82**(3): p. 340-1.

61. Pico, G.A. and C. Houssier, *Bile salts-bovine serum albumin binding: spectroscopic and thermodynamic studies.* Biochim Biophys Acta, 1989. **999**(2): p. 128-34.

62. Myszka, D.G. and T.A. Morton, *CLAMP (c): A biosensor kinetic data analysis program.* Trends in Biochemical Sciences, 1998. **23**(4): p. 149-150.

63. Meisel, P., et al., *Albumin binding of photobilirubin II.* Biochem J, 1983. **213**(1): p. 25-9.

64. Olsen, H., et al., *Pharmaceutical-grade albumin: impaired drug-binding capacity in vitro.* BMC Clin Pharmacol, 2004. **4**: p. 4.

65. Costarino, A.T., et al., *Bilirubin photoisomerization in premature neonates under low- and high-dose phototherapy.* Pediatrics, 1985. **75**(3): p. 519-22.

66. Zahir, H., et al., *Changes in tacrolimus distribution in blood and plasma protein binding following liver transplantation.* Ther Drug Monit, 2004. **26**(5): p. 506-15.

67. Clark, W.R., et al., *Plasma protein adsorption to highly permeable hemodialysis membranes.* Kidney Int, 1995. **48**(2): p. 481-8.

68. Membrana. [cited 2012 2/6/2012]; Available from: www.membrana.com.

69. Stange, J., et al., *A new procedure for the removal of protein bound drugs and toxins.* ASAIO J, 1993. **39**(3): p. M621-5.

70. Morti, S.M. and A.L. Zydney, *Protein-membrane interactions during hemodialysis: effects on solute transport.* ASAIO J, 1998. **44**(4): p. 319-26.

71. Clark, W.R., et al., *Membrane adsorption of beta 2-microglobulin: equilibrium and kinetic characterization.* Kidney Int, 1994. **46**(4): p. 1140-6.

72. Fujimori, A., H. Naito, and T. Miyazaki, *Adsorption of complement, cytokines, and proteins by different dialysis membrane materials: evaluation by confocal laser scanning fluorescence microscopy.* Artif Organs, 1998. **22**(12): p. 1014-7.

73. Clark, W. and D. Gao, *Properties of membranes used for hemodialysis therapy.* Seminars in Dialysis, 2002. **15**(3): p. 191-195.